The sedimentary record of subglacial erosion beneath the Laurentide Ice Sheet

Gregory A. Balco

A dissertation submitted in partial fulfillment
of the requirements for the degree of

Doctor of Philosophy

University of Washington

2004

Program Authorized to Offer Degree: Earth and Space Sciences – Geological Sciences

University of Washington

Graduate School

This is to certify that I have examined this copy of a doctoral dissertation by

Gregory A. Balco

and have found that it is complete and satisfactory in all respects,
and that any and all revisions required by the final
examining committee have been made.

Chair of Supervisory Committee:

_____

John O.H. Stone

Reading Committee:

_____

John O.H. Stone

_____

Bernard Hallet

_____

Stephen C. Porter

Date: _____

In presenting this dissertation in partial fulfillment of the requirements for the Doctoral degree at the University of Washington, I agree that the Library shall make its copies freely available for inspection. I further agree that extensive copying of this dissertation is allowable only for scholarly purposes, consistent with "fair use" as prescribed in the U.S. Copyright Law. Requests for copying or reproduction of this dissertation may be referred to Bell and Howell Information and Learning, 300 North Zeeb Road, Ann Arbor, MI 48106-1346, or to the author.

Signature_____

Date_____

University of Washington

Abstract

The sedimentary record of subglacial erosion beneath the Laurentide Ice Sheet

by Gregory A. Balco

Chair of Supervisory Committee:

Associate Professor John O.H. Stone
Quaternary Research Center and Earth and Space Sciences

I use measurements of the cosmic-ray-produced radionuclides ^{10}Be and ^{26}Al to investigate the age and source of subglacial sediment exported by the Laurentide Ice Sheet during the last 2 million years. This is important because the processes of subglacial erosion and sediment transport regulate the size and stability of ice sheets, which in turn affect global climate and sea level. These processes are difficult to study, both because they take place at the bottom of large ice sheets and because, as in all eroding landscapes, the record of change is continually effaced as the surface is removed. However, there do exist thick sequences of glacial sediment, which record past subglacial erosion and transport, preserved around the margins of present and former ice sheets; these are the subject of this study.

First, I describe a method for dating such sequences by measuring ^{10}Be and ^{26}Al in quartz from paleosols intercalated with glacial sediments. The method consists of measuring nuclide concentrations at various depths in the soil, assembling a mathematical model that predicts expected nuclide concentrations given unknown parameters that include the durations of soil exposure and burial, and using an optimization method to find ages that best fit the measured data. The method is most successful for paleosols that formed over relatively long periods of time, ($\sim$50,000 yr), in which case the precision of the age determination is limited by ^{10}Be and ^{26}Al measurement uncertainty. For paleosols that were exposed for short periods of time, uncertainties in below-ground nuclide production rates become important. Under ideal circumstances, the precision of the age determination is $\sim$5-8%. In most cases this is insufficient for correlating individual tills

with marine oxygen-isotope stages, but presents a significant, and widely applicable, improvement on existing means of dating most Plio-Pleistocene clastic sediments. Attempts to apply a similar method to outwash and river sediment intercalated with tills failed, because fluvial sediments in glaciated regions have complex exposure histories, and their nuclide concentrations at the time of their final burial usually cannot be determined. This is interesting in that it provides a means of distinguishing outwash from nonglacial fluvial sediment, but it means that buried outwash cannot be accurately dated.

Second, I use atmospherically-produced ^{10}Be, which accumulates in soil and regolith formation but is absent in fresh rock, as a geochemical tracer to determine the source of Plio-Pleistocene tills of the Laurentide Ice Sheet. Tills derived from erosion of unweathered bedrock can be distinguished from those derived from deeply weathered regolith that likely predates ice sheet formation. The Laurentide Ice Sheet exported ^{10}Be–rich sediment in two major pulses, first at the onset of glaciation and then again in the middle Pleistocene during an apparent expansion of either the ice sheet or the area of wet-based conditions.

TABLE OF CONTENTS

LIST OF FIGURES

LIST OF TABLES

ACKNOWLEDGMENTS

Carrie Patterson of the Minnesota Geological Survey, Kelli McCormick of the South Dakota Geological Survey, Joe Mason of the Conservation and Survey Division, University of Nebraska, and Chuck Rovey of Southwest Missouri State University made this project feasible and relevant by providing access to drill core and field locations, information about local and regional geology, and the stratigraphic context for the entire project. Marc Caffee of Purdue University's PRIME Lab and Bob Finkel of the Center for Accelerator Mass Spectrometry, Lawrence Livermore National Laboratories, as well as the rest of the PRIME and CAMS accelerator staffs, made ^{10}Be and ^{26}Al analyses possible. Pat Jaybush and Derrick Johnson of the UW helped with analytical work. The Fannie and John Hertz Foundation, DOSECC, Inc., the Geological Society of America, the ARCS Foundation, the American Federation of Mineralogical Societies, the UW Dept. of Geological Sciences, and the National Science Foundation all provided financial support.

Chapter 1

INTRODUCTION AND SUMMARY

Large ice sheets are the defining feature of the Quaternary Earth. We know from the oxygen isotopic composition of marine sediments [Emiliani, 1955, Shackleton and Opdyke, 1973] that large ice sheets have formed and disappeared regularly and repeatedly throughout the Pleistocene. We infer from this, from physical arguments, and from the barren and streamlined terrain they leave behind, that ice sheets are a critical part of the global climate system as well as the primary geomorphic agent responsible for arctic and northern-temperate landscapes.

Despite the fact that most of these ice sheets were located on the continents, most of what is known about their chronology prior to the last glacial maximum (LGM) comes from marine records. This is because the terrestrial stratigraphic record of earlier glaciations, although extensive, is fragmentary and mostly older than the range of radiocarbon dating. This forces us to rely on long-distance correlation with a very few volcanic ashes and magnetostratigraphic boundaries even to widely bracket the age of glacial deposits. The object of this project is to a) develop new means of dating Pleistocene glacial sediments, with the goal of better correlating marine and terrestrial records of glaciation, and b) to exploit terrestrial glacial sediments as a record of subglacial processes.

The project is motivated by several aspects of the stratigraphic and paleoclimatic record of the last few million years that are particularly difficult to understand. First, the relationship between of ice sheets and Pleistocene climate is deeply confused by an inconsistency between the size of marine δ^{18}O excursions and the size of terrestrial ice sheets. The most southerly deposits of the Laurentide Ice Sheet (LIS) are known from intercalated volcanic ashes to be 1-2 Myr old [Roy et al., 2004, Boellstorff, 1978c], which means that the first instances of the LIS were geographically as large or larger than more recent ones. However, Pleistocene marine δ^{18}O excursions, which reflect total continental ice volume, were much larger in the late Pleistocene than in the early Pleistocene. This observation, that the geographic area of the LIS has been constant but the volume has drastically increased, suggests major changes in ice dynamics during the Pleistocene. This in turn makes it

difficult to construct consistent models to simulate Pleistocene climate variability, and casts doubt on the results of any model that assumes that ice dynamics were much the same over time.

A second controversy concerns the origin of the streamlined and polished landscapes of the northern continents that we intuitively attribute to deep erosion of resistant bedrock. Flint [1947] calculated from the relatively small volume of terrestrial glacial sediment around the margin of the LIS that subglacial erosion had been minimal. White [1972] pointed out that vastly more glacial sediment was deposited in the ocean, and argued that the Precambrian rocks of Canada and Fennoscandia were exhumed by hundreds of meters of glacial abrasion. Since that time, a wide variety of evidence has been marshaled to support one or the other of these positions. Estimates of marine sediment volumes suggest that the mean depth of erosion by the Pleistocene LIS was on the order of 100 m [Bell and Laine, 1985]. This disagrees with geomorphic evidence for the survival of pre-glacial landscapes and rock surfaces in glaciated areas [Sugden, 1976, 1978, 1989, Hall and Sugden, 1987, Kleman, 1994, Briner and Swanson, 1998, Bierman et al., 1999, Harbor et al., 1999], the persistence of Tertiary planation surfaces across ice sheet boundaries [Sugden, 1976], the morphologic similarity between glacially eroded surfaces and the chemical weathering front beneath deeply weathered terrains [Feininger, 1971, Lidmar-Bergstrom, 1988, 1997, Patterson and Boerboom, 1999], and numerous examples of surviving pre-glacial regolith in glaciated regions. These all indicate that Pleistocene ice sheets may have accomplished little more than removing a pre-existing blanket of deeply weathered regolith, the legacy of a temperate Tertiary climate acting on the low-relief interiors of continental shields for millions of years.

These geomorphic and paleoclimatic questions are drawn together by the importance of subglacial sediment to ice sheet dynamics. Both theory [Cuffey and Alley, 1996] and observations from the West Antarctic ice sheet [Blankenship et al., 2001, Bindschadler et al., 2001] suggest that a supply of deformable subglacial sediment is essential for initiating and maintaining fast, low-gradient flow within ice sheets. MacAyeal [1993a] [also MacAyeal, 1993b, MacAyeal and Dupont, 1994] explained Heinrich events – massive discharges of ice-rafted debris into the North Atlantic, accompanied by global climate changes [Heinrich, 1988] – as a physical instability of the LIS in which coupled changes in thickness and basal temperature alternately froze and thawed basal sediments. This showed that it was possible for subglacial conditions to directly affect global climate. Clark and Pollard [1998] coupled these ideas and suggested that the early Pleistocene LIS, underlain by a thick layer of weak regolith that could support little shear stress, was thin and fast-flowing. Being relatively thin and thus low in volume, it could form and decay rapidly in response to the 41,000-year inclination cycle. As repeated ice advances removed the lubricating regolith and left

resistant bedrock, increased basal shear stress resulted in thicker ice sheets with a longer response time. This hypothesis may explain the apparent mismatch between the large geographic extent and small inferred ice volume of the early Pleistocene LIS. It may also explain the mid-Pleistocene climate transition: the long response time of the thick late Pleistocene ice sheet forced the global climate system into longer-period variability.

This theory relies upon the idea that the supply of deformable material beneath ice sheets is limited. Cuffey and Alley [1996] suggest this as well, pointing out that subglacial bedrock erosion is too slow to replace subglacial sediment evacuated by streaming flow. Therefore Antarctic ice streams (at present exporting marine sediments from Cenozoic basins in West Antarctica), and possibly unstable ice sheets in general, rely on a pre-existing supply of unconsolidated sediment. Exhausting this supply would cause a fundamental change in ice sheet dynamics. Clark and Pollard's hypothesis suggests that this happened to the LIS; the work of Blankenship, Bindschadler, and others suggests that it may happen to West Antarctica in future. The focus of this project is to investigate this idea by studying the erosion and removal of pre-Pleistocene regolith from beneath the Laurentide ice sheet.

This poses two challenges. First, it is necessary to date the Plio-Pleistocene glacial sediments that surround the former ice sheet. Second, some method is needed to identify pre-glacial regolith in subglacial sediments, differentiate it from the products of bedrock erosion, and determine the rate and timing of its removal. In this project, I address both of these using cosmogenic isotope geochemistry, as follows.

Chapters 2 and 3 address the first of these requirements, the need for new means of dating terrestrial glacial deposits. I use the cosmic-ray-produced radionuclides ^{26}Al and ^{10}Be which are produced in quartz, for this purpose. These two nuclides are produced at a ratio which is fixed by the chemical composition of the target quartz, but have different decay constants: if sedimentary quartz that was exposed at the Earth's surface for a time is then deeply buried and removed from the cosmic-ray flux, the ^{26}Al inventory decreases by decay faster than the ^{10}Be inventory, and the ^{26}Al/^{10}Be ratio diverges from the production ratio. This means that the ^{26}Al/^{10}Be ratio in a particular sedimentary unit is directly related to the age of its overburden. Most glacial sediment sequences consist of tills intercalated with interglacial deposits, river sands in particular, which were demonstrably exposed at the surface between ice sheet advances. Thus it should be possible to determine the age of tills by the ^{26}Al and ^{10}Be concentrations in such sands. However, this requires simplifying assumptions about the ^{26}Al and ^{10}Be concentrations in the sand at the time of burial. I show that these assumptions are not valid for river sediment in glaciated regions. ^{26}Al

and ^{10}Be analyses of such sediment do not provide accurate ages for these tills, although they do yield limiting ages in some cases.

I overcome this difficulty by instead measuring ^{26}Al and ^{10}Be in quartz from paleosols that are buried by tills, then using a more general mathematical approach to determine the initial nuclide concentrations in the paleosol at the time it was buried, as well as the duration of burial. As paleosols intercalated with tills are common, this technique provides a widely applicable improvement on other means of dating Plio-Pleistocene terrestrial glacial sediments. I apply it to pre-Wisconsinan glacial sediment sequences in eastern Nebraska, southwest Minnesota and eastern South Dakota.

Chapters 4 and 5 address the second requirement for learning about the origin and fate of subglacial sediment from Plio-Pleistocene, that is, some means of investigating the sources of subglacial sediment exported from the Canadian Shield by the LIS. I measure atmospherically-produced $^{\mathbf{10}}$Be, which is abundant in deeply weathered soils but absent in fresh bedrock, in a series of Plio-Pleistocene tills in boreholes from Minnesota and adjacent South Dakota. Tills derived from erosion of fresh bedrock have low ^{10}Be concentrations, and can be easily distinguished from ^{10}Be-rich tills derived from regolith that predated glaciation. The lowest one or two tills in each borehole are enriched in ^{10}Be and are directly overlain by ^{10}Be-poor tills, suggesting that the entire preglacial ^{10}Be inventory was rapidly removed from the core area of the LIS by its earliest advances. This is not consistent with the idea that regolith persisted until $\sim$ 1 Ma and could have provided an internal trigger for ice sheet growth at the mid-Pleistocene climate transition. Some boreholes, however, also contained additional ^{10}Be-rich tills higher up in the section, which are younger than 1 Ma and record an additional source of previously undisturbed regolith, either by an increase in the area of the ice sheet or in the extent of thawed bed which was subject to erosion. It appears, therefore, that the initial supply of regolith in the core area of the LIS was exhausted by the first one or two major Pliocene ice sheet advances, and the later renewed export of ^{10}Be-rich till was a consequence, and not a cause, of some change in ice dynamics.

Chapter 2

NUMERICAL AGES FOR PLIO-PLEISTOCENE GLACIAL SEDIMENT SEQUENCES BY $^{26}Al/^{10}Be$ DATING OF QUARTZ IN BURIED PALEOSOLS

This chapter was submitted to the journal *Earth and Planetary Science Letters*. John Stone and Joe Mason were co-authors.

2.1 Introduction

In this paper we describe a means of dating Plio-Pleistocene paleosols using the cosmic-ray-produced radionuclides ^{26}Al and ^{10}Be. This work is motivated by the need to date and correlate terrestrial glacial deposits that predate the last two glaciations. Although there are many thick sequences of tills and associated glacial and interglacial sediments in North America and Eurasia, most of the existing information about the timing of continental glaciations prior to the last one comes from oxygen-isotope records in marine sediment cores that are dated by paleomagnetic stratigraphy and astronomical tuning [Emiliani, 1955, Shackleton and Opdyke, 1973]. Such marine $\delta^{18}O$ time series record only global ice volume: except in rare cases where ice-rafted debris can be associated with a particular source [Shackleton et al., 1984, Mangerud et al., 1996, Hambrey et al., 2002], they give no information about the location of ice sheets on the continents or the distribution of ice between different ice sheets. The continental deposits that would provide this information, although widespread, are extremely difficult to date. In the case of the sedimentary sequences surrounding the former Laurentide Ice Sheet, the only means available for dating sediments older than the useful ranges of radiocarbon (∼50,000 yr) or optical dating techniques (∼150,000 yr) are by bracketing them between two easily recognized magnetic reversals at 0.78 and 2.58 Ma [Cande and Kent, 1995] and three widespread volcanic ashes from the Yellowstone volcanic center at 0.6, 1.3, and 2.0 Ma [Gansecki et al., 1998] – and only a few sections contain any of these time markers at all. At present, it is impossible to associate most individual pre-Wisconsinan tills with particular marine oxygen isotope stages, and there exists little direct evidence to show whether or not the configuration of ice sheets during most older glaciations was or was not similar to that during the

most recent one.

In an effort to better date terrestrial glacial sediments and improve correlation of marine paleoclimate records with terrestrial glacial records, therefore, we are applying cosmogenic-nuclide techniques to determine the age of glacial sediment sequences. In this paper we describe such a method for dating buried paleosols, which are common in Plio-Pleistocene glacial sequences surrounding the Laurentide and other ice sheets. Although we are concerned here with glacial sediments, our approach is very general and could be adapted to date quartz-bearing sediments in many other depositional settings.

2.2 Basic principles of the method

^{26}Al and ^{10}Be are rare radionuclides that are produced at a fixed ratio in quartz grains subjected to cosmic ray bombardment at the Earth's surface, but have different decay constants. They are commonly used in exposure-dating studies [Gosse and Phillips, 2001]. If quartz exposed at the Earths surface for enough time to develop measurable quantities of these nuclides is then deeply buried – and thus isolated from the cosmic-ray flux – the two nuclides decay at different rates, and the ^{26}Al/^{10}Be ratio can be used as a burial clock. This principle is the basis of the "burial dating" method described by Klein et al. [1988] and Granger and Muzikar [2001], which has been used primarily to date fluvial sediments carried into caves and abandoned [Partridge et al., 2003]. In this form, the technique consists of assuming that the sediment sample has experienced a single episode of surface exposure during erosion and transport through the river system, followed by a single episode of burial at a depth sufficient to greatly reduce the cosmic ray flux. With these assumptions, there are two unknown parameters: the erosion rate at the sediment source, and the duration of burial. As there are also two measurements – ^{26}Al and ^{10}Be concentrations in the sediment – these parameters are single-valued functions of the measurements. Granger and Muzikar [2001] provide formulae for determining the burial age in this situation.

Determining the burial age for a sediment sample is more complicated if the sample was gradually buried, buried at a shallow depth, or had a complex history of repeated burial and re-exposure prior to the final burial event. In these cases, additional parameters, consisting of initial nuclide concentrations or burial rates, depths, and times, are necessary to describe the shielding history of the sample. Once the number of unknown parameters grows beyond two, we need a larger number of measurements, on a set of samples whose shielding histories are somehow linked, for the problem to be tractable. A more complex stratigraphic setting also provides more geological information, in the form of stratigraphic relationships, correlation of units to dated deposits else-

where, and paleoenvironmental information, that is pertinent to the age of the sample and which we would like to explicitly incorporate into our age determination. Thus, we require a different mathematical framework that will allow us to both determine more parameters and incorporate more analytical data as well as geologic information. In this paper, we develop an exposure model that predicts the expected nuclide concentrations in a set of samples from a paleosol that is, a) developed on till with unknown initial nuclide concentrations, b) buried by units of unknown age, and c) further buried by units of known age. The parameters of this model include the age of the undated part of the stratigraphic section as well as the time required for soil formation. We then find the parameters which yield nuclide concentrations that best fit our observations while satisfying geological constraints.

2.3 Glacial sediments in borehole 3-B-99, eastern Nebraska

Nebraska Conservation and Survey Division borehole 3-B-99 penetrates four loess units which are separated by paleosols and which overlie another paleosol developed in till (Figure 2.1; Mason [2001]). This till is likely correlative with a till in nearby sections that is normally magnetized and underlies the 0.6 Ma Lava Creek ash [Roy et al., 2004, Boellstorff, 1978a]. Table 2.1 gives details about the paleosol which forms the top of this till. This paleosol is overlain by 8.5 m of clay-rich, pedogenically altered loess of unknown age, then by 7.6 m of Loveland loess (deposited ca. 135,000 - 150,000 yr B.P.), and finally by 10.3 m of Gilman Canyon Formation and Peoria Loess (deposited 35,000 - 12,000 yr B.P) [Mason, 2001, Forman et al., 1992, Forman and Pierson, 2002, Bettis III et al., 2003]. Thus, we are interested in determining the ages of the lowest loess unit and of the till itself.

2.4 Analytical methods

2.4.1 Quartz separation and Al/Be extraction

We measured ^{26}Al and ^{10}Be concentrations in quartz extracted from core samples of pedogenically altered till between 26.0 and 28.1 m depth. We disaggregated core samples by soaking in water and $(NaPO_3)_6$ ("Calgon") in an ultrasonic bath, then isolated the 0.125-0.85 mm grain size by wet-sieving. We extracted and purified quartz by repeated etching in 2% HF, heavy-liquid separation to remove refractory heavy minerals, soaking in hot KOH to remove secondary fluoride precipitated during the HF treatment, and a final 2% HF etch. This procedure yielded quartz with 60-80 ppm total Al. We extracted Al and Be from quartz using standard methods [Ditchburn and Whitehead,

1994, Stone, 2004], prepared Al cathodes by Al/Ag coprecipitation [Stone et al., 2004 in press], and measured isotope ratios at the Lawrence Livermore National Laboratory, Center for Accelerator Mass Spectrometry. Combined process and carrier blanks were $6.3 \pm 6.5 \times 10^4$ atoms ^{26}Al and $2.6 \pm 0.3 \times 10^5$ atoms ^{10}Be. Table 2.2 shows our analytical results.

2.4.2 Density measurements

In order to calculate nuclide production rates, we need to know the shielding depth of samples below the surface in $g \cdot cm^{-2}$. To determine this, we measured the density of our samples by an adaptation of the procedure outlined in Sheldrick [1984] (also see Balco [2004a]). We used the dry density determined by this method (1.92 ± 0.08 $g \cdot cm^{-3}$) to calculate shielding depths during soil formation. We based our calculation of shielding depths during burial by loess units on previous measurements of loess density in eastern Nebraska (J. Mason, unpublished data). We assumed that, at any time, the upper 15 m of loess was not water-saturated and had a bulk density of 1.9 $g \cdot cm^{-3}$; underlying loess was water-saturated, with a bulk density of 2.3 $g \cdot cm^{-3}$.

2.5 Exposure model

The unknown parameters in the model are the initial nuclide concentrations in the till prior to soil formation, the exposure time of the soil surface prior to burial, and the duration of burial. The goal is to construct an objective function M of these four parameters that describes the misfit between the nuclide concentrations computed using the exposure model, and the actual measured nuclide concentrations. We can then use a numerical optimization algorithm to find parameter values that minimise the objective function, *i.e.*, that predict nuclide concentrations which best fit the observed data.

The data to be fit are the measurements of nuclide concentrations ($atoms \cdot g^{-1}$) in samples from different depths (Table 2.2). Denote these $N_{i,j}^M$ for sample i and nuclide j, the superscript M denoting measured concentrations. The subscript i indicates the sample number, where $i = 1 \ldots 6$. The subscript j indicates the nuclide measured, *i.e.*, $j = 10$ for ^{10}Be and $j = 26$ for ^{26}Al. The samples consist of drillcore segments with top and bottom depths $z_{i,1}^{top}$ and $z_{i,1}^{bot}$ ($g \cdot cm^{-2}$) below the soil surface. The soil surface is at 26 m depth in the borehole. Note that z increases with depth so $z_{i,1}^{bot} > z_{i,1}^{top}$.

The samples are emplaced with initial nuclide concentrations $N_{j,0}$. Most geochemical measurements show that massive till is well-mixed at the outcrop scale. Thus, the initial nuclide concentrations are the same for all samples i. These values $N_{10,0}$ and $N_{26,0}$ are unknown. The

samples then experience several periods of exposure or burial. We denote these time periods by the index $k = 1 \ldots K$. Our example soil experiences one period of surface exposure and three periods of steadily deeper burial; hence $K = 4$. At the end of time period k, the nuclide concentration in the sample is $N_{i,j,k}$, such that:

$$N_{i,j,k} = N_{i,j,(k-1)} e^{-\lambda_j t_k} + \frac{P_j(z_{i,k})}{\lambda_j} \left(1 - e^{-\lambda_j t_k}\right) \tag{2.1}$$

where t_k is the duration of time period k (yr), the function $P_j(z)$ is the production rate (atoms $\cdot$ g^{-1} $\cdot$ yr^{-1}) of nuclide j at depth z (g $\cdot$ cm^{-2}), and $z_{i,k}$ is the depth (g $\cdot$ cm^{-2}) of sample i during time period k. For the decay constants λ_j, we use $\lambda_{10} = 4.62 \times 10^{-7}$ and $\lambda_{26} = 9.83 \times 10^{-7}$. There is some evidence that this value for λ_{10}, which is the most commonly used value to date, may be incorrect (Caffee, M., Southon, J., unpublished data); pending resolution of this ambiguity we continue to use it.

Beginning with the initial nuclide concentrations $N_{j,0}$, we apply Equation 2.1 repeatedly to arrive at the values $N_{i,j,K}$, which are the predicted nuclide concentrations at the present time which we will compare to the measured values $N_{i,j}^M$. We then use the χ^2 statistic to describe the misfit M between measured and simulated nuclide concentrations:

$$M = \sum_i \sum_j \left(\frac{N_{i,j,K} - N_{i,j}^M}{\sigma N_{i,j}^M} \right)^2 \tag{2.2}$$

where the values $\sigma N_{i,j}^M$ are the standard errors of the ^{10}Be and ^{26}Al measurements.

2.5.1 Parameters of the exposure model

We have already discussed the initial nuclide concentrations $N_{j,0}$, which are unknown parameters of the model. The other parameters we need in order to evaluate M are the exposure and burial times t_k and the nuclide production rates $P_j(z_{i,k})$.

The first time period of interest is the period of surface exposure and soil formation after the emplacement of the till. The length of this time period t_1 is an unknown parameter. The production rate for sample i and nuclide j during soil formation is:

$$P_j(z_{i,1}) = \frac{1}{\left(z_i^{bot} - z_i^{top}\right)} \int_{z_{i,1}^{top}}^{z_{i,1}^{bot}} P_j(z) dz \tag{2.3}$$

The values $z_{i,1}^{top}$ and $z_{i,1}^{bot}$ are the top and bottom depths (g $\cdot$ cm^{-2}) of each sample below the soil surface (Table 2.2). During soil formation, when all samples are near the surface, spallogenic

nuclide production predominates and production by muon interactions is unimportant. Thus, during soil production the nuclide production rates as a function of depth are $P_j(z) = P_j^{surf} e^{-z/\Lambda}$, where P_j^{surf} is the surface production rate (atoms $\cdot$ g^{-1} $\cdot$ yr^{-1}) for nuclide j. We choose $P_{j,surf}$ to be 6.9 atoms $\cdot$ g^{-1} $\cdot$ yr^{-1} for ^{10}Be and 42.1 atoms $\cdot$ g^{-1} $\cdot$ yr^{-1} for ^{26}Al based on the latitude and present altitude of the borehole [Stone, 2000], and use a value of 160 g $\cdot$ cm^{-2} for Λ, the characteristic length for spallogenic production.

Our choice of $P_j(z)$ here incorporates two important assumptions. First, in using the surface value for P_j^{surf}, we assume that the true soil surface is preserved in the section. In this example, the presence of an Ab horizon indicates that the entire soil profile is preserved. If we were applying this technique in a situation where the soil profile had been truncated during deposition of the overlying material, we would either have to infer the amount of truncation from the soil characteristics, or treat P_j^{surf} as an additional unknown parameter. Second, we assume that the coarse-grained fraction of the soil which we have sampled was not mixed vertically. Illuvial clay coatings in the Bt horizons of the paleosol, as well as the presence of atmospherically produced ^{10}Be 1 m below the soil surface [Balco, 2004b], do indicate some vertical transport of fine particles. However, the measured ^{10}Be and ^{26}Al concentrations in the soil are indistinguishable from an exponential profile with attenuation length Λ (Figure 2.2). If mixing of coarse sand between samples had been significant, this could not be the case. Although bioturbation and rooting must have taken place during soil formation, it was apparently confined to the uppermost 30 cm, the thickness of our shallowest sample.

We have also made an additional assumption in our choice of Equation 2.1 to describe nuclide production during soil formation, that is, we have disregarded erosion of the soil surface. It is likely that the soil surface was eroding during soil formation, which would affect nuclide concentrations. Alternatively, we could add the soil erosion rate as an additional free parameter, but we would not be able to accurately discriminate exposure time and erosion rate [Gillespie and Bierman, 1995]. Either approach yields a nuclide concentration profile with the same exponential form prior to burial, and thus the burial time t_2 that we eventually compute is not affected. However, the parameter t_1 that we determine will reflect both the exposure time and the erosion rate of the soil surface. Without independent evidence as to whether the soil surface was stable or eroding, we must regard our estimate of t_1 as the minumum time between emplacement of the parent material and the burial of the soil profile by the overlying loess. Thus, in this particular setting we can only determine the age of the overlying loess explicitly; the age we infer for the emplacement of the till and onset of soil formation depends on assumptions about the soil erosion rate.

During the subsequent time periods ($k = 2 \ldots 4$) the soil surface is buried by an episodically increasing overburden of loess. The duration of the first burial period t_2 is an unknown parameter. The duration of the second and third burial periods, defined by the onset of deposition of the upper loess units with known age, are $t_3 = 115,000$ yr and $t_4 = 35,000$ yr. To determine the burial depths of the samples during these periods, we replace the top and bottom depths of the samples below the soil surface with their average depths $z_{i,1}^{avg}$. This is reasonable because at large depths below the surface nuclide production rates change slowly with depth and are close to linear over small depth ranges. Then, $z_{i,k}^{avg} = z_{i,1}^{avg} + Z_k$ where Z_k is the overburden thickness above the soil surface during period k. Here Z_2 is 1600 g $\cdot$ cm^{-2}, Z_3 is 3100 g $\cdot$ cm^{-2}, and Z_4 is 5100 g $\cdot$ cm^{-2}, the present overburden thickness.

In this part of the model we cannot approximate $P(z)$ by an exponential function but must include nuclide production by negative muon capture and fast muon interactions [Stone et al., 1998, Heisinger et al., 2002a,b]. The depth dependence of muogenic nuclide production is the subject of active research at present. Here, for simplicity, we use the compilation of sea level/high latitude measurements of the muon flux at various depths from Heisinger et al. [Heisinger et al., 2002a]. At the location of our site (41.5°N, 400 m elevation), we expect this to be a good approximation for the actual muon flux at depths greater than ~2000 g $\cdot$ cm^{-2}. We then use nuclear cross-sections for muon interactions inferred from calibration measurements in samples at Wyangla, Australia (Stone, unpublished data). In this particular problem, it happens that the parameter t_2 that we are interested in is relatively insensitive to the choice of muon interaction cross-sections: best-fit burial ages calculated with our cross-sections and those of Heisinger et al. [2002a] differ only by 0.2% . This occurs because nuclide concentrations in the samples are relatively large, and the time of burial is relatively short: thus, nuclide production during the burial period is small relative to nuclide loss through decay. In other situations, in particular for shorter periods of soil formation, the details of muogenic production would be more important.

Our choice for Equation 2.1 also implies that burial by the full thickness of each loess unit was instantaneous at the beginning of the burial period. As there is evidence for soil formation during deposition of the lowest loess, this is not likely to be strictly true. The uncertainty produced by this approximation, however, is small relative to other sources of uncertainty, in particular the analytical precision of our ^{26}Al measurements.

To summarize, the model has four unknown parameters: the initial nuclide concentrations in the soil parent material $N_{j,0}$; the nominal time of soil exposure t_1, and the duration of the first period of burial by loess t_2. The actual age (yr B.P) of the lowermost loess, which is the unknown

quantity we are most interested in, is $t_2 + t_3 + t_4$.

2.5.2 Constraints

There are several constraints on the allowed values of the parameters $N_{j,0}$, t_0, and t_1. First, all parameters must be nonnegative. Second, the $N_{j,0}$ must not be in the so-called forbidden zone [Lal, 1991]. This means not only that $N_{j,0} < P_j^{surf}/\lambda_j$, where P_j^{surf}/λ_j is the surface steady-state concentration, but also that initial nuclide concentrations must lie within or below the simple exposure region on Figure 2.3, *i.e.*,

$$N_{26,0} < \frac{P_{26}^{surf}}{\lambda_{26}} \left[1 - \left(1 - \frac{N_{10,0}\lambda_{10}}{P_{10}^{surf}} \right)^{\frac{\lambda_{26}}{\lambda_{10}}} \right] \tag{2.4}$$

This latter constraint is nonlinear and potentially undefined for some parameter values, which presents difficulties for the optimization algorithm. Furthermore, if the samples had been exposed in the past at a significantly different elevation, it would not be appropriate to use the value of P_j^{surf} for the present sample location in this constraint. For this particular example, we expect the $N_{j,0}$ to be small, so we avoid this difficulty by requiring instead that $N_{26,0}/N_{10,0} < 6.1$.

2.6 Optimisation procedure; results

We used the constrained nonlinear multidimensional minimization algorithm in the MATLAB Optimization Toolbox [Mathworks, Inc., 2000] to find the optimal values for the parameters. The objective function M is not convex, but has only one minimum. The only numerical difficulty arises from the asymptotic behaviour of Equation 2.1: the partial derivatives of M with respect to the time parameters t_k are very small when the t_k are large. This is easily addressed by using an appropriate initial guess and limiting the maximum permitted step size. Figure 2.3 shows the exposure history that best fits the measured data. This yields best-fit parameters as follows: $N_{10,0} = 0.99 \times 10^5$ atoms $\cdot$ g^{-1}; $N_{26,0} = 4.3 \times 10^5$ atoms $\cdot$ g^{-1}; $t_1 = 51,000$ yr; and $t_2 = 430,000$ yr.

2.7 Error analysis

The dominant uncertainties in this procedure are the $\sigma N_{i,j}^M$. Other sources of error include a) uncertainties in surface production rates, muon interaction cross-sections, and density measurements; b) our assumption of instantaneous rather than gradual deposition; and c) another assumption,

that no significant thicknesses of overburden were deposited and then eroded without leaving any evidence. We found that these sources of error are either much less important than the $\sigma N_{i,j}^M$ (production rate uncertainties, instantaneous rather than gradual deposition) or difficult to quantify (no significant missing overburden). Furthermore, in this work we focus on the basic principles of this dating method and not on detailed correlation of our dates with other paleoclimate records. Thus, we included only the dominant error in our error analysis. We propagated this error into our estimate of t_2, the parameter of most interest, using a Monte Carlo simulation in which we repeatedly carried out the optimization procedure using measured nuclide concentrations generated from normal random distributions with mean $N_{i,j}^M$ and standard deviation $\sigma N_{i,j}^M$. Figure 2.4 shows the results of the error analysis for t_1, which indicates that the lowermost loess unit was deposited $580,000 \pm 110,000$ yr B.P. The nominal soil exposure time t_1 is $51,000 \pm 4300$ yr. The initial nuclide concentrations $N_{10,0}$ and $N_{26,0}$ are $0.99 \pm 0.04 \times 10^5$ atoms $\cdot$ g^{-1} and $4.3 \pm 0.43 \times 10^5$ atoms $\cdot$ g^{-1} respectively. The error analysis also showed that the analytical uncertainty for ^{26}Al measurements is more important than that for the ^{10}Be measurements in limiting the total precision of our age determination.

2.8 Conclusions

The most likely age of deposition of the lowermost loess unit is 580,000 yr. If, by analogy to modern low-gradient soils in the region, we believe that the erosion rate of the soil surface was small, then we can interpret t_1 as the duration of soil formation. For example, for erosion rates of 5 and 10 μm $\cdot$ yr^{-1}, the duration of soil formation would have been 60,000 and 80,000 yr respectively. A soil formation time of 50,000–70,000 yr. is also consistent with the degree of soil development and with another soil age estimate of 66,000 yr derived from accumulation of atmospherically-produced ^{10}Be [Balco, 2004b]. Considering the results of the error analysis, it is most likely that the lowermost loess was deposited 550,000–600,000 yr B.P., during marine isotope stages 14 and 15, and that the till was deposited during marine isotope stage 16 at approximately 620,000-640,000 yr B.P. This is consistent with the stratigraphy of nearby outcrops in eastern Nebraska and adjacent Iowa, in which the 0.6 Ma Lava Creek ash occurs a short distance above the uppermost till.

The estimated initial ^{10}Be and ^{26}Al concentrations in the till, near 1×10^5 and 4.3×10^5 atoms $\cdot$ g^{-1} respectively, are similar to concentrations we have observed in other Pleistocene tills, as well as modern river sediments derived therefrom, in the north-central U.S. [Balco, 2004b]. The initial ^{26}Al/^{10}Be ratio of 4.3 is significantly less than the production ratio of 6.1, which indicates a complex exposure and burial history of more than 600,000 yr prior to incorporation in the till. This

observation underscores the need for the very general approach we have used here: the conventional assumptions used in burial dating would yield wildly misleading ages in this situation.

As we discuss above, the analytical uncertainties cause our final error estimate to be large: we cannot uniquely associate the age of the loess with a specific marine δ^{18}O event. However, our approach provides a widely applicable means of assigning numerical ages to many Plio-Pleistocene terrestrial sediment sequences that cannot be dated by other means. It can be used wherever quartz-bearing paleosols are embedded within sedimentary sequences, and promises a significant improvement on our present ability to date and correlate Plio-Pleistocene terrestrial sediments. Because the accuracy of the technique depends on precise ^{10}Be and ^{26}Al measurements, it also provides a strong incentive toward improving analytical techniques for cosmic-ray-produced nuclides, as well as incorporating other nuclides such as ^{36}Cl that would provide a more favorable set of decay constants.

Table 2.1: Soil description for paleosol in core 3-B-99.

Borehole depth(m)	Description
26.00-26.21	Ab. 10YR 4/3 clay, strong fine subangular blocky structure.
26.21-26.58	Bt1b. 10YR 5/3 clay (5% gravel), strong fine subangular blocky structure, clay coatings on ped faces.
26.58-27.11	Bt2b. 7.5YR 4/4 clay (5% gravel), moderate fine subangular blocky parting to moderate very fine subangular blocky structure.
27.11 - 27.40	BCb. 10YR 5/6 clay (5% gravel), moderate fine subangular blocky structure, clay coatings on ped faces.
27.40-28.65+	C. 2.5Y 5/6 clay (10% gravel), moderate medium subangular blocky structure, effervescent in 10% HCl.

Table 2.2: ^{10}Be and ^{26}Al concentrations in paleosol in borehole 3-B-99

Sample ID	Borehole depth(m)	Depth below soil surface ($g \cdot cm^{-2}$)	^{10}Be[a] (10^4 atoms $\cdot g^{-1}$)	^{26}Al[a] (10^4 atoms $\cdot g^{-1}$)
3-B-99-87	26.01-26.31	0-58	31.88 ±1.08	133.8 ± 4.3
3-B-99-88	26.31-26.62	58-117	26.83 ± 0.93	112.7 ± 3.3
3-B-99-89	26.62-26.92	117-175	19.75 ± 0.58	85.6 ± 3.8
3-B-99-90	27.07-27.23	204-234	16.14 ± 0.49	67.6 ± 3.5
3-B-99-91	27.32-27.46	234-278	15.75 ± 0.47	57.9 ± 2.1
3-B-99-93[b]	27.76-28.14	336-410	11.92 ±0.28	48.7 ± 1.9

[a]Measured relative to LLNL internal standards. Uncertainties are shown at $\pm 1\sigma$ and include all known sources of analytical error.

[b]Mean of two analyses

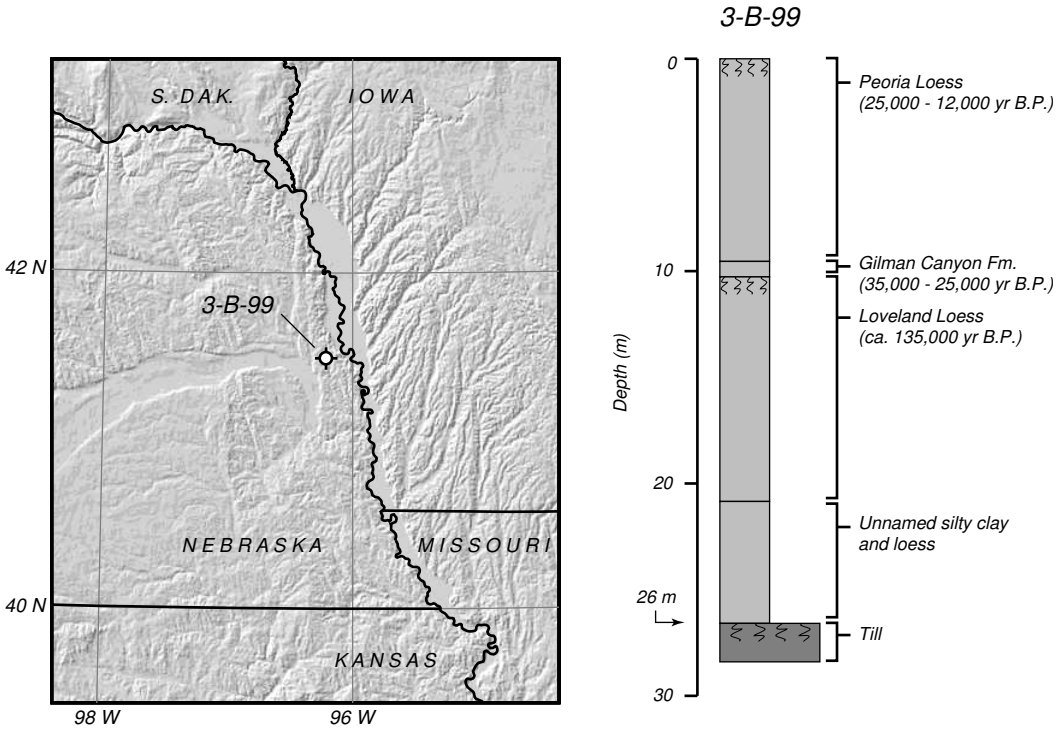

Figure 2.1: Location map and core log for Nebraska Conservation and Survey Division borehole 3-B-99 [Mason, 2001].

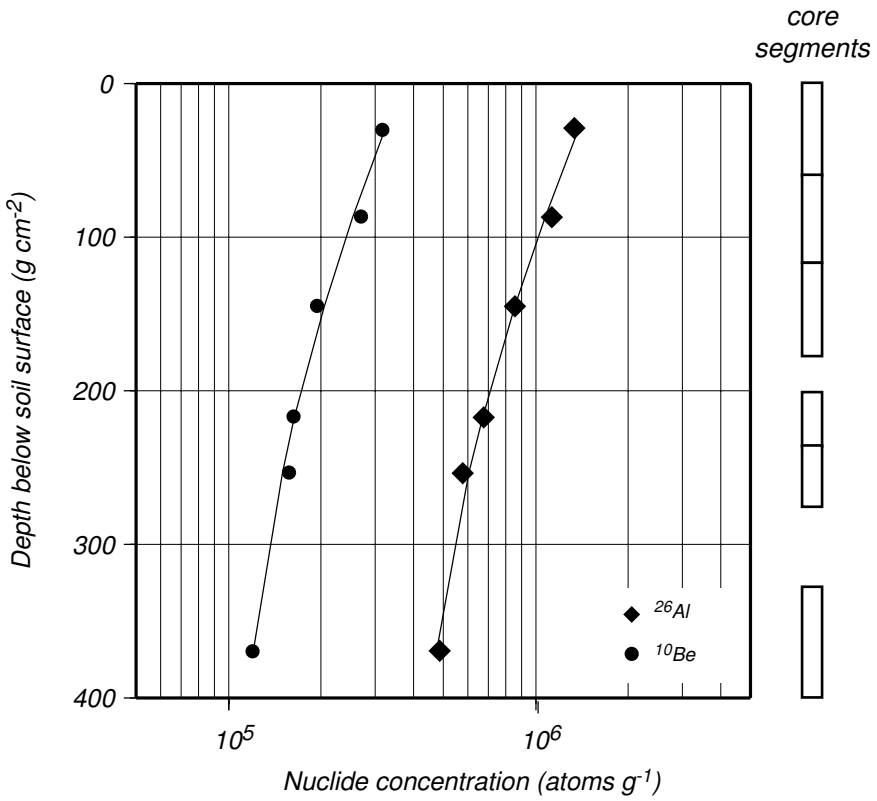

Figure 2.2: ^{26}Al and ^{10}Be concentrations measured in soil profile in borehole 3-B-99. The data points show measured concentrations. Error bars would be similar in size to the symbols at this scale (Table 2.2). Each sample consisted of quartz extracted from a ~ 30 cm segment of core, the boundaries of which are shown at right. The lines show the nuclide concentrations predicted by our best-fit exposure model.

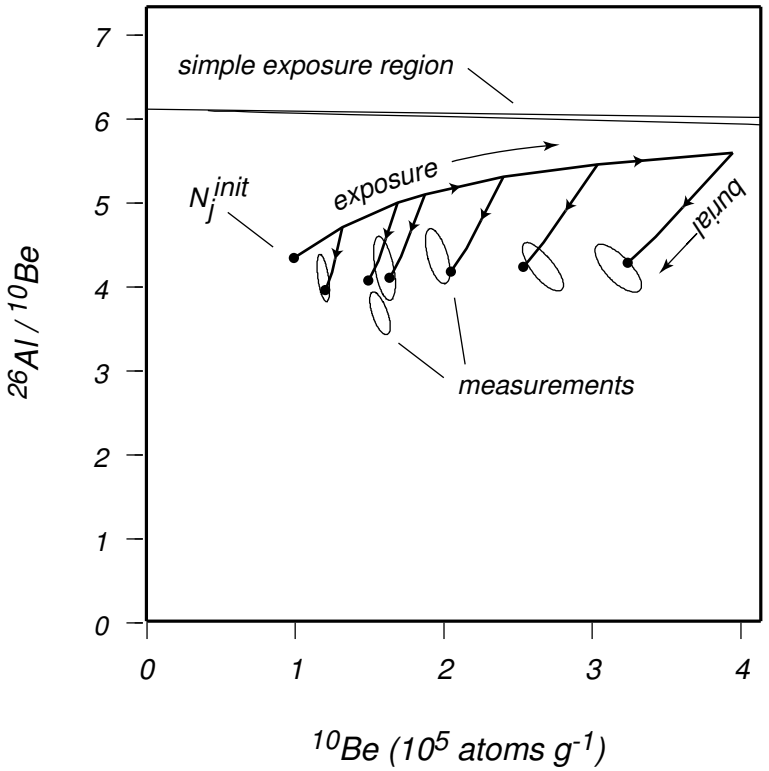

Figure 2.3: Two-nuclide parametric diagram showing the exposure history that best fits our measurements. Ellipses show 68% confidence regions for measured nuclide concentrations.

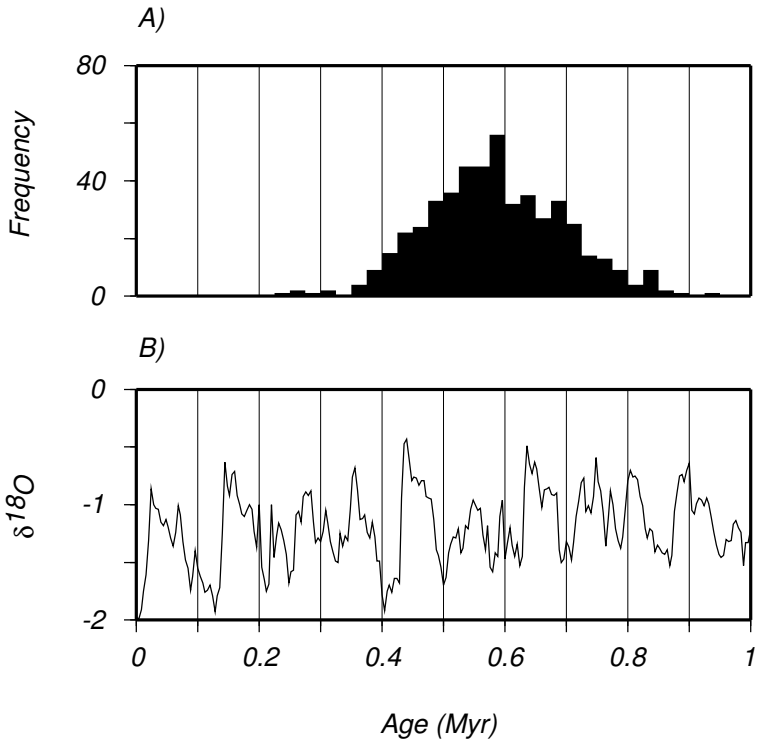

Figure 2.4: Histogram of best-fit burial ages for lowermost loess unit generated by 1000-point Monte Carlo simulation, compared with the benthic oxygen-isotope record from ODP core 806 [Berger et al., 1993].

Chapter 3

DATING PLIO-PLEISTOCENE GLACIAL SEDIMENTS USING THE COSMIC-RAY-PRODUCED RADIONUCLIDES ^{10}BE AND ^{26}AL

This chapter was submitted to *American Journal of Science*. John Stone and Carrie Jennings were co-authors. Section 3.8 was included as an appendix to this manuscript.

3.1 Introduction; purpose of this study

In this paper we describe our efforts to better determine the timing of Plio-Pleistocene ice sheet advances by using the cosmic-ray-produced nuclides ^{10}Be and ^{26}Al to date glacial sediments.

The chief motivation for this work is the need for new methods to determine the age of the thick sequences of tills and associated ice-marginal sediments that surround the locations of former continental ice sheets in North America and Eurasia. These deposits are important because they record the advances and retreats of the large ice sheets that are the defining feature of global climate changes during the last several million years. Despite this direct stratigraphic evidence of many glaciations, however, most information about the timing of ice sheet advances prior to the most recent Wisconsinan glaciation comes from oxygen-isotope records in marine sediment cores that are dated by paleomagnetic stratigraphy and astronomical tuning [Emiliani, 1955, Shackleton and Opdyke, 1973]. These δ^{18}O time-series record only global ice volume. Except in rare cases where ice-rafted debris in sediment cores can be associated with a specific source [e.g., Shackleton et al., 1984, Mangerud et al., 1996, Hambrey et al., 2002], marine records give little information about the location of ice on the continents or the partitioning of ice between different ice sheets. The continental deposits that would provide this information are extremely difficult to date. In the region formerly occupied by the Laurentide Ice Sheet, for example, the only means available for dating sediments older than the useful ranges of radiocarbon (∼50,000 yr) or optical dating techniques (∼150,000 yr) are by bracketing them between two easily recognized magnetic reversals (0.78, 2.58 Ma; Cande and Kent [1995]) or three widespread ashes from the Yellowstone volcanic center(0.6, 1.3, and 2.0 Ma; Gansecki et al. [1998]). As only a few sections contain any of these time markers at all, it is impossible to associate most individual pre-Wisconsinan tills with particular

marine oxygen isotope stages, and there exists little direct evidence to show whether or not the configuration of ice sheets during most older glaciations was or was not similar to that during the most recent one.

Besides this particular question of the age of Plio-Pleistocene glacial sediments, we are interested in expanding the range of applications of cosmogenic-nuclide geochronology. To date, measurements of cosmic-ray-produced radionuclides have been used almost exclusively for exposure-age dating of surface rocks [Gosse and Phillips, 2001]. Only a few authors have attempted to use more complicated methods that rely on the decay of these nuclides as well as their initial accumulation [e.g., Granger and Muzikar, 2001]. Here we describe methods for using the two radionuclides ^{10}Be and ^{26}Al to date stratified deposits in much more complex geologic settings. These nuclides have decay constants that are particularly suited to dating sediments 0.5-3 Myr old, and occur in quartz, which is ubiquitous in sedimentary systems. Although we discuss only glacial sediments in this paper, the methods we describe apply to Plio-Pleistocene clastic sediments in general, and could be used in many sedimentary environments.

3.2 The basics of ^{26}Al/^{10}Be dating methods

^{26}Al and ^{10}Be are rare radionuclides that accumulate in quartz subjected to cosmic ray bombardment near the Earth‘s surface. These nuclides are commonly used for exposure-age dating, which relies on the fact that they are produced at a known rate in rock surfaces exposed to the surface cosmic ray flux [e.g., Gosse and Phillips, 2001]. Here we are not concerned with exposure dating of surfaces, but with another technique, sometimes known as “burial dating,” which relies on the fact that ^{26}Al and ^{10}Be are produced at a fixed ratio, but have different decay constants. If sedimentary quartz exposed at the Earth‘s surface for enough time to develop measurable quantities of these nuclides is then buried below the surface – and thus isolated from the cosmic-ray flux – the two nuclides decay at different rates and the ^{26}Al/^{10}Be ratio is related to the duration of burial [e.g., Klein et al., 1988]. In this section, we first describe the basis for previous uses of burial dating to determine the age of fluvial sediment deposited in caves, and then describe the additional complications that arise, and the different approach that is required, to use the technique in more complicated situations.

3.2.1 Depth dependence of ^{26}Al and ^{10}Be production

At the Earth’s surface, ^{26}Al and ^{10}Be production in quartz is mostly by spallation reactions on O and Si, and to a much lesser extent by negative muon capture and fast muon interactions [Lal and

Peters, 1967]. The total surface production rates of these nuclides in quartz at sea level and high latitude are approximately 5.1 and 31.1 atoms $\cdot$ g^{-1} $\cdot$ yr^{-1}for ^{10}Be and ^{26}Al respectively [Stone, 2000]. These production rates vary predictably with latitude, altitude, and magnetic field variation [Lal, 1991, Stone, 2000, Gosse and Phillips, 2001], but the ratio of ^{26}Al and ^{10}Be production rates is fixed at 6.1 [Nishiizumi et al., 1989]. Some details of surface production are still the subject of active research. These remaining uncertainties in surface production rate estimates are not significant in the context of this paper and we do not dwell on them.

Nuclide production rates decrease with depth below the ground surface (Figure 3.1). In order to simplify the text and mathematics in this paper, we describe depth in units of g $\cdot$ cm^{-2} to reflect the attenuation of the cosmic-ray flux according to the amount of mass traversed. This measure of depth is sometimes referred to as "mass depth" or "shielding depth." If d is linear depth below the surface (cm) and ρ is the density of the overburden (g $\cdot$ cm^{-3}), $z = d\rho$.

The depth dependence of the production rate of nuclide j due to spallation is:

$$P_{sp,j}(z) = P_{sp,j}(0)e^{\left(-\frac{z}{\Lambda_{sp}}\right)} \tag{3.1}$$

where z is depth below the surface (g $\cdot$ cm^{-2}), $P_{sp,j}(z)$ the production rate due to spallation at depth z (atoms $\cdot$ g^{-1} $\cdot$ yr^{-1}), $P_{sp,j}(0)$ the surface production rate due to spallation (atoms $\cdot$ g^{-1} $\cdot$ yr^{-1}), and Λ_{sp} the effective attenuation length (g $\cdot$ cm^{-2}) for spallation. Here we use $\Lambda_{sp} = 160$ g $\cdot$ cm^{-2}. For depths less than approximately 500 g $\cdot$ cm^{-2}, production by spallation dominates and Equation 3.1 is a good approximation for the total production rate $P_j(z)$.

Production due to muon reactions is attenuated much less rapidly than spallogenic production, and predominates at greater depths (Figure 3.1). The depth dependence of muogenic production is also the subject of active research at present. In this work we wish to estimate how important the uncertainty in this function is to our results, without quantifying it in a way that may later prove to be wrong. The few measurements of the relevant quantities, in particular nuclear cross-sections for muon interactions, are subject to systematic as well as random errors, and offer no basis for selecting a Gaussian or any other probability distribution to describe the uncertainty. Thus, we proceed as follows. We use the compilation of sea level/high latitude measurements of the subsurface muon flux from Heisinger et al. [2002a]. As our sites are near 45°N latitude and at 400-600 m elevation, we expect this to be a good approximation for the actual muon flux at depths greater than 2000 g $\cdot$ cm^{-2}. We then perform most calculations using two sets of cross-sections for production of ^{10}Be and ^{26}Al by negative muon capture and fast muon interactions: first, those measured experimentally by Heisinger et al. [2002a,b], and second, those inferred from a quarry

profile at Wyangla, Australia (Stone, J., unpublished data). These latter values are as follows: The energy dependence exponent for fast muon interactions α is 0.8 [see Heisinger et al., 2002a, Equation 13]; and the effective nuclide production probabilities after muon capture f^* are 0.1212 % and 0.62 % for ^{10}Be from O in SiO_2 and ^{26}Al from Si in SiO_2, respectively [see Heisinger et al., 2002b, Equation 11]. The range in production rates generated by these two sets of parameters is representative of the uncertainty in our present knowledge of muogenic production. The resulting subsurface production rates differ by a factor of two or more at depths of 500-2000 $g \cdot cm^{-2}$, but are similar near the surface and at depths greater than 10,000 $g \cdot cm^{-2}$(Figure 3.1). Thus, the uncertainty in these parameters is most important when samples are buried at shallow depths for long periods of time, and is not important when samples are deeply buried. Where important, we discuss the variation in results caused by these two parameter sets at the appropriate points in the text.

3.2.2 ^{26}Al/^{10}Be *dating of buried sediments in simple situations*

Here we describe the approach used in previous studies that used ^{26}Al and ^{10}Be measurements to date buried sediments [Klein et al., 1988, Granger and Muzikar, 2001]. We are interested in samples of quartz that were exposed at the surface for a time and then buried at a known depth below the surface. First, we consider the period of exposure. If a sample begins with zero initial ^{26}Al and ^{10}Be concentrations, then is continuously exposed at the surface for an exposure time t_{exp} (yr), while eroding at a constant rate ϵ ($g \cdot cm^{-2} \cdot yr^{-1}$), the concentration $N_j(t_{exp})$ ($atoms \cdot g^{-1}$) of nuclide j is:

$$N_j(t_{exp}) = \frac{P_j(0)}{\lambda_j + \frac{\epsilon}{\Lambda_{sp}}} \left(1 - e^{-\left(\lambda_j + \frac{\epsilon}{\Lambda_{sp}}\right) t_{exp}}\right) \tag{3.2}$$

where $P_j(0)$ is the surface production rate of nuclide j. The decay constants λ_{10} and λ_{26} are 4.62×10^{-7} and 9.83×10^{-7} yr^{-1}, respectively, which correspond to half-lives of 1.5 Myr for ^{10}Be and 0.7 Myr for ^{26}Al. There is some evidence that this value for λ_{10}, which is the most commonly used value to date, may be incorrect (Caffee, M., Southon, J., unpub. data); pending resolution of this ambiguity we continue to use it here. We disregard nuclide production by muons in Equation 3.2 because, except in the case of very high erosion rates (which do not occur in the context of this work), it is unimportant relative to nuclide production by spallation near the surface.

The range of possible ^{10}Be and ^{26}Al concentrations that can be generated by Equation 3.2 for all positive values of t_{exp} and ϵ define the so-called "simple exposure island." Lal [1991] describes this in detail. Figure 3.2A shows it graphically. Samples with nuclide concentrations that do not

lie within the simple exposure island cannot be explained by surface exposure alone, but must have a complex exposure history involving exposure at the surface as well as burial. [Strictly, as the location of the simple exposure island is specific to the surface production rate at a particular site, samples that are exposed at the surface in one location, and then moved to another location where the production rate is lower, can lie outside the island corresponding to the first site without having been buried. However, this possibility does not become important in this paper.]

We now describe burial of a previously exposed sample. If a sample with some initial nuclide concentrations that developed during a previous period of exposure is buried, the subsequent nuclide concentrations are related to the burial duration as follows: For a quartz sample with concentration of nuclide j at the time of burial $N_{j,0}$ (atoms $\cdot$ g^{-1}), the nuclide concentration $N_j(t_b)$, after burial duration t_b (yr), at a depth below the surface z (g $\cdot$ cm^{-2}) is:

$$N_j(t_b) = N_{j,0}e^{-\lambda_j t_b} + \frac{P_j(z)}{\lambda_j}\left(1 - e^{-\lambda_j t_b}\right) \tag{3.3}$$

where $P_j(z)$ is the production rate (atoms $\cdot$ g^{-1} $\cdot$ yr^{-1}) of nuclide j at depth z. Here we have disregarded the effect of surface erosion because the change in nuclide production rates with depth is very small at large depths.

If we measure both ^{26}Al and ^{10}Be in a single buried sample, we can write Equation 3.3 for each nuclide. This yields three unknowns: the burial time t_b and the initial nuclide concentrations $N_{10,0}$ and $N_{26,0}$. With only two measurements (the concentrations of ^{26}Al and ^{10}Be), we must make additional assumptions to determine t_b uniquely. The assumptions that are commonly used to accomplish this are based on the idea that samples have only experienced a single period of surface exposure and/or steady erosion before burial, in which case Equation 3.2 provides the needed relationships between ^{26}Al and ^{10}Be concentrations at the time of burial. Three examples of such assumptions follow.

First, for short exposure times ($<\sim 50,000$ yr) or high erosion rates ($>\sim 0.003$ g $\cdot$ cm^{-2} $\cdot$ yr^{-1}), we can disregard radioactive decay, in which case the ^{10}Be and ^{26}Al concentrations in a surface sample are related by

$$\frac{N_{26}}{N_{10}} = R_0 \tag{3.4}$$

where R_0 is the production ratio. $R_0 = 6.1$ [Nishiizumi et al., 1989]. This relation between the initial concentrations of ^{26}Al and ^{10}Be would allow us to calculate both the initial nuclide concentrations and the burial time t_b from ^{10}Be and ^{26}Al measurements on a buried sample.

Second, we can follow Granger et al. [1997, 2001] and Partridge et al. [2003], who dated samples of fluvial sediment deposited in caves. They assumed that their samples were derived from surfaces that had been continuously exposed for long enough that surface nuclide concentrations had reached a steady-state balance between production and loss by erosion and radioactive decay. In this case, the initial nuclide concentrations at the time of burial are related by:

$$\left[\frac{P_{26}(0)\Lambda}{N_{26}} - \lambda_{26}\Lambda\right] = \epsilon = \left[\frac{P_{10}(0)\Lambda}{N_{10}} - \lambda_{10}\Lambda\right] \tag{3.5}$$

where $P_j(0)$ is the surface production rate, and ϵ is the erosion rate, at the location where the sample originated. In effect this parameterizes the initial nuclide concentrations $N_{10,0}$ and $N_{26,0}$ in terms of the erosion rate ϵ. Thus, both ϵ and t_b are single-valued functions of the ^{26}Al and ^{10}Be measurements in a buried sample. Granger and Muzikar [2001] give formulae for this calculation. Note that in this case, as the next, we must specify the surface production rates during the time of exposure. For sediments whose source is not well known, this assumption contributes some uncertainty to ϵ, but in most cases does not significantly affect the value of t_b that we eventually determine.

Third, we can assume that the samples originated from a surface that was continuously exposed, without any erosion, for a time t_{exp}. In this case, the relationship between the initial nuclide concentrations is:

$$\left[\frac{-1}{\lambda_{26}}\ln\left(1 - \frac{N_{26}\lambda_{26}}{P_{26}(0)}\right)\right] = t_{exp} = \left[\frac{-1}{\lambda_{10}}\ln\left(1 - \frac{N_{10}\lambda_{10}}{P_{10}(0)}\right)\right] \tag{3.6}$$

that is, we parameterize $N_{10,0}$ and $N_{26,0}$ in terms of the exposure time t_{exp}, and we can then calculate t_{exp} and the burial time t_b from the two measurements.

Many authors have described this procedure graphically instead of mathematically [e.g., Lal, 1991, Bierman et al., 1999]. In graphical form, Equation 3.4 above is equivalent to assuming that nuclide concentrations at the time of burial are restricted to the extreme "left side" of the simple exposure island in Figure 3.2A. Equations 3.5 and 3.6 above are equivalent to assuming that nuclide concentrations at the time of burial are restricted to the "lower" and "upper" boundaries of the simple exposure island, respectively. Having made one of these assumptions, one can then use Equation 3.3 to draw isolines of the erosion rate and burial time, or the exposure time and burial time, corresponding to any measured nuclide concentrations. In Figures 3.2B-3.2E we provide isolines of exposure time and burial time drawn with the assumption that Equation 3.6 holds at the time of burial. The form of this diagram varies depending on the depth of burial and thus the

production rate during the period of burial; thus the burial depth determines the age resolution that can be attained given a certain analytical precision.

One more possible scenario, which we discuss later in this paper, concerns a sample which has been exposed for a time, buried at a lower production rate for a time, and then re-exposed at the surface, that is, a sample which is brought to the surface with nuclide concentrations well outside the simple exposure island. Equation 3.3 applies in this case as well, and the nuclide concentrations in the sample will asymptotically approach the simple exposure island along the re-exposure trajectories shown in Figure 3.2F.

The important points of this section are as follows:

1. If the measured ^{26}Al and ^{10}Be concentrations in a sample fall "below" the simple exposure island defined by the surface production rates $P_j(0)$ at the location they were originally exposed, that is,

$$\left[\frac{P_{26}(0)}{N_{26}} - \lambda_{26}\right] > \left[\frac{P_{10}(0)}{N_{10}} - \lambda_{10}\right] \tag{3.7}$$

   then the history of the sample must include burial as well as surface exposure. In the rest of this paper, we use the phrase "inconsistent with surface exposure" to describe this situation.

2. If we make at least one of the assumptions in Equations 3.4-3.6 about the relationship of ^{26}Al and ^{10}Be concentrations at the time of burial, we can calculate the duration of burial (as well as one additional parameter) from measured ^{26}Al and ^{10}Be concentrations.

3.2.3 ^{26}Al/^{10}Be *dating of buried sediments in complicated situations*

In effect the procedure that we describe above treats Equation 3.3 as a predictive model that tells us the nuclide concentrations we expect in the sample as a function of the unknown parameters $N_{26,0}$, $N_{10,0}$, and t_b. We then seek the values of these parameters that best predict the nuclide concentrations we actually measure. For a single sample, the number of parameters (3) exceeds the number of measurements (2), so we use the assumptions in Equations 3.4,3.5, and 3.6 to reduce the number of unknowns to equal the number of measurements. The unknown parameters are then single-valued functions of the measurements, and can be found by relatively simple analytical formulae.

The difficulty with this approach, in which we make assumptions to reduce the number of unknown parameters, is that these assumptions are only valid in very restricted geological situations.

Fluvial sediments that originate from a slowly eroding landscape and are deposited in caves are one of these. In general, however, we expect that sediments in many environments will have already had a complicated exposure history, including many periods of exposure, burial, erosion, transportation, and redeposition, before the final burial of interest, and that these assumptions will not be valid. In the first part of this paper (Section 3.5), we show that this is true of fluvial sediments intercalated with tills in glacial sedimentary sequences: therefore we cannot use assumptions based on Equation 3.2 to determine when these sediments were buried by overlying tills.

An alternative, to the simple approach of reducing the number of parameters by making convenient assumptions, is to collect more samples, whose exposure histories are somehow linked, and use this larger data set to determine a larger number of unknown parameters. In the second part of the paper (Section 3.6, we take this approach to determine the burial age of paleosols developed on one till and then buried by subsequent units. We measure ^{26}Al and ^{10}Be concentrations in samples of quartz from various depths in the buried paleosol. These measured nuclide concentrations reflect the initial nuclide concentrations in the lower till at the time it was emplaced, the duration of near-surface exposure during soil development, and the duration of several periods of burial by successively increasing thicknesses of overburden. Thus, an exposure model that we use to predict the present nuclide concentrations in our samples has several parameters: the initial nuclide concentrations in quartz in the lower till, and the lengths of exposure and burial periods. We use whatever geological data are available to estimate some of these parameters independently, and then use a numerical optimization method (rather than the analytical solutions we can use in the simple method) to determine the values for the remaining parameters that best explain the measured nuclide concentrations.

The mathematical description of this procedure is as follows. We extend Equation 3.3 to cover multiple samples and multi-stage burial histories by denoting the concentration of nuclide j in sample i at the end of time period k by $N_{i,j,k}$. The subscripts k go from $1 \ldots K$ where K is the total number of exposure or burial periods in the sample history. Then,

$$N_{i,j,k} = N_{i,j,(k-1)} e^{-\lambda_j t_k} + \frac{P_j(z_{i,k})}{\lambda_j} \left(1 - e^{-\lambda_j t_k}\right) \tag{3.8}$$

where $P_j(z_{i,k})$ is the production rate of nuclide j at depth $z_{i,k}$, and $z_{i,k}$ is the depth of sample i during time period k. For multiple samples from a paleosol that experiences surface exposure during period $k = 1$, the depths $z_{i,1}$ are the depths of the samples below the paleosol surface. For the periods of burial where $k > 1$, the depths $z_{i,k} = z_{i,1} + Z_k$ where Z_k is the depth of overburden covering the soil surface during period k. The depths of the samples below the present land surface

are $z_{i,K} = z_{i,1} + Z_K$. We start with initial nuclide concentrations at the beginning of the first time period $N_{i,j,0}$ and apply this equation K times to arrive at the final nuclide concentrations $N_{i,j,K}$.

We can estimate the production rates during the different time periods $P_j(z_{i,k})$ from the present stratigraphy and the depth dependence of nuclide production rates. Some of the durations of exposure or burial periods t_k may be known from correlation to nearby units or other age information, and some are unknown. The initial nuclide concentrations $N_{i,j,0}$ are in most cases unknown. This yields a predictive model for the final nuclide concentrations $N_{i,j,K}$ as a function of one or more unknown parameters; we use standard mathematical optimization methods to select the parameters that minimize the difference between predictions and actual measurements. Balco et al. [2004b in review] describe this optimization procedure in more detail.

3.3 The stratigraphic record of Plio-Pleistocene advances of the Laurentide Ice Sheet

The former location of the Laurentide Ice Sheet is today delimited by a broad arc of exposed, lake-riddled, and glacially scoured Precambrian bedrock surrounded by an outer zone near the past ice margin where thick sequences of glacial sediment have been deposited. Here we are interested in the portion of this arc of deposition within the north-central United States (Figure 3.3). In northernmost Minnesota, the glacial section consists only of thin deposits of the last glaciation overlying eroded bedrock. Glacial deposits thicken to the south, and eastern South Dakota, southwestern Minnesota, and western Iowa are covered by up to 250 m of Plio-Pleistocene glacial sediment, which consists mostly of laterally extensive till sheets interbedded with fluvial or glaciofluvial sediment. Paleosols and loess are rare in this region. Farther south, in southern Iowa, eastern Nebraska, and Missouri, the total glacial section is thinner, fewer till sheets are present, tills are separated by well-developed paleosols, and loess is common. It appears that the northernmost part of the region experienced mostly glacial erosion, and areas south of central Minnesota experienced deposition of till and ice-marginal sediment during nearly all ice advances. The area of thickest sediment in southwest Minnesota, where the largest number of tills is present, likely experienced numerous and relatively frequent glaciations; the southernmost glaciated regions experienced fewer glaciations and longer intervening periods [Soller and Packard, 1998, Hallberg, 1986, Hallberg and Kemmis, 1986, Roy et al., 2004, Boellstorff, 1978c, Patterson, 1997, 1999, Setterholm, 1995]. Here we focus on two areas: the region of thickest glacial sediment in southwestern Minnesota and adjacent states, and the region of thinner sediment, fewer tills, and better-developed interglacial deposits in eastern Nebraska and adjacent Iowa (Figure 3.3).

3.3.1 Southwestern Minnesota and adjacent states

The thickest sequences of Pleistocene tills in southwestern Minnesota and adjacent states occur under the Prairie Coteau highland near the Minnesota-South Dakota border. Here multiple till sheets are interbedded with sands and silts that record either ice-marginal glaciofluvial and glaciolacustrine deposition or fluvial systems that existed during interglaciations. Individual boreholes penetrate up to 12 distinct tills, indicating that at least this number of ice sheet advances took place. Some boreholes that reach bedrock penetrate mature quartz sands containing charcoal, woody plant debris, and mammal bones and teeth, suggesting a lowland riverine environment that predates Pleistocene glaciation. Patterson [1997], Setterholm [1995], Gilbertson and Lehr [1989], and Lineburg [1993] describe this stratigraphy.

The age of these tills is uncertain. The lower part of the section is correlated with magnetically reversed sediments, indicating that at least some ice advances occured prior to 0.78 Ma [Patterson, 1997]. The Lava Creek B ash (0.6 Ma) occurs between tills somewhat to the west [Flint, 1955], but correlation from this borehole into our study area is uncertain. Wisconsinan ice covered only the edges of the Prairie Coteau.

The Minnesota River lowland to the northeast of the Prairie Coteau also contains a thick sequence of tills. These tills are associated with the Des Moines lobe of the Laurentide Ice Sheet and are generally of northwestern provenance. Correlation between these tills and those in the Prairie Coteau section is uncertain. Here several Wisconsinan tills at the surface are underlain by at least five distinct pre-Wisconsinan tills. The pre-Wisconsinan tills form at least two unconformity-bounded packages, each of which presumably records a single glacial-interglacial cycle. These packages are separated by laterally extensive, linear sand units apparently deposited by well-developed interglacial fluvial systems. The age of these tills is unknown. Patterson [1999] describes this stratigraphy.

3.3.2 Eastern Nebraska and adjacent Iowa

Boellstorff [1978a,b,c] and Roy et al. [2004] describe the sequence of tills in eastern Nebraska and adjacent Iowa. The earliest of these tills, the "C" tills of Boellstorff and the "R2" tills of Roy et al., consist of at least two tills that have distinctive clay mineralogy, are magnetically reversed, and underlie the 2.0 Ma Huckleberry Ridge ash. There are no known tills that lie between the 2.0 Myr and 1.2 Myr ashes. The "B" tills of Boellstorff [1978c] ("R1" in Roy et al. [2004]) comprise at least two tills that are magnetically reversed and overlie the 1.3 Ma Mesa Falls ash, suggesting deposition between 1.3 Ma and 0.78 Ma. The uppermost set of tills ("A" tills of Boellstorff [1978c]; "N" of

Roy et al. [2004]) comprises at least three tills that have normal magnetic polarity. At least one of these is younger than the 0.6 Ma Lava Creek B ash. Wisconsinan ice did not cover this region. Thick sand units are rare in this area. Surfaces of individual till units are commonly oxidized or weathered, and often exhibit well-developed paleosols, suggesting long periods of exposure between ice advances. The uppermost till is commonly covered by one or more loess units separated by paleosols. The uppermost two loess units, designated the Peoria and Loveland formations in eastern Nebraska, were deposited 35,000-12,000 yr B.P. and 150,000-135,000 yr B.P. respectively [Forman et al., 1992, Forman and Pierson, 2002]. The age of loess units below these uppermost two is unknown.

3.4 Analytical methods

3.4.1 Quartz separation and Al/Be extraction

We disaggregated samples of till, sand, silt, and soil by drying, crushing, soaking in water, KOH, HNO_3, or $(NaPO_3)_6$ ("Calgon"), sonic bath treatment, or some combination thereof, then isolated the appropriate grain size by wet-sieving. In most cases we used the 0.25-0.85 mm grain size, but for small samples we used material as fine as 0.125 mm in order to obtain sufficient quartz. ^{26}Al and ^{10}Be analyses of separate coarse (0.25-0.85 mm) and fine (0.125-0.25 mm) grain-size fractions for samples of outwash (two samples) and till (one sample) were indistinguishable, as expected for glacial sediment which is likely to be immature, well-mixed, and poorly sorted. We extracted and purified quartz by repeated etching in 2% HF, heavy-liquid separation to remove acid-insoluble heavy minerals, soaking in hot KOH to remove secondary fluoride precipitated during the HF treatment, and a final 2% HF etch. This procedure yielded quartz with 35-80 ppm Al in all cases. We extracted Al and Be from 25-35 g of quartz using standard methods [Ditchburn and Whitehead, 1994, Stone, 2004], prepared Al cathodes by Al/Ag coprecipitation [Stone et al., 2004 in press], and measured isotope ratios at the Lawrence Livermore National Laboratory, Center for Accelerator Mass Spectrometry.

Our combined process and carrier blanks were $6.3 \pm 6.5 \times 10^4$ atoms ^{26}Al, $2.6 \pm 2.5 \times 10^4$ atoms ^{10}Be for analyses conducted in 2002, and $2.6 \pm 0.3 \times 10^5$ atoms ^{10}Be for analyses conducted in 2003. Although process blanks run simultaneously with samples in 2003 yielded repeatable results at the level noted above, we discovered later that some, but not all, of the aluminum metal cathodes used to hold BeO samples for AMS analysis during 2003 contained large quantities of ^{10}Be ($> 3 \times 10^7$ atoms $\cdot$ g(Al)$^{-1}$). Sputtering of exposed Al metal during AMS analysis may have

contributed spurious ^{10}Be counts to some samples that are not fully reflected in the process blank measurements. Thus, it is likely that we have undercorrected a small, but unknown, number of our ^{10}Be measurements. We discuss the results that may have been affected by this undercorrection later in the text.

3.4.2 Density measurements

In order to estimate subsurface nuclide production rates at our sample sites, we measured the density of 132 samples from our set of drillcores. For a few samples of non-cohesive sand and silt, we measured density by packing a container of known volume to approximate the natural compaction of the material. The majority of the samples consisted of irregular blocks of till or weakly cemented sand and silt. We measured their density by an adaptation of the procedure outlined by Sheldrick [1984] [also see Balco, 2004a]. We weighed each sample, placed it in a container of known volume, filled the remainder of the container with 1-mm glass beads, and weighed sample, container, and beads. Having already measured the density of packed glass beads, we could subtract the volume of beads from the volume of the container to determine the volume of the sample and thence the density. By repeatedly measuring the density of quartz ($\rho = 2.65$ g $\cdot$ cm^{-3}) samples, we determined the accuracy of this procedure to be ± 0.08 g $\cdot$ cm^{-3}.

The drillcore samples available to us had been air-dried to atmospheric moisture content during 3-30 yr of storage. However, the units we sampled, and nearly all of their overburden, are actually water-saturated in the field, so we require their wet density in order to calculate shielding depths. We inferred the wet density of samples by assuming that the dried sample consisted entirely of quartz grains: if such a sample were fully water-saturated, the wet density would be:

$$\rho_{wet} = \left(1 - \frac{\rho_{dry}}{\rho_{quartz}}\right) + \rho_{dry} \tag{3.9}$$

where ρ_{dry} is the dry density of the sample and ρ_{quartz} is the density of quartz ($2.65 \mathrm{g} \cdot \mathrm{cm}^{-3}$). We evaluated this assumption by measuring wet and dry densities for the following: a) naturally water-saturated samples of till collected at outcrops and mine excavations that we then dried, and b) dry drillcore samples of sand, silt, and till that we then saturated with distilled water. We found that measured wet densities for both naturally wet samples and saturation experiments coincided with those calculated using Equation 3.9 within measurement error (Figure 3.4).

For units whose density we did not actually measure, we assigned average densities for the appropriate type of sediment. These average wet bulk densities are 2.24 ± 0.07 g $\cdot$ cm^{-3} for glacial till ($n = 90$), 2.13 ± 0.16 g $\cdot$ cm^{-3} for sand ($n = 35$), and 2.01 ± 0.1 g $\cdot$ cm^{-3} for silt ($n = 7$).

We assigned compacted loess a wet density of 2.3 $g \cdot cm^{-3}$ based on measurements by J. Mason (personal comunication).

3.5 Results and discussion I: buried river sands and outwash

In this paper we report results of ^{26}Al and ^{10}Be analyses of two types of glacial sediment: first, sandy fluvial sediment and outwash intercalated with tills; and second, paleosols developed on tills and then buried by other glacial sediment. In this first section we discuss analyses of fluvial sediment and outwash. We discuss paleosols in the next section.

The buried fluvial and glaciofluvial sands whose burial age we wish to determine consist of fine sand to gravel interbedded with till in five boreholes from southwest Minnesota and adjacent South Dakota (Figures 3.3, 3.5). These sand units are up to 20 m thick and, in many cases, can be correlated between drillholes to reveal channel networks that presumably record river systems developed during interglacial periods [Patterson, 1999]. The reason we became interested in these sands at first is that nearly all modern river sands for which ^{26}Al and ^{10}Be have previously been measured have nuclide concentrations that comply with Equation 3.5 [Granger et al., 2001, 1997, Partridge et al., 2003, Granger et al., 1996, Clapp et al., 2000]. Thus, we thought that we could use the simple approach previously described in Section 3.2.2 to determine the time that these sediments were buried by overlying tills, and thus the age of the tills. However, we found that this was not the case, and that we could not constrain the initial nuclide concentrations in these sediments at the time they were buried. In this section we describe the reasoning that led us to this conclusion and summarize the limited age information that we could obtain from our measurements.

We measured ^{26}Al and ^{10}Be in 33 samples from sand units intercalated with pre-Wisconsinan tills in five boreholes from Minnesota and adjacent South Dakota (Figure 3.5; Table 3.2). Many of these samples belonged to the thick, laterally extensive, and well-sorted sand units deposited by river systems that developed during interglaciations, and others belonged to thinner, less extensive, and less well-sorted sands that could have been rapidly deposited near the ice margin. We observed no systematic difference between samples from these two stratigraphic contexts. We found that $^{26}Al/^{10}Be$ ratios decreased with depth in nearly all cases, that $^{26}Al/^{10}Be$ ratios of correlative sand units from different boreholes agreed, and that nuclide concentrations in buried sands were near expected values for sediments that had experienced 10,000-50,000 yr of surface exposure and 0.5-1.5 Myr of burial below several meters depth. The fact that we obtained plausible results, did not infer age reversals, and did not violate stratigraphic constraints suggested at first that we were

justified in assuming that ^{26}Al and ^{10}Be concentrations at the time of burial were consistent with surface exposure.

3.5.1 Results from modern fluvial systems

In order to better evaluate our assumptions about ^{10}Be and ^{26}Al concentrations at the time of burial, we measured ^{26}Al and ^{10}Be concentrations in samples of sand being transported in modern rivers (Figure 3.6; Tables 3.3, 3.4; sample locations shown in Figure 3.3). We found that nuclide concentrations in these samples are not consistent with surface exposure. We also measured ^{26}Al and ^{10}Be concentrations in subsurface samples from tills and ice-marginal deposits of latest Wisconsinan age (Figure 3.6; Table 3.5). Nuclide concentrations in sand from the modern Minnesota River and its tributaries (samples MNR-01, MNR-02, YMR-01) were indistinguishable from those in Wisconsinan glacial sediments deposited by the Des Moines lobe. If this modern river sand was derived from slow erosion of nearby soil surfaces that had been exposed to the cosmic ray flux since deglaciation 15,000 yr ago, it would have higher ^{26}Al and ^{10}Be concentrations than Wisconsinan glacial sediments that have remained buried since emplacement. The fact that this is not the case shows that most of the sediment in the river systems is derived from rapid undermining of steep riverbank bluffs that expose glacial deposits, rather than from gradual erosion of soil surfaces over large areas. The remarkable agreement of nuclide concentrations in latest Wisconsinan glacial sediment from a variety of environments, all ultimately derived from subglacial erosion of older glacial sediments, also indicates that the last ice sheet advance was very effective in mixing and homogenizing the sediment that it transported. Thus, the Wisconsinan advance of the Des Moines Lobe into the Minnesota River valley mobilized, mixed, and redeposited older glacial sediment that already had experienced an exposure/burial history of at least 500,000 yr, and this sediment is now moving directly into rivers without being measurably exposed to the surface cosmic ray flux. If modern river sands were buried by future glacier advances and we subsequently attempted to calculate their burial age by assuming that nuclide concentrations were consistent with surface exposure at the time of burial, we would obtain wildly incorrect ages.

3.5.2 ^{26}Al/^{10}Be ratios below the production ratio in river sands from prior interglacials?

If river sands in previous interglaciations had a similar history to modern river sands, we cannot assume that nuclide concentrations in these sands when they were buried by overlying tills were anywhere near consistent with surface exposure. Thus, we looked for further evidence that would tell us whether or not nuclide concentrations in pre-Wisconsinan river sediment were anything like

those that we observe in modern river sands. First, we considered the possibility that recycling of older glacial sediment into the modern river system has been particularly pronounced in the Minnesota River Valley during the present interglaciation. The modern Minnesota River occupies a deep valley, cut through the entire glacial section by drainage from glacial Lake Agassiz, and tributary streams have incised several hundred feet of glacial sediment to reach the valley floor. However, we analyzed two samples of river sand from farther south and west (02-TILL-008-VERM from the Vermilion River in South Dakota and 02-TILL-005-PLA from the Platte River in Nebraska; see Figure 3.3) and found ^{26}Al and ^{10}Be concentrations that were different from Minnesota River samples, but were also inconsistent with surface exposure.

Direct measurements from buried sands of known age

The ^{26}Al and ^{10}Be concentrations of modern river sediment show that nuclide concentrations that are inconsistent with surface exposure appear to be the rule for river sands in regions covered by glacial sediment in the present interglaciation. We evaluated whether or not this was true in previous interglaciations by collecting samples of middle Pleistocene fluvial sands whose burial ages were constrained by independent evidence, and back-calculating the nuclide concentrations in these samples at the time they were buried (Figure 3.7; Table 3.6).

In borehole 4-A-75 [Boellstorff, 1978b], we sampled a coarse sand unit overlain by a normally magnetized till (the "A3" till of Boellstorff [1978b]) which was deposited 0.78-0.6 Ma. This till was overlain by loess containing the 0.6 Ma Lava Creek ash, and then by two pre-Wisconsinan tills ("A1" and "A2") that were emplaced 0.6-0.15 Ma (Figure 3.7). We estimated the nuclide concentrations in the sand at the time it was buried with a Monte Carlo simulation, as follows: We generated 1000 plausible burial histories by assuming that the loess unit was deposited 0.6 Ma, and selecting random ages for the other two units that were uniformly distributed between the age constraints. Then, for each of these permissible burial histories, we applied Equation 3.3 repeatedly to back-calculate the initial ^{10}Be and ^{26}Al concentrations in the sample at the time of burial. This yields the range of nuclide concentrations at the time of burial that are permitted by the constraints on the age of the overburden.

In borehole 1-A-76 [Boellstorff, 1978b], we sampled a sand unit that was overlain by a loess containing the 1.2 Ma Mesa Falls ash, by two tills (the "B2" and "A3" tills) that were deposited 1.2-0.6 Ma, and then by another sand unit that was deposited 0.6-0 Ma, and used the same procedure to estimate nuclide concentrations in the sample at the time of burial.

Figure 3.7 summarizes these results. Nuclide concentrations consistent with surface exposure

at burial are not completely excluded for either sample, but are very unlikely in both cases.

At a gravel pit exposure in eastern Iowa [the Kraft locality of Bettis III, 1990] we sampled sand and gravel, thought to be distal outwash from a former tributary to the Missouri River, that contains the 0.6 Ma Lava Creek B ash (Figure 3.7; Table 3.6). The samples are now buried under 6-10 m ($\sim$ 1200-2000 g $\cdot$ cm^{-2}) of sand and loess, but field relationships show that this overburden has been eroded significantly. Thus, the burial history of these samples is poorly constrained. However, we can obtain a maximum limit for the ^{26}Al/^{10}Be ratio at the time of burial by assuming that the samples have been buried at infinite depth since the time of ash deposition, and applying Equation 3.3. Figure 3.7 summarizes this calculation. Regardless of the burial depth, the ^{26}Al/^{10}Be ratio in these samples was well below the production ratio, and nuclide concentrations were not consistent with surface exposure, when the samples were buried. This suggests an outwash origin for these sediments. The alternative, Missouri River alluvium, would be expected to contain both outwash and western-derived nonglacial river sediment, and have nuclide concentrations such as we observed in sand from the nearby Platte River (sample 02-TILL-005-PLA; Figures 3.3,3.6).

Nuclide concentrations near and below steady-state values

After very long burial times ($\sim 5 \times 10^6$ yr), the concentration of nuclide j in a sample buried at depth z will asymptotically approach a steady state $N_{j,ss}$ where nuclide production and decay are balanced, that is, $P_j(z) = N_{j,ss}\lambda_j$ (see Figures 3.2C-3.2E). Many of the surface and subsurface samples we analysed had nuclide concentrations which are close to steady-state values at burial depths of 4000-8000 g $\cdot$ cm^{-2} (compare Figure 3.5 with Figures 3.2C-3.2E). If these samples had nuclide concentrations consistent with surface exposure at the time of burial, their present nuclide concentrations would imply burial ages exceeding 5 Myr, which is unlikely in light of the lack of evidence for Northern Hemisphere glaciation at that time. It is more likely that these sediments were buried with nuclide concentrations near steady-state at their eventual burial depth, *i.e.*, with ^{26}Al/^{10}Be ratios well below the production ratio. Furthermore, near-steady-state concentrations make it nearly impossible to calculate accurate burial ages even if initial nuclide concentrations at the time of burial are known exactly, for two reasons. First, the closer the initial concentrations are to the steady-state values, the less time resolution is available. Second, the calculated burial age becomes very sensitive to the choice of model for nuclide production by muons.

We also found that some samples had nuclide concentrations that were below the steady-state nuclide concentrations expected at their burial depth. These occurred in the upper parts of UMRB-1 and UMRB-3. This inconsistency reflects either erosion at these sites or redeposition of material

that was previously more deeply buried. Patterson [1999] inferred from stratigraphic evidence that the Des Moines Lobe had removed pre-existing older tills in this region; thus we favor erosion as an explanation for these data.

3.5.3 Summary: we can not determine the burial age of pre-Wisconsinan fluvial sediment from ^{26}Al and ^{10}Be measurements.

We conclude that coarse-grained interglacial sediments intercalated with pre-Wisconsinan tills, like modern fluvial sediments in Minnesota, were deposited and buried with initial nuclide concentrations that were not consistent with surface exposure. Therefore, we cannot use the simple burial dating methods described in Section 3.2.2, which rely on assuming that initial nuclide concentrations were consistent with surface exposure, to date the tills.

3.5.4 Limiting ages derived from conservative assumptions

Even though we cannot determine the exact age for most samples of pre-Wisconsinan sand, we can compute maximum and minimum limiting ages by making conservative assumptions.

First, given a sample buried by some thickness of overburden, we can estimate its minimum age by making the following assumptions:

1. The^{26}Al/^{10}Be ratio of the sample at the time of burial was 4.3 (70 % of the production ratio of 6.1), the average of our analyses of Wisconsinan glacial sediment from the Minnesota River Valley. We justify this value as the minimum ^{26}Al/^{10}Be ratio that any Pleistocene fluvial sediment could reasonably be expected to have had by the observation that nuclide concentrations in modern fluvial sediments directly reflect those in Wisconsinan glacial sediments, which are near the average ^{26}Al/^{10}Be ratio observed for all our analyses of the entire Pleistocene section. If each ice sheet advance remobilizes a representative sample of the sedimentary section that exists at that time, the ^{26}Al/^{10}Be ratio of fluvial sediments at burial should decrease with each glaciation. Although this is not strictly assured, only very complicated scenarios can produce lower fluvial ^{26}Al/^{10}Be ratios at burial in pre-Wisconsinan river sands than in modern river sands. Our estimates of the ^{26}Al/^{10}Be ratio at burial for pre-Wisconsinan sands, discussed above, are all greater than 4.3.

2. The sample was immediately buried at infinite depth and remained so until the present time, i.e., $P_j(z) = 0$. This ensures an underestimate of the true burial age.

With these assumptions, the minimum age for a given sample is given by:

$$t_{min} = \frac{-\ln\left(\frac{R}{4.3}\right)}{\lambda_{26} - \lambda_{10}} \tag{3.10}$$

where R is the measured $^{26}Al/^{10}Be$ ratio. We cannot calculate a meaningful minimum age with these assumptions for samples whose nuclide concentrations are not clearly distinguishable from those of modern fluvial sediments (as is the case for all samples in borehole UMRB-2, and several others). This calculation yields the minimum age for the sample, which by the principle of superposition also applies to all units below it. For boreholes with multiple samples at different stratigraphic levels, minimum ages relative to higher samples supersede those that relate to lower samples, again following the principle of superposition. Figure 3.8 summarizes these results. We have not considered analytical uncertainty in calculating these minimum ages.

Estimating the maximum burial age associated with a sample is more complicated, because of the fact that, until the sample is buried deeply enough that the nuclide concentration in the sample lies above the steady-state nuclide concentration at that depth, infinitely long cyclical burial histories are permitted. Thus, we cannot associate a maximum age with a particular unit that we have sampled, but we can use a particular sample to provide maximum ages for stratigraphic units that lie above it by some critical amount. In effect this is done by assuming that, at the time of emplacement of the overlying unit of interest, the sample had nuclide concentrations in equilibrium with surface exposure, and since that time the sample has been buried at the minimum possible depth allowed by the stratigraphy. We provide a mathematical description in Section 3.8.

Figure 3.8 shows the results of these calculations, which provide slightly more information on the age of the tills than was previously available. Intermediate-depth tills in borehole UMRB-1 (unit 8 of Patterson [1999] and adjacent tills) are constrained to be between ca. 0.6 and ca. 1.5 Myr old. The oldest tills in the Prairie Coteau section (boreholes SWRA-3 and SD-BR) must be older than 1-1.25 Myr; the youngest tills in this section are younger than 1.5 Myr. These data are little help in correlating individual tills on the basis of age, but do indicate that the lower tills are older than previously believed.

3.5.5 Explicit burial ages for one special case

We collected two samples from the basal sand unit in borehole SD-CO (samples SD-CO-402 and -406; Figure 3.9; Table 3.2). This unit directly overlies saprolite, and it and similar sands in other boreholes underlie all known tills in the region. If it predated all ice sheet advances, the fact that modern river sands in unglaciated regions have ^{26}Al and ^{10}Be concentrations that comply

with Equation 3.5 suggests that this unit would, at burial, have had nuclide concentrations consistent with surface exposure as well. In addition, this unit has extremely high concentrations of atmospherically produced ^{10}Be [Balco, 2004b], which further suggests that it originated from a preglacial landscape and reflects a long period of surface exposure. Thus, the available evidence indicates that these samples was buried with nuclide concentrations in equilibrium with surface exposure, and we can use them to determine the age of the overlying till by the simple burial dating approach described in Section 3.2.2. The major remaining uncertainty in this calculation concerns the burial history of this sample after the emplacement of the lowest till unit. If we calculate the burial age under the assumption that only the lowest till was emplaced at the time of interest, and the rest of the section was emplaced recently, we will overestimate the true burial age; likewise, if we assume that the entire present overburden was emplaced at once we will underestimate the true age. Neither of these end-member scenarios are likely to be true, so we used the following assumptions, which we believe to be the most reasonable:

1. Nuclide concentrations at the time of burial by the lowest till reflect equilibrium with steady erosion, *i.e.*, Equation 3.5 applies. In applying Equation 3.5, we use approximate regional average surface production rates of 7.5 and 45.8 atoms $\cdot$ g^{-1} $\cdot$ yr^{-1} for ^{10}Be and ^{26}Al respectively. Note that the choice of surface production rates here does not affect the burial age, only the erosion rate in the sediment source area ϵ that we might also infer from the samples.

2. There have been four subsequent periods of burial, that is, $K = 4$ in Equation 3.8, as follows: First, the samples were buried at 2500 g $\cdot$ cm^{-2} depth at an unknown time by the till immediately overlying them. Second, they were buried at 10,100 g $\cdot$ cm^{-2} depth, by the till whose top is now 77 m below the surface, at 1 Ma. This age estimate is based on the analysis of the truncated paleosol that we discuss below in Section 3.6.5. Third, they were buried to 23,500 g $\cdot$ cm^{-2} depth, by the sequence of tills whose top is now 17 m below the surface, at 0.5 Ma. This age estimate is speculative but, as the samples are already very deeply buried at this point, has a minimal effect on the actual burial age. Fourth, they were buried to their present depth of 27,200 g $\cdot$ cm^{-2} by the uppermost, late Wisconsinan, till 30,000 yr ago. In the framework of Equation 3.8, $z_{i,1} = 2500$, $z_{i,2} = 10,100$, $z_{i,3} = 23,500$, $z_4 = 27,200$, $t_2 = 0.5 \times 10^6$ yr, $t_3 = 0.47 \times 10^6$ yr, and $t_4 = 30,000$ yr. t_1 is the unknown parameter of interest, and $t_1 + t_2 + t_3 + t_4$ is the age of the till overlying the samples.

With these assumptions we can determine t_1 and the nominal erosion rate prior to burial ϵ by using Equations 3.5 and 3.8 to predict the expected nuclide concentrations as a function of

these unknown parameters, and then finding ϵ and t_1 that best explain the measured nuclide concentrations. We are not interested in ϵ so we treat it as a nuisance parameter. For sample SD-CO-402, this calculation yields ages for the lowermost till of 1.90 ± 0.24 Ma and 2.03 ± 0.30 Ma, using muon interaction cross-sections of Stone and Heisinger, respectively. Sample SD-CO-406 yields ages of 1.43 ± 0.18 Ma and 1.50 ± 0.22 Ma, respectively. These standard errors include only analytical uncertainty.

These age estimates are surprisingly young, because the existence of tills in Nebraska and Iowa that underlie the 2 Ma Huckleberry Ridge ash [Boellstorff, 1978c, Roy et al., 2004] suggests that the oldest tills in eastern South Dakota should also be older than 2 Ma. Our analysis of SD-CO-402 is consistent with this idea; that of SD-CO-406 is not. If the disagreement between the two samples were the result of analytical error, the true age of the lowest till in SD-CO would be near 1.7 Ma; If our assumption that the nuclide concentrations in these samples were consistent with surface exposure were incorrect for SD-CO-402, this sample would overestimate the age of the till, and the true age would be near 1.5 Ma. In any case, we were not able to find any plausible burial history that would be consistent with both the data for SD-CO-406 and an age greater than 2 Ma for the till. Thus, absent additional information, we cannot confidently associate the lowermost till here with pre-2 Ma tills further to the south.

3.6 Results and discussion II: pre-Wisconsinan paleosols

We show in the previous section that fluvial and glaciofluvial sands intercalated with glacial tills are not suitable for burial dating using ^{26}Al and ^{10}Be. We were more successful applying the technique to paleosols developed on till and buried by younger sediments. Paleosols are common in Plio-Pleistocene glacial sediment sections, especially in the southern part of our field area. Starting with the first explorations of the north-central U.S., glacial geologists took particular note of prominent paleosols as a possible means of correlating major glacial-interglacial cycles: thus, there exist numerous well-described sections where paleosols are buried by younger glacial sediment.

There are two particular advantages to using paleosols rather than fluvial sediments from our perspective. First, the existence of a well-developed paleosol implies a long period of surface exposure. In contrast to river sands, which appear to experience very short periods of surface exposure between exhumation from old glacial deposits and transport out of the glaciated area, we expect quartz in paleosols to have higher ^{26}Al and ^{10}Be concentrations than quartz in fluvial sand. This makes for more precise analyses and also suggests that, whatever the inherited nuclide

concentrations in the parent material on which the soil is developed, nuclide concentrations may return to values within the simple exposure island if the soil surface is exposed for long enough.

Second, samples from different depths in a paleosol share a similar exposure history. This enables us to collect more samples and obtain a tractable problem in which the number of measurements exceeds the number of unknown parameters. In contrast, there is no assurance that sediment from different stratigraphic levels in a single fluvial sand unit will have a similar provenance and exposure history.

3.6.1 Examples from modern soils

We began by measuring nuclide concentrations in modern surface soils to determine whether or not they were consistent with surface exposure. Figure 3.3 and Table 3.7 show the locations of these samples. Figure 3.10 and Table 3.8 show nuclide concentrations. As we expected, nuclide concentrations in quartz near the soil surface were higher, and closer to the simple exposure island, than nuclide concentrations in quartz from the soil parent material, that is, Wisconsinan glacial sediment, well below the surface.

In borehole SD-CO, we analysed samples from a soil developed on the uppermost (Wisconsinan) till, which is associated with the Verdi ice-marginal position of the Des Moines lobe and was deposited ca. 30,000 ^{14}C yr B.P. [Patterson, 1997, Setterholm, 1995]. A sample at 13 m depth (SD-CO-43), which reflects only the inherited nuclide concentration in the till when it was emplaced, had low nuclide concentrations that were inconsistent with surface exposure, like other samples of Wisconsinan glacial sediment (compare Figures 3.10A and 3.6). A sample from 1.2 m depth in the same borehole (SD-CO-4) had higher nuclide concentrations that lay along an appropriate resetting curve relative to the lower sample (Figures 3.10A and 3.9). Differencing the two samples yields exposure ages of $43,000 \pm 5000$ yr and $38,000 \pm 4000$ yr for the ^{10}Be and ^{26}Al measurements respectively. This is somewhat older than the age of the till inferred from correlation to the Verdi ice margin, but the difference in ages can be accounted for by our uncertainty in determining the exact depth of sample SD-CO-4 prior to disturbance of the drilling site.

We also sampled the uppermost part of the modern soil profile at three other locations (Figure 3.10; Tables 3.7, 3.8; locations in Figure 3.3). We collected sample 02-TILL-007-PIT from the surface of a soil developed on Wisconsinan outwash associated with the Bemis ice-marginal position [14,000 ^{14}C yr B.P.; Patterson, 1997, Setterholm, 1995]. We did not measure nuclide concentrations at depth here; however, if they were similar to those in other latest Wisconsinan deposits of the Des Moines Lobe that we sampled, this sample would reflect 15,000 years of exposure, which is

consistent with the age of the unit. We collected sample 02-TILL-006-GRA from what we believed to be an undisturbed soil surface developed on pre-Wisconsinan till [Patterson, 1997, Setterholm, 1995]. This sample had surprisingly low nuclide concentrations, equivalent to 10,000 - 15,000 yr of surface exposure if the parent material had nuclide concentrations similar to late Wisconsinan tills. It is difficult to explain this unless much of the quartz in the surface soil originated from late-glacial or Holocene eolian deposition, and not from the older till on which the soil is developed. Finally, we collected sample MN-SAL-20 from the upper 20 cm of a soil developed on Wisconsinan till deposited 12,000 - 14,000 radiocarbon yr B.P. The difference between the ^{10}Be concentration in this sample and that in Wisconsinan glacial sediments elsewhere indicated 15,000 years of exposure. The ^{26}Al concentration in this sample was surprisingly low (suggesting only 8000 yr of exposure with equivalent assumptions); this suggests that the inherited nuclide concentrations in the till at this site were somewhat lower than in the other Wisconsinan glacial sediment we sampled.

3.6.2 Direct measurements on buried paleosols of known age

Our measurements from modern soils show, as we expect from Figure 3.2F and the nuclide concentrations we measured in Wisconsinan glacial sediments (Figure 3.6), that the present interglaciation has been too short to "reset" nuclide concentrations in modern soils to the simple exposure island. However, many paleosols found intercalated with early and middle Wisconsinan tills display soil development that suggests much longer periods of surface exposure. In these cases the assumption, that nuclide concentrations in these soils were consistent with surface exposure when buried by overlying tills, would be more plausible.

We evaluated this by analyzing samples from two paleosols of approximately known age in drillcores from southeast Iowa collected by Boellstorff [1978a] (Figure 3.11; Table 3.6). Both paleosols are developed on the "C1" till of Boellstorff [1978a,b,c], which is equivalent to the upper of the two "R2" tills of Roy et al. [2004]. This till is magnetically reversed and underlies the 2.0 Myr Huckleberry Ridge ash. We used a Monte Carlo simulation similar to the one we describe above in Section 3.5.2 to generate random burial histories that fit the existing age constraints, and thus compute the initial nuclide concentrations that the samples could have had when they were buried.

In borehole 5-A-75 [Boellstorff, 1978b], our sample is overlain by silt containing the Huckleberry Ridge ash, which we assumed was deposited 2.0 Ma, then by a magnetically reversed till ("B" or "R1" till) deposited 1.2-0.78 Myr ago, and then by two magnetically normal tills ("A1" and "A2" or "N") deposited 0.78-0.15 Myr ago. Only very few burial histories that fit these constraints result

in nuclide concentrations at burial that are consistent with surface exposure (Figure 3.11).

In borehole 17-A-76, our sample is overlain by silt which is likely correlative with sand and silt in nearby boreholes that was deposited 2-1.2 Ma, then by two tills ("A2" and "A3") deposited 0.78-0.62 Ma, then by a third till ("A1") deposited 0.62-0.15 Ma. Many plausible burial histories that fit these constraints yield initial nuclide concentrations close to the simple exposure island (Figure 3.11), suggesting that the sample most likely had nuclide concentrations at burial that were consistent with surface exposure. The difference in our results for these two samples is consistent with with the relative degree of development of the two paleosols (J. Mason, unpublished core logs) as well as the higher overall ^{10}Be and ^{26}Al concentrations in 17-A-76-146 than in 5-A-75-167.

3.6.3 General method for calculating burial ages for paleosols

We conclude from these measurements that pre-Wisconsinan paleosols that were formed during particularly long interglaciations may well contain quartz with nuclide concentrations near the simple exposure island, but this will not always be the case. Thus, we cannot in general use simplifying assumptions to estimate the ^{26}Al and ^{10}Be concentrations in soil quartz at the time of burial, but must treat them as unknown parameters. Although this presented a fatal difficulty for buried fluvial sediments, it does not present the same difficulty for paleosols. A paleosol developed on a well-mixed parent material such as till contains quartz grains that, on average, were emplaced with the same initial nuclide concentrations. The additional nuclide inventory produced by exposure during soil formation will vary throughout the soil profile as a known function of depth. The entire paleosol has the same exposure and burial history. This means that we can determine the burial age of a paleosol using an exposure model with only four unknown parameters: initial ^{10}Be and ^{26}Al concentrations at the time of till emplacement, the duration of soil formation, and the duration of burial. In contrast to the case for fluvial sediment, where we could not simultaneously determine all of these parameters because none of them were shared between different samples, we can collect multiple samples from various depths in a paleosol to obtain a tractable problem in which the number of measurements greatly exceeds the number of unknowns. The mathematical procedure for doing this is the same as we have previously described: we use Equation 3.8 to predict the measured nuclide concentrations for given parameters, then use an optimization method to determine the parameters which best reproduce the observations. We have previously described this method in more detail in Balco et al. [2004b in review].

3.6.4 Example paleosol from eastern Nebraska

Here we briefly describe results which we have previously reported elsewhere [Balco et al., 2004b in review]. We measured ^{26}Al and ^{10}Be concentrations at six depths below the surface of a paleosol developed on the youngest till in eastern Nebraska and buried by three loess units. Figure 3.12 and Table 3.9 show the stratigraphy of this borehole and the nuclide concentrations in the paleosol. Here the initial nuclide concentrations at the time of emplacement of the till $N_{j,0}$ are unknown parameters that are the same for all samples. The upper two loess units, the Peoria and Loveland formations, were deposited 12,000-35,000 and 135,000-150,000 yr ago, respectively [Forman et al., 1992, Forman and Pierson, 2002]. Thus, $K = 4$, $t_3 = 135,000$ yr, and $t_4 = 35,000$ yr. t_2, the time between emplacement of the first and second loess units, is unknown, and the age of the lowermost loess, *i.e.,* $t_2 + t_3 + t_4$, is the unknown parameter of most interest. t_1, the nominal duration of soil formation, cannot be determined exactly without knowing the erosion rate during soil formation, and we treat it as a nuisance parameter. The burial depths for the various time periods are $Z_2 = 1600$ g $\cdot$ cm^{-2}, $Z_3 = 3100$ g $\cdot$ cm^{-2}, and $Z_4 = 5100$ g $\cdot$ cm^{-2}.

To summarize, the unknown parameters in this problem are the initial nuclide concentrations $N_{j,0}$ and the durations of exposure and initial burial, t_1 and t_2. The parameters that best fit our data are as follows: $N_{10,0} = 0.99 \times 10^5$ atoms $\cdot$ g^{-1}; $N_{26,0} = 4.3 \times 10^5$ atoms $\cdot$ g^{-1}; $t_1 = 51,000$ yr; and $t_2 = 430,000$ yr., *i.e.*, the most likely age of the lowermost loess is 0.58 Ma.

We also carried out an error analysis to determine the uncertainty in this age estimate. We used a Monte Carlo simulation in which we repeatedly generated random sets of measurements drawn from normal probability distributions with mean and standard deviation given by our actual measurements and their analytical uncertainties. We then found the age that best fit each simulated data set. This exercise indicated that age of the lowermost loess was 0.58 ± 0.11 Ma. Figure 3.13 shows the results of this simulation. Our error analysis also shows that the analytical error in our measurements of ^{26}Al concentrations is the dominant source of uncertainty. The uncertainty in muon interaction cross-sections is unimportant in this particular case because of the relatively high ^{26}Al and ^{10}Be concentrations in the paleosol and the relatively short duration of burial: reduction of the preexisting nuclide inventory by decay is much more important than nuclide production during burial. Thus, the choice of muon interaction cross-sections only affected the age estimate by 0.2%. We conclude that the loess was emplaced during marine δ^{18}O stages 13-15. We cannot determine the duration of soil formation, and thence the age of the underlying till, very accurately because we lack information about the surface erosion rate during soil development. However, it is most likely that this till was emplaced during marine δ^{18}O stage 16 near 0.62 Ma. The $N_{j,0}$,

the initial nuclide concentrations in the till at the time of emplacement, are similar to those we observed in Wisconsinan tills.

3.6.5 Example paleosol in borehole SD-CO

We also applied this method to the oxidized upper portion of a till at 103.8 m depth in borehole SD-CO from eastern South Dakota (Table 3.10; Figures 3.9, 3.14).

This example presented several difficulties compared to the soil in core 3-B-99 described above. First, in contrast to the complete, well-developed soil profile in 3-B-99, oxidation and a weakly developed blocky structure are the only indications of soil development. Nuclide concentrations near the surface of this till (with the exception of one anomalous ^{10}Be measurement which we discuss below) decrease exponentially with the appropriate attentuation length (Figure 3.14). This confirms that exposure within several meters of the surface did in fact take place. However, the upper part of the soil profile is not preserved. This indeterminate amount of truncation of the soil profile makes it impossible to determine the exposure time of the soil prior to burial (because we cannot accurately estimate nuclide production rates during soil formation), but does not affect our estimate of the burial age for the soil. Thus, we again treat the duration of exposure during soil formation t_1 as a nuisance parameter. On the other hand, the fact that we have only the deepest part of the soil profile to work with indicates that we can disregard vertical mixing of quartz during soil development, which simplifies the problem.

Second, we have little information about the age of any of the overlying units. The till immediately overlying the samples, whose age is the unknown parameter of interest, is 4300 g $\cdot$ cm^{-2} thick; at present the samples are buried by 22,300 g $\cdot$ cm^{-2} of overburden, of which the uppermost 3800 g $\cdot$ cm^{-2} is late Wisconsinan in age. In the framework of Equation 3.8, $K = 2$, t_1 is the parameter of interest, and the Wisconsinan burial history is represented by $t_2 = 25,000$ yr,and $z_{i,2} = 22,300$ g $\cdot$ cm^{-2}. The uncertainty in the time at which the intermediate 14,200 g $\cdot$ cm^{-2} of material was deposited leads to an uncertainty in the parameters $z_{i,1}$. To evaluate the importance of this uncertainty, we carried out the calculation with the two end member scenarios of a) $Z_1 = 4300$ g $\cdot$ cm^{-2}, that is, all the overburden above the till of interest was emplaced 25,000 yr ago, and b) $Z_1 = 18,500$ g $\cdot$ cm^{-2}, that is, all the overburden below the Wisconsinan was emplaced at once at the time of interest. Table 3.11 summarizes these results.

Third, as nuclide concentrations in the sample are much lower than in 3-B-99, nuclide production during burial, which is predominantly by muon interactions, is correspondingly more important relative to decay of the initial nuclide inventory. Thus the uncertainty in rates of nuclide produc-

tion by muons is important. We evaluated its importance by carrying out the calculation with both sets of muon interaction cross-sections (Table 3.11). As expected, the choice of cross-sections is most important when most of the burial takes place at shallow depths.

Fourth, the nuclide concentrations in these samples are low, and have correspondingly large analytical uncertainties. Furthermore, nuclide concentrations are close to steady-state values for depths of 8000-12000 $g \cdot cm^{-2}$, which causes analytical errors in nuclide concentration to propagate into large errors in age. In addition, it means that implausible burial histories, in which the initial nuclide concentrations $N_{j,0}$ are very close to the measured concentrations, and the exposure and burial times $t_1 = t_2 = 0$, fit the full data set better than stratigraphically plausible burial histories with t_1 on the order of 10^4 yr and t_2 on the order of 10^6 yr. However, neither of these scenarios fit the data acceptably well. This problem is evident in the error analysis (which we carried out using a Monte Carlo simulation as described above) by the large population of possible results with burial age equal to zero, and the uniformly poor fit of the model to the data (reduced $\chi^2 \simeq 5 \pm 3$; Figure 3.15). We found that this difficulty in fitting the data was largely explained by a single analysis, our ^{10}Be measurement for the lowest sample (SD-CO-354). When we did not consider this measurement in determining the best-fit burial history, the plausible burial histories fit the data well, (reduced $\chi^2 \simeq 1$; Figure 3.15). As an anomalously high ^{10}Be concentration is consistent with the possibility of undercorrection for spurious ^{10}Be in the cathodes used for AMS analysis (discussed above in Section 3.4), we discarded this analysis. Regardless, the relatively large analytical uncertainties, and the proximity of measured nuclide concentrations to steady-state concentrations, result in a larger uncertainty in our age estimate for this paleosol than for the one in borehole 3-B-99.

Figure 3.16 summarizes the results of Monte Carlo simulations for bracketing assumptions about muon cross-sections and burial history. With assumptions that minimize nuclide production rates after burial, the age of the till overlying this paleosol is fairly well constrained to be near 0.9 Myr old. For the opposite assumptions, the probability distribution of the age of the till is very wide, with a modal age near 1.45 Myr. As the most likely burial history is intermediate between the bounding assumptions, we conclude that the till was deposited 1-1.2 Myr ago. To summarize, analytical uncertainty, uncertainty in subsurface production rates, and uncertainty in the age of the overburden all contribute significant uncertainty to our age estimate for this till, although the uncertainty in the age of the overburden could be reduced by making additional measurements on tills higher up in the section.

3.7 Conclusions

1. *Outwash and river sediment.* Unlike modern river sediment in unglaciated areas, both modern and ancient river sands in glaciated areas are nearly all derived from the recycling of older glacial deposits exposed in river cut banks. This sediment moves rapidly into fluvial systems without being appreciably exposed to the cosmic ray flux, and, when buried by later glacier advances, retains ^{10}Be and ^{26}Al concentrations that are inconsistent with surface exposure. Thus, neither glacial outwash or river sediment from glaciated regions is a good candidate for ^{10}Be– ^{26}Al burial dating. On the other hand, the ^{26}Al and ^{10}Be concentrations of river sand can likely be used to distinguish glacially- and nonglacially-derived sediment in many rivers.

2. *Paleosols.* ^{26}Al and ^{10}Be measurements on quartz in paleosols developed on tills and then buried by later glacier advances can be used to date the overlying units. This method is most successful for soils that developed over a long period of exposure and consequently have high nuclide concentrations: the higher the nuclide concentrations at the time of burial, the less important many of the methodological uncertainties become. In contrast to exposure dating techniques [Putkonen and Swanson, 2003], the accuracy of this technique is at present limited by analytical uncertainties in AMS measurement. This provides an incentive for further analytical improvements. As paleosols buried by later ice sheet advances are common in the stratigraphic record around the Laurentide Ice Sheet (and others), this method is widely applicable to dating and correlating Plio-Pleistocene glacial sediments.

3. *Contributions to regional glacial chronology.* We report several age determinations of regional interest in this paper. First, limiting ages derived from analyses of pre-Wisconsinan outwash and river sands from boreholes in the Minnesota River Valley indicate that the lower part of this section is 1.5-0.5 Myr old, which is older than we previously believed. Second, similar limiting ages in boreholes from the Prairie Coteau region of Minnesota and South Dakota indicate that the lower part of the till section here is greater than 1 Myr old. Also, analyses of river sand underlying the lowest till in the Prairie Coteau section indicate that this lowest till is 2-1.5 Myr old, and analyses of a paleosol interbedded with tills in this section suggest at least one ice sheet advance 1-1.2 Myr ago. Thus, the sequence of tills beneath the Prairie Coteau may contain a nearly complete record of late Pliocene through middle Pleistocene advances of the Laurentide Ice Sheet.

3.8 Maximum limiting ages from ^{26}Al *and* ^{10}Be *measurements*

Here we describe how ^{26}Al and ^{10}Be analyses of a sample at a particular depth can be used to infer maximum limiting ages for some portion of their overburden.

Equation 3.3 can be rearranged to yield:

$$t_b = -\frac{1}{\lambda_j} \log \left[\frac{\left(N_j - \frac{P_j(z)}{\lambda_j} \right)}{\left(N_{j,0} - \frac{P_j(z)}{\lambda_j} \right)} \right] \tag{3.11}$$

We measure the present nuclide concentrations in a sample N_j and seek to choose the parameters z and $N_{j,0}$ to maximize the burial time t_b. We can only evaluate this formula if N_j and $N_{j,0}$ are both greater than, or both less than, $P_j(z)/\lambda_j$, the steady-state value at depth z. This reflects the fact that the nuclide concentration must always approach, and cannot cross, the steady-state value. Here we consider only the case where both are greater than the steady-state value. Because t_b must be greater than zero, this assumption also requires that $N_{j,0} > N_j$, i.e. the initial nuclide concentration must be higher than the final nuclide concentration. Thus, if we have a a sample whose present depth is z^M and a unit of overburden whose top has present depth z^*, we can only use this approach to infer a maximum age for this unit of overburden if $P_j(z^M - z^*) > N_j^M \lambda_j$ for both j. It is important that we are not inferring a maximum age for a sample, but a maximum age for a portion of the overburden which lies above some critical depth z^{crit}, where $P_j(z^M - z^{crit}) = N_j^M \lambda_j$. Figure 3.8 shows this relationship. In order to maximize t_b, we note that:

$$\frac{\partial t_b}{\partial P_j(z)} = \frac{1}{\lambda_j^2} \left[\frac{1}{N_j - \frac{P_j(z)}{\lambda_j}} - \frac{1}{N_{j,0} - \frac{P_j(z)}{\lambda_j}} \right] \tag{3.12}$$

and

$$\frac{\partial t_b}{\partial N_{j,0}} = \frac{1}{\lambda_j \left(N_{j,0} - \frac{P(z)}{\lambda_j} \right)} \tag{3.13}$$

First, if $N_j > P_j(z)/\lambda_j$ and $N_{j,0} > N_j$ (as we have assumed above), $\partial t_b / \partial N_{j,0}(z) > 0$ always. As expected, to maximize the burial time t_b we should choose the maximum possible initial nuclide concentration $N_{j,0}$.

Second, $N_j > P_j(z)/\lambda_j$ and $N_{j,0} > N_j$ also imply that $\partial t_b / \partial P_j(z) > 0$ always. This means that to maximize t_b we should choose the maximum possible $P(z)$, *i.e.* the minimum depth that the sample could have been buried at after deposition of the unit at depth z^*. This minimum depth

is $z^M - z^*$. In effect, we are assuming that all of the overburden above the unit of interest was deposited instantaneously just before the present time, thus choosing the minimum possible burial depth for the sample since deposition of the unit of interest. The fact that the unit of overburden still exists shows that the sample could not have been less deeply buried since the deposition of that unit. Furthermore, we choose muon interaction cross-sections appropriately to yield the maximum $P_j(z)$.

We measure two nuclides j, so once we have chosen $z = z^M - z^*$, the choice of the $N_{j,0}$ is constrained by the relationship of the λ_j, *i.e.*, nuclide concentrations must have followed a burial trajectory defined by the production rates at the chosen burial depth, and the choice of nuclide concentrations that maximizes t_b is defined by the intersection of that burial trajectory with the simple exposure line. We obtain this maximum age, t_b^{max}, by solving the system of three equations consisting of Equation 3.3 written for both ^{10}Be and ^{26}Al and Equation 3.6.

Thus, each sample allows us to calculate a maximum limiting age for any unit of overburden whose top is above the critical depth z^{crit}. The unit whose top is at the critical depth z^{crit}, as the measured nuclide concentration is at steady state relative to that depth, could be infinitely old. The age of units higher up in the section is more closely limited, and the maximum age for units high up in the section asymptotically approaches the burial age for the sample calculated assuming initial nuclide concentrations on the simple exposure line and burial at infinite depth (Figure 3.8). If there are multiple samples in a single borehole, a maximum age calculated for a particular unit relative to a particular sample must also apply to all units above it according to the principle of superposition: thus, the maximum age limits for complete boreholes in Figure 3.8 reflect the combination of several maximum age-depth curves such as those shown in Figure 3.8. We have not taken analytical error into account in generating the maximum age limits in Figure 3.8.

Table 3.2: ^{26}Al and ^{10}Be concentrations in pre-Wisconsinan fluvial sands and outwash in boreholes. In this and subsequent tables, ^{10}Be concentrations are reported relative to LLNL internal standards, which are traceable to the ICN ^{10}Be standard. ^{26}Al concentrations are reported relative to LLNL internal standards. Uncertainties are reported at $\pm 1\sigma$ and include all known sources of analytical error. Blank corrections are described in the text.

Sample name	Borehole	Depth (m)	[^{10}Be] (10^4 atoms $\cdot$ g^{-1})	[^{26}Al] (10^4 atoms $\cdot$ g^{-1})
UMRB-1-62	UMRB-1	18.9	7.3 ± 0.23	27.38 ± 1.72
UMRB-1-75	UMRB-1	22.9	9.69 ± 0.22	39.34 ± 3.07
UMRB-1-97	UMRB-1	29.6	10.35 ± 0.29	39.4 ± 2.40
UMRB-1-100*	UMRB-1	30.5	7.87 ± 0.17	25.39 ± 1.11
UMRB-1-159	UMRB-1	48.5	10.19 ± 0.28	31.85 ± 1.66
UMRB-1-192	UMRB-1	58.5	11.6 ± 0.55	38.29 ± 1.75
UMRB-1-216	UMRB-1	65.9	10.56 ± 0.31	33.88 ± 2.11
UMRB-2-149	UMRB-2	45.4	5.3 ± 0.16	17.58 ± 2.29
UMRB-2-168	UMRB-2	51.2	6.31 ± 0.18	25.82 ± 1.67
UMRB-2-185	UMRB-2	56.4	6.15 ± 0.24	24.02 ± 1.71
UMRB-2-201F	UMRB-2	61.3	4.07 ± 0.15	20.56 ± 1.81
UMRB-2-207	UMRB-2	63.1	4.81 ± 0.18	18.52 ± 5.74
UMRB-2-209	UMRB-2	63.7	4.38 ± 0.23	17.02 ± 1.39
UMRB-3-49	UMRB-3	14.9	5.54 ± 0.18	22.47 ± 1.54
UMRB-3-52	UMRB-3	15.9	5.64 ± 0.17	25.67 ± 1.64
UMRB-3-127	UMRB-3	38.7	6.25 ± 0.16	22.53 ± 1.31
UMRB-3-138	UMRB-3	42.1	6.4 ± 0.19	20.91 ± 1.52
UMRB-3-150C	UMRB-3	45.7	3.59 ± 0.14	14.73 ± 1.00
UMRB-3-165	UMRB-3	50.3	3.79 ± 0.13	12.81 ± 1.19

continued on next page

Table 3.2: *continued*

Sample name	Borehole	Depth (m)	[^{10}Be] (10^4 atoms $\cdot$ g^{-1})	[^{26}Al] (10^4 atoms $\cdot$ g^{-1})
UMRB-3-168C	UMRB-3	51.2	2.64 ± 0.14	8.92 ± 0.95
SWRA-3-196	SWRA-3	59.8	6.74 ± 0.19	18.44 ± 1.54
SWRA-3-205	SWRA-3	62.5	6.45 ± 0.19	18.96 ± 1.25
SWRA-3-241	SWRA-3	73.5	6.5 ± 0.19	14.55 ± 1.05
SDBR-305M	SD-BR	93.0	14.64 ± 0.42	39.87 ± 2.33
SD-CO-402	SD-CO	122.6	13.89 ± 0.4	35.36 ± 2.79
SD-CO-406	SD-CO	123.8	12.49 ± 0.53	38.16 ± 2.33

* Mean of two analyses

Table 3.1: Locations and nuclide production rates for boreholes and excavations mentioned in text. Production rates calculated according to Stone [2000].

Designation (in this work)	Latitude	Longitude	Wellhead elevation (m)	Approx. nuclide production rates in quartz at surface (atoms $\cdot$ g^{-1} $\cdot$ yr^{-1}) ^{10}Be	^{26}Al	Reference
UMRB-1	44.8970 N	96.4125 W	358	6.9	42.3	Patterson [1999]
UMRB-2	45.3823 N	96.3467 W	335	6.8	41.7	Patterson [1999]
UMRB-3	45.3012 N	95.7066 W	334	6.8	41.6	Patterson [1999]
SWRA-3	44.0821 N	96.3888 W	529	8.0	48.6	Setterholm [1995]
SD-BR	44.3478 N	96.7175 W	507	7.8	47.9	Lineburg [1993]
SD-CO	45.0186 N	97.1847 W	547	8.2	49.9	S.D. Geol. Surv., unpub. data
4-A-75	40.6819 N	94.1144 W	347	6.6	40.1	Boellstorff [1978a]
5-A-75	40.9983 N	94.2000 W	354	6.6	40.5	Boellstorff [1978a]
1-A-76	41.2225 N	97.0992 W	494	7.5	45.7	Boellstorff [1978a]
17-A-76	41.2303 N	94.7936 W	396	6.9	42.1	Boellstorff [1978a]
3-B-99	41.4908 N	96.2129 W	398	6.9	42.3	Mason [2001]
Kraft site	41.8616 N	95.9925 W	332	6.6	40.1	Bettis III [1990]

Table 3.3: Location of samples of modern river sediment and Wisconsinan glacial deposits.

Designation (in this work)	Latitude	Longitude	elevation (m)	Description
RWT-01	44.6750 N	95.2828 W	306	Gravel pit near Granite Falls, MN, in terrace of glacial River Warren
MNR-01	44.5297 N	95.9019 W	218	Channel of Minnesota River
MNR-02	44.6950 N	95.3403 W	261	”
YMR-01	44.7389 N	95.4294 W	264	Channel of Yellow Medicine River
02-TILL-005-PLA	41.4092 N	96.5176 W	365	Channel of Platte River
02-TILL-008-VERM	42.8033 N	96.9509 W	361	Channel of Vermilion River

Table 3.4: ^{26}Al and ^{10}Be concentrations in modern river sands.

Sample name	[^{10}Be] (10^4 atoms $\cdot$ g^{-1})	[^{26}Al] (10^4 atoms $\cdot$ g^{-1})	Description
MNR-01	5.15 $\pm$ 0.17	23.27 $\pm$ 2	Minnesota River, MN
MNR-02	6.11 $\pm$ 0.18	25.1 $\pm$ 1.95	Minnesota River, MN
YMR-01	6.78 $\pm$ 0.25	29.01 $\pm$ 1.8	Yellow Medicine River, MN
02-TILL-005-PLA	24.02 $\pm$ 0.84	97.6 $\pm$ 5.58	Platte River, NB
02-TILL-008-VERM	11.42 $\pm$ 0.42	43.4 $\pm$ 2.82	Vermilion River, SD

Table 3.5: ^{26}Al and ^{10}Be concentrations in Wisconsinan glacial sediment in southwest Minnesota and adjacent South Dakota.

Sample name	[^{10}Be] (10^4 atoms $\cdot$ g^{-1})	[^{26}Al] (10^4 atoms $\cdot$ g^{-1})	Description
UMRB-3-11	5.47 $\pm$ 0.18	22.71 $\pm$ 1.55	Late Wisconsinan glaciolacustrine silt at 3.4 m in core UMRB-3
UMRB-3-16	5.23 $\pm$ 0.18	23.32 $\pm$ 1.4	Same, at 4.9 m depth
RWT-01	7.01 $\pm$ 0.2	31.25 $\pm$ 1.62	Late Wisconsinan outwash from terrace of glacial River Warren
SD-CO-43	6.88 $\pm$ 0.27	31.64 $\pm$ 1.62	Wisconsinan till at 13.1 m depth in borehole SD-CO

Table 3.6: ^{26}Al and ^{10}Be concentrations in pre-Wisconsinan samples of known age.

Sample name	Borehole	Depth (m)	[^{10}Be] (10^4 atoms $\cdot$ g^{-1})	[^{26}Al] (10^4 atoms $\cdot$ g^{-1})	Description
5-A-75-167*	5-A-75	50.9	7.84 ± 0.2	23.1 ± 1.09	Paleosol
17-A-76-146*	17-A-76	44.5	14.8 ± 0.37	40.3 ± 1.99	Paleosol
4-A-75-107	4-A-75	32.6	18.02 ± 0.54	65.65 ± 2.33	Sand and silt
1-A-76-204	1-A-76	62.2	25.27 ± 0.67	58.57 ± 3.35	Sand and silt
02-TILL-000-KRA	n/a	n/a	9.12 ± 0.38	30.02 ± 1.68	Sand and gravel 1.5 m above Lava Creek ash
02-TILL-002-KRA	n/a	n/a	5.05 ± 0.24	18.42 ± 1.32	Sand and gravel immediately below ash
02-TILL-003-KRA	n/a	n/a	4.41 ± 0.24	15.55 ± 1.85	Sand and gravel 15 cm below ash
02-TILL-004-KRA	n/a	n/a	6.31 ± 0.31	14.96 ± 1.01	Sand and gravel 30 cm below ash

* Mean of two analyses

Table 3.7: Location of surface soil samples. Production rates calculated according to Stone [2000].

Designation (in this work)	Latitude	Longitude	elevation (m)	Approx. nuclide production rates at surface in quartz (atoms $\cdot$ g^{-1} $\cdot$ yr^{-1}) ^{10}Be	^{26}Al	Description
MN-SAL	44.5575 N	93.8749 W	277	6.4	39.2	Road cut, Salisbury, MN
02-TILL-006-GRA	44.0516 N	96.2852 W	558	8.2	49.8	Soil pit, Grange, MN
02-TILL-007-PIT	44.0980 N	96.3380 W	527	8.0	48.5	Excavation,Grange, MN

Table 3.8: ^{26}Al and ^{10}Be concentrations in surface soil samples.

Sample name	[^{10}Be] (10^4 atoms $\cdot$ g^{-1})	[^{26}Al] (10^4 atoms $\cdot$ g^{-1})	Description
MN-SAL-20	15.95 ± 0.57	56.16 ± 2.35	Upper 20 cm of soil on Wisconsinan till
02-TILL-006-GRA	12.6 ± 0.36	70.12 ± 2.32	Surface sample of soil on pre-Wisconsinan till
02-TILL-007-PIT	17.85 ± 0.53	86.89 ± 2.32	Surface sample of soil on Wisconsinan outwash
SD-CO-4	14.36 ± 0.4	71.99 ± 2.89	Soil on Wisconsinan till at 1.3 m depth in borehole SD-CO

Table 3.9: Sample depths and nuclide concentrations, paleosol at 26 m in borehole 3-B-99. This table reproduces data previously reported in Balco et al. [2004b in review].

Sample name	Borehole depth(m)	Depth below soil surface ($g \cdot cm^{-2}$)	^{10}Be (10^4 atoms $\cdot g^{-1}$)	^{26}Al (10^4 atoms $\cdot g^{-1}$)
3-B-99-87	26.01-26.31	0-58	31.88 ±1.08	133.8 ± 4.3
3-B-99-88	26.31-26.62	58-117	26.83 ± 0.93	112.7 ± 3.3
3-B-99-89	26.62-26.92	117-175	19.75 ± 0.58	85.6 ± 3.8
3-B-99-90	27.07-27.23	204-234	16.14 ± 0.49	67.6 ± 3.5
3-B-99-91	27.32-27.46	234-278	15.75 ± 0.47	57.9 ± 2.1
3-B-99-93*	27.76-28.14	336-410	11.92 ±0.28	48.7 ± 1.9

*Mean of two analyses

Table 3.10: Sample depths and nuclide concentrations, paleosol at 104.7 m depth in borehole SD-CO.

Sample name	Borehole depth (m)	Depth below till surface $z_{i,0}$ ($g \cdot cm^{-2}$)	[^{10}Be] (10^4 atoms $\cdot g^{-1}$)	[^{26}Al] (10^4 atoms $\cdot g^{-1}$)
SD-CO-344	104.7-105.0	0-58	7.28 ± 0.44	27.8 ± 2.0
SD-CO-351	107.0-107.3	434-492	5.48 ± 0.28	22.1 ± 0.4
SD-CO-354	107.9-108.2	608-666	6.71 ± 0.27	20.5 ± 1.6

Table 3.11: Modal ages derived from Monte Carlo simulations, for till unit overlying paleosol at 104.5 m in borehole SD-CO, calculated with bracketing assumptions for burial depths and nuclide production by muons. Figure 3.16 shows the corresponding error analysis.

	Muon cross-sections	
	Stone	Heisinger
$z_1 = 18,500$ g $\cdot$ cm^{-2}	0.91 Myr	0.92 Myr
$z_1 = 4300$ g $\cdot$ cm^{-2}	1.29 Myr	1.45 Myr

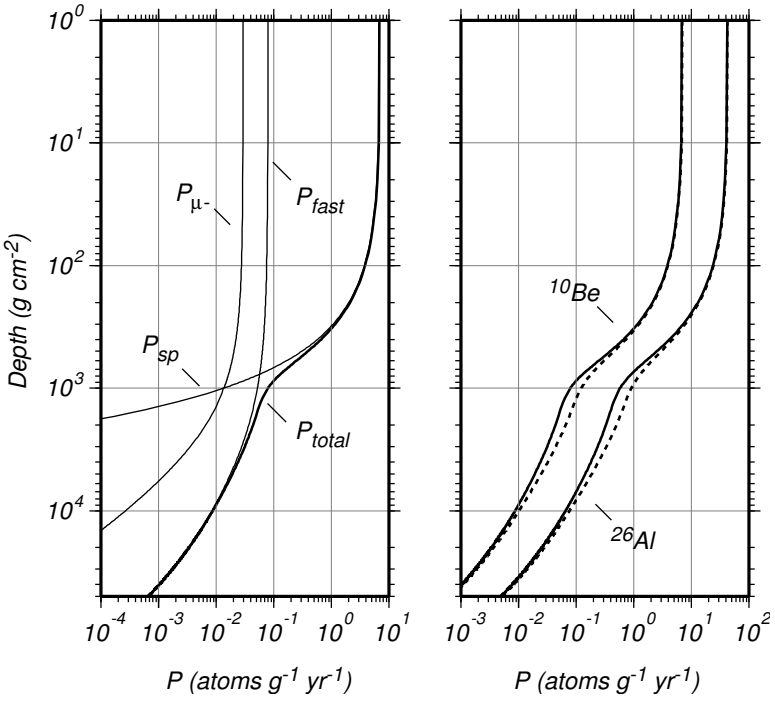

Figure 3.1: Depth dependence of ^{26}Al and ^{10}Be production rates. Left panel, contribution of spallation (P_{sp}), negative muon capture ($P_{\mu-}$), and fast muon interactions (P_{fast}) to ^{10}Be production in quartz. Surface production rate of ^{10}Be by spallation assumed to be 7 atoms $\cdot$ g^{-1} $\cdot$ yr^{-1}. P_{fast} and $P_{\mu-}$ are calculated using muon interaction cross-sections inferred from measurements at Wyangla quarry, Australia, as described in text (J. Stone, unpublished data). Right panel, effect of uncertainty in muon interaction cross-sections on total production rates of ^{10}Be and ^{26}Al. Solid lines, Wyangla quarry cross-sections; dashed lines, cross-sections from [Heisinger et al., 2002b,a].

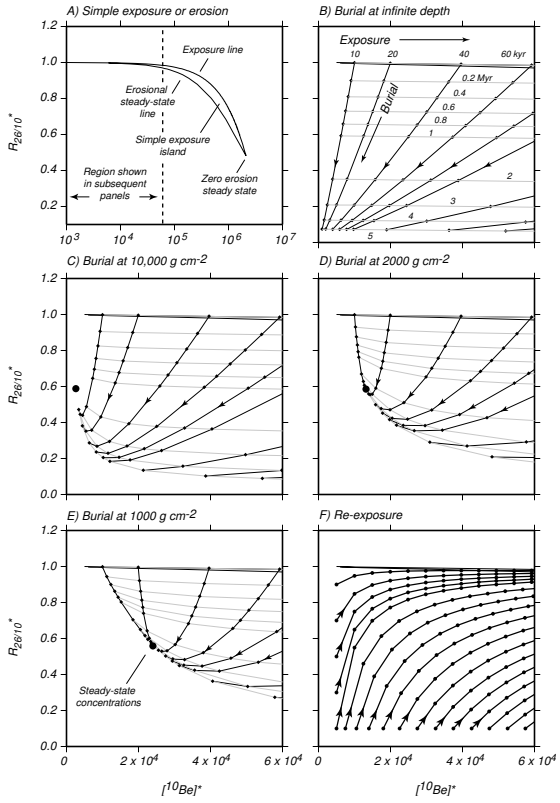

Figure 3.2: Effect of surface exposure, burial, and re-exposure on ^{10}Be and ^{26}Al concentrations. In this and subsequent diagrams, the superscripted star indicates that measured nuclide concentrations have been normalized to the surface production rates of each nuclide. That is, $[^{10}\mathrm{Be}]^* = N_{10}/P_{10}(0)$, where N_{10} is the measured concentration of ^{10}Be (atoms $\cdot$ g^{-1}) and $P_{10}(0)$ is the surface production rate of ^{10}Be at the sample location (atoms $\cdot$ g^{-1} $\cdot$ yr^{-1}). $[^{10}\mathrm{Be}]^*$ has units of yr. The normalized ^{26}Al/^{10}Be ratio $R^*_{26/10}$ is equal to R/R_0, where R is the measured ^{26}Al/^{10}Be ratio in a sample and R_0 is the surface production ratio ($R_0 = 6.1$). A), the simple exposure island of Lal [1991], that is, the region of nuclide concentrations consistent with surface exposure that can be generated by Equation 3.2. B), nuclide concentrations expected after a single period of surface exposure and a single period of burial at infinite depth. Dark lines show burial trajectories; light lines show burial isochrons. Note change from semi-logarithmic to linear axes. C), D), and E), burial trajectories and isochrons for a single period of surface exposure and a single period of burial at 10,000, 2000, and 1000 g $\cdot$ cm^{-2} respectively. Black circles denote steady-state nuclide concentrations at the respective depths. We used subsurface production rates generated with the Wyangla quarry muon interaction cross-sections (Figure 3.1) to construct these diagrams. F), re-exposure trajectories. If a sample with nuclide concentrations outside the simple exposure island is re-exposed at the surface, its nuclide concentrations will progress upward and to the right along the dark lines. Black dots indicate 5,000-yr increments of exposure time.

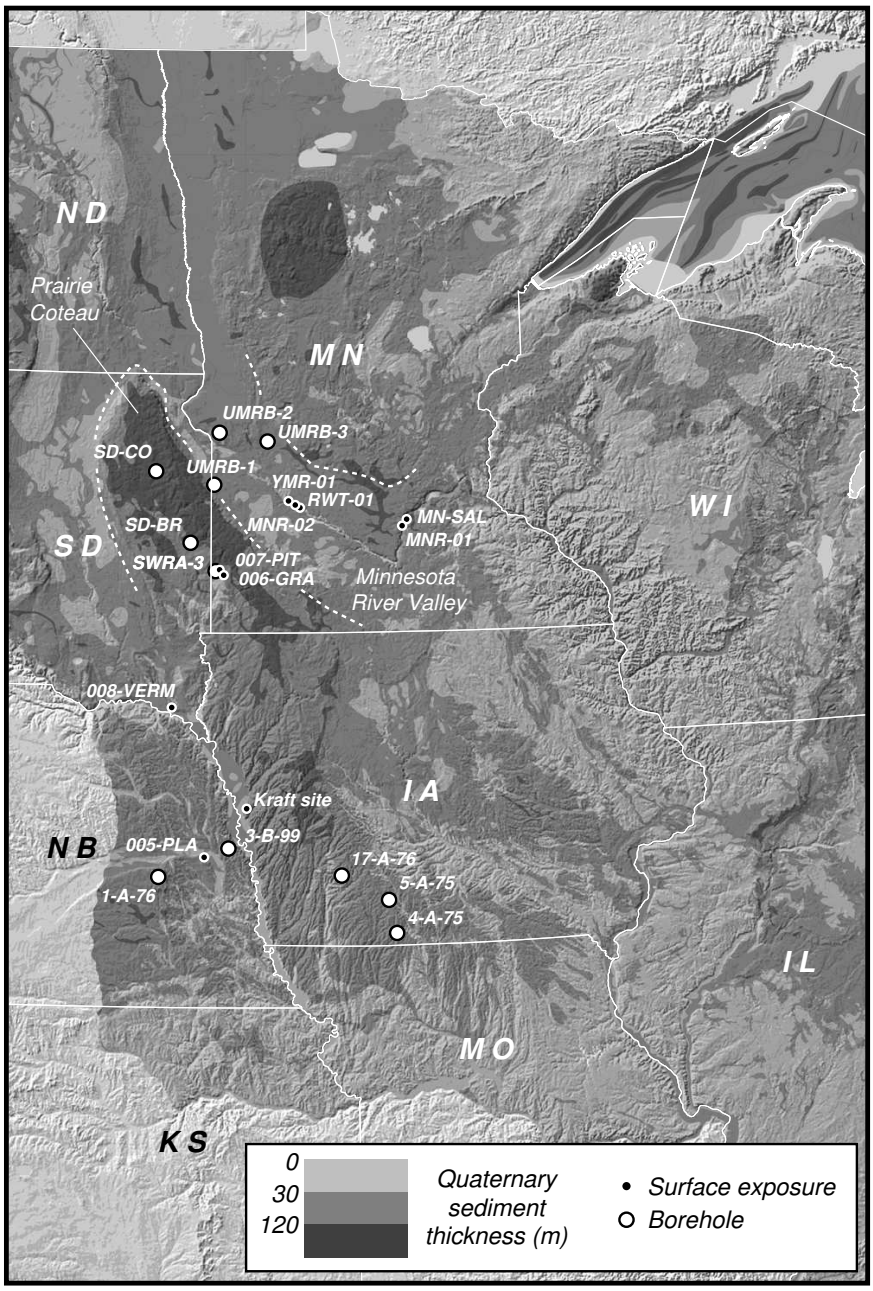

Figure 3.3: Locations of boreholes and other samples discussed in text. Background shows shaded relief overlain by total Quaternary sediment thickness, for areas within the U.S., from Soller and Packard [1998].

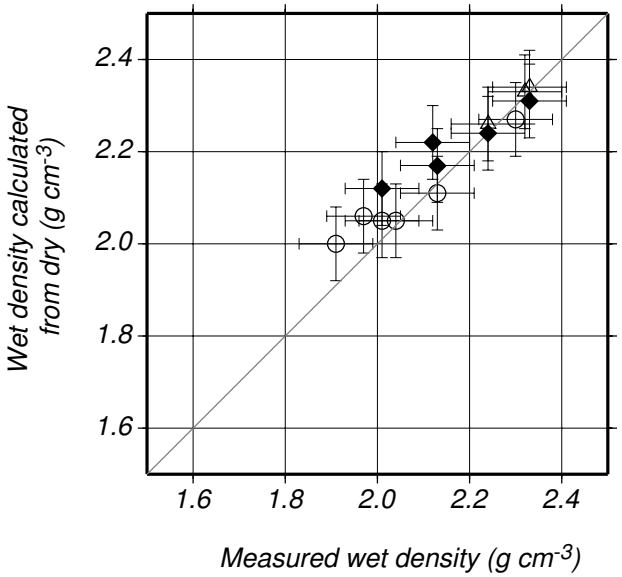

Figure 3.4: Comparison of measured wet bulk densities, with wet densities calculated from dry density measurements using Equation 3.9. Open circles, unconsolidated sand collected dry from drill core and then resaturated. Solid diamonds, till collected wet in the field and then dried. Open diamonds, till collected dry from drill core and then resaturated.

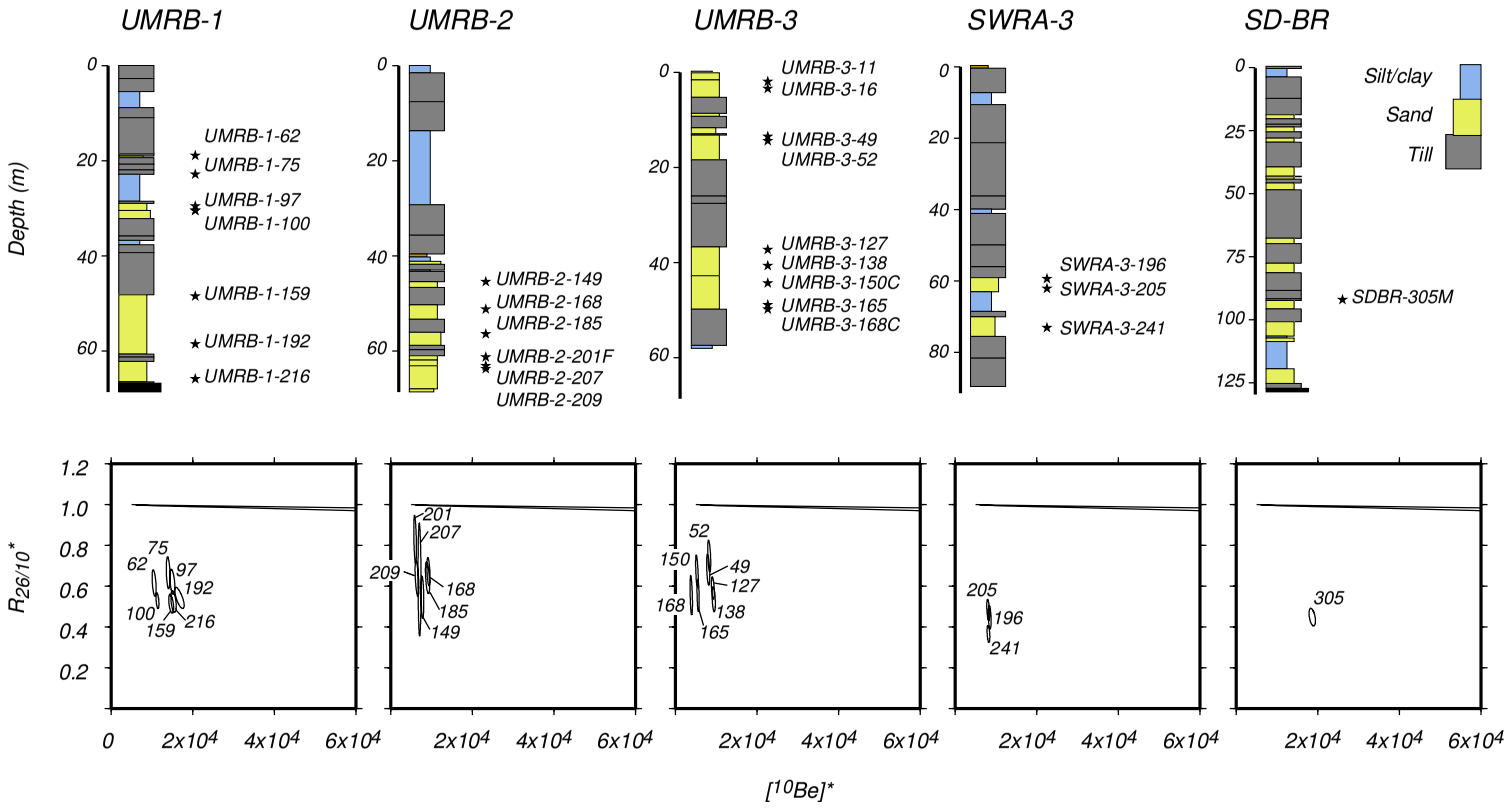

Figure 3.5: Stratigraphic context of pre-Wisconsinan fluvial sand and outwash samples. Stars and accompanying sample names indicate locations of samples in boreholes. Lower panels show 68% confidence ellipses for ^{10}Be and ^{26}Al analyses on the same axes as Figures 3.2B-3.2F. Figure 3.3 shows location of boreholes.

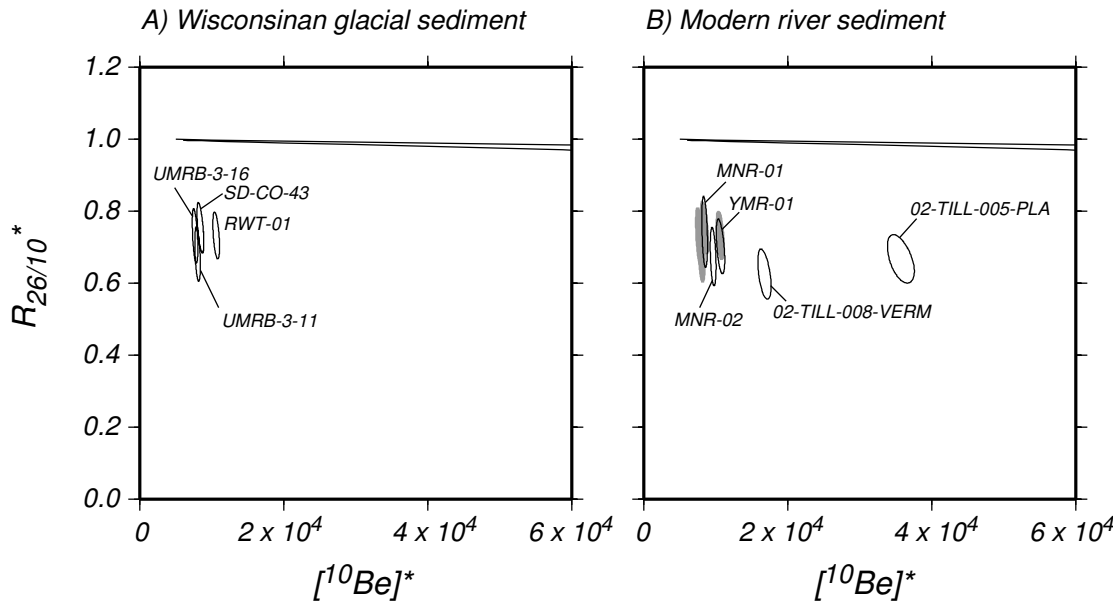

Figure 3.6: A), ^{26}Al and ^{10}Be concentrations in Wisconsinan glacial sediment from southwest Minnesota and adjacent South Dakota. UMRB-3-11 and -16 are samples of glaciolacustrine sand and silt from borehole UMRB-3; RWT-01 is a sample of sandy outwash from a terrace of the glacial River Warren; and SD-CO-43 consists of quartz extracted from the uppermost till in borehole SD-CO. Figure 3.3 shows sample locations. B), ^{26}Al and ^{10}Be concentrations in modern river sands. Figure 3.3 shows sample locations. Data from A) are reproduced in gray to highlight the close agreement between nuclide concentrations in Wisconsinan glacial sediment and modern river sand from the Minnesota River Valley. Measured nuclide concentrations in this figure have been normalized to typical regional surface production rates of 7 and 42.5 atoms $\cdot$ g^{-1} $\cdot$ yr^{-1}for ^{10}Be and ^{26}Al respectively.

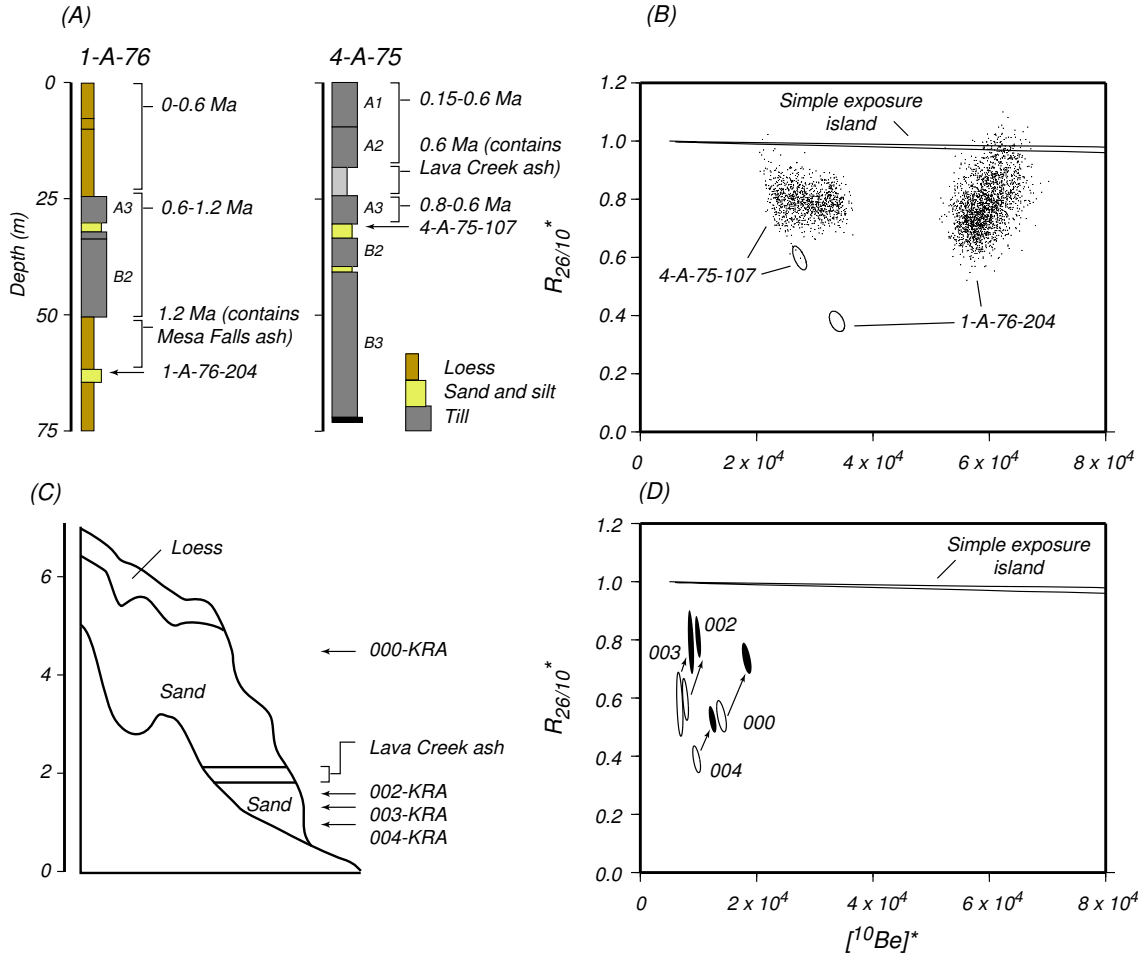

Figure 3.7: ^{26}Al and ^{10}Be concentrations at time of burial inferred from samples of fluvial sediment of approximately known age. A), stratigraphy of boreholes 1-A-76 and 4-A-75 [Boellstorff, 1978a], showing age constraints on units overlying our samples. samples from boreholes 4-A-75 and 1-A-76. B), measured nuclide concentrations in samples (68 % confidence ellipses) and possible nuclide concentrations at the time of burial (dots) generated from Monte Carlo simulation described in text. C), diagrammatic stratigraphy of Kraft exposure of Lava Creek ash showing sample locations relative to the ash [Bettis III, 1990]. D), measured nuclide concentrations in samples from Kraft site (unfilled ellipses) and inferred nuclide concentrations at the time of burial, calculated as described in text.

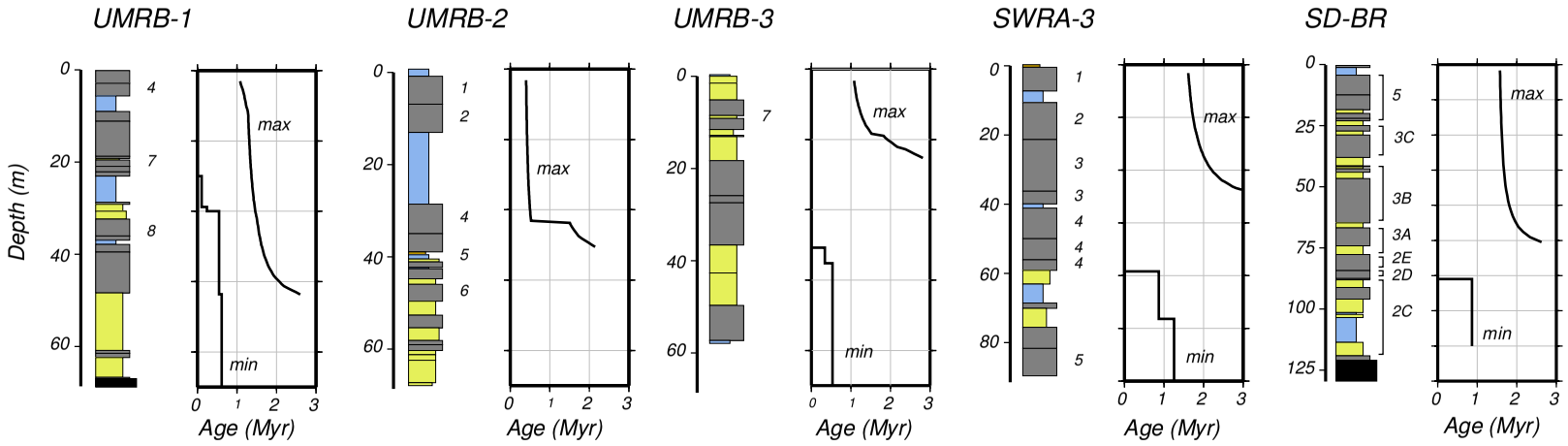

Figure 3.8: Minimum and maximum limiting age models inferred from ^{26}Al and ^{10}Be measurements for boreholes that contained pre-Wisconsinan sand samples, calculated as described in Section 3.5.4 and Appendix 3.8. Lithologic symbols are the same as those in Figure 3.5. Numbers for till units in boreholes UMRB-1, -2, and -3 follow Patterson [1999], those in SWRA-3 follow Patterson [1997], and those in SD-BR follow Lineburg [1993].

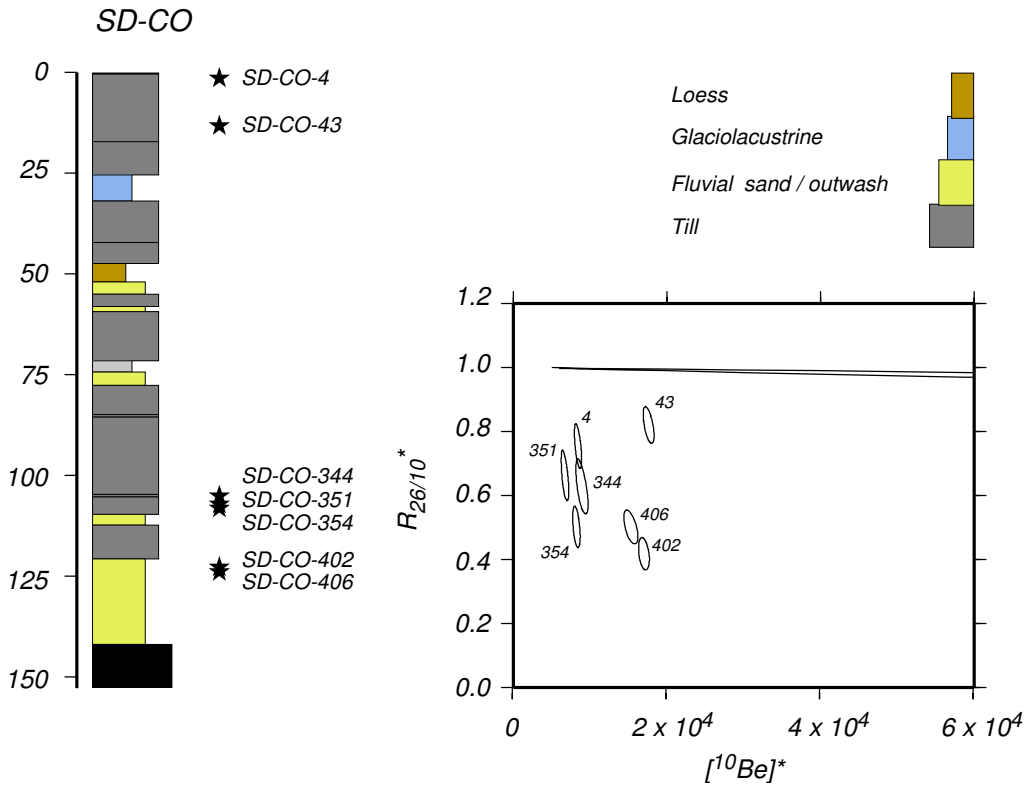

Figure 3.9: Stratigraphy and analytical data for borehole SD-CO. Left panel, borehole stratigraphy. Stars and accompanying sample names denote sample locations in boreholes. Right panel, nuclide concentrations in these samples.

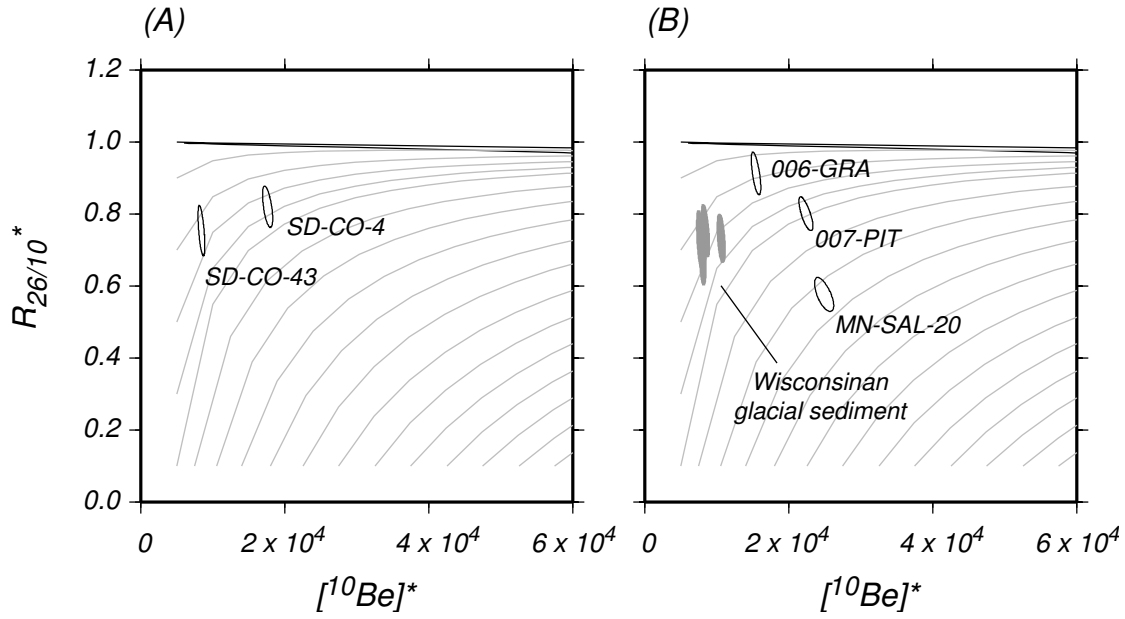

Figure 3.10: Nuclide concentrations in quartz from modern surface soils in southwest Minnesota and adjacent South Dakota. A), nuclide concentrations in a near-surface sample (SD-CO-4) and a sample from 13 m depth (SD-CO-43) in the uppermost (Wisconsinan) till from borehole SD-CO in eastern South Dakota. The excess ^{10}Be and ^{26}Al in the surface sample are the result of exposure since deposition of the till. Light lines in background are resetting curves from Figure 3.2F. B), nuclide concentrations in quartz from soils in southwest Minnesota. Light lines in background are resetting curves from Figure 3.2F. Gray ellipses are nuclide concentrations in nearby Wisconsinan glacial sediments from Figure 3.6.

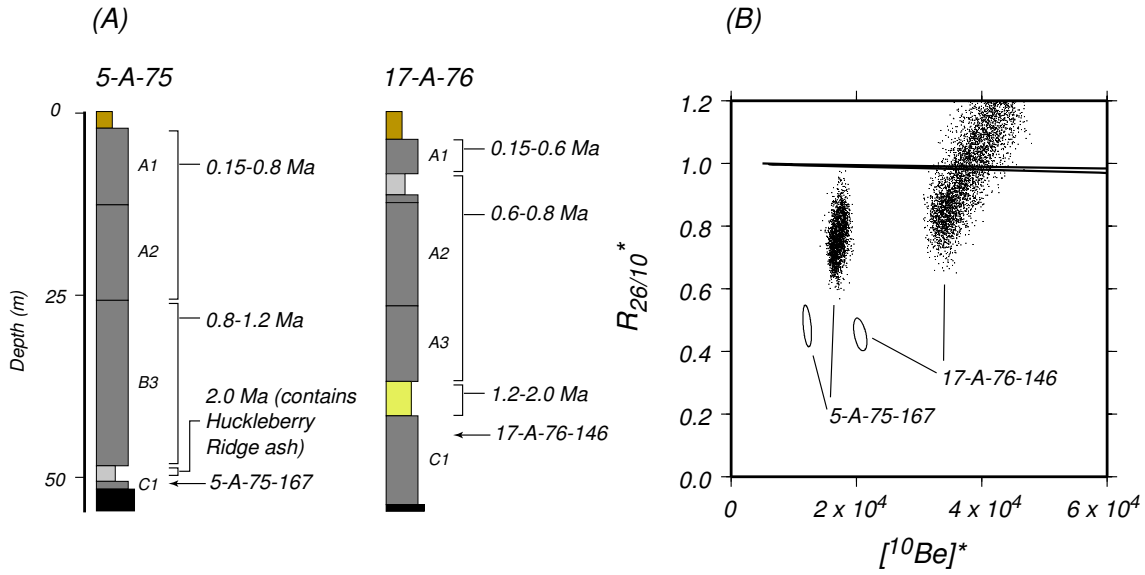

Figure 3.11: A). stratigraphy of boreholes 5-A-75 and 17-A-76, showing age constraints for units overlying our samples [Boellstorff, 1978a]. B), measured nuclide concentrations in samples (68 % confidence ellipses) and possible nuclide concentrations at the time of burial (dots) generated from Monte Carlo simulation described in text. Inferred nuclide concentrations at the time of burial that have $R^*_{26/10} > 1$ indicate that the corresponding burial histories cannot be correct even though they fit the independent age constraints; however, we have retained them to show that the probability distribution is centered on the simple exposure island.

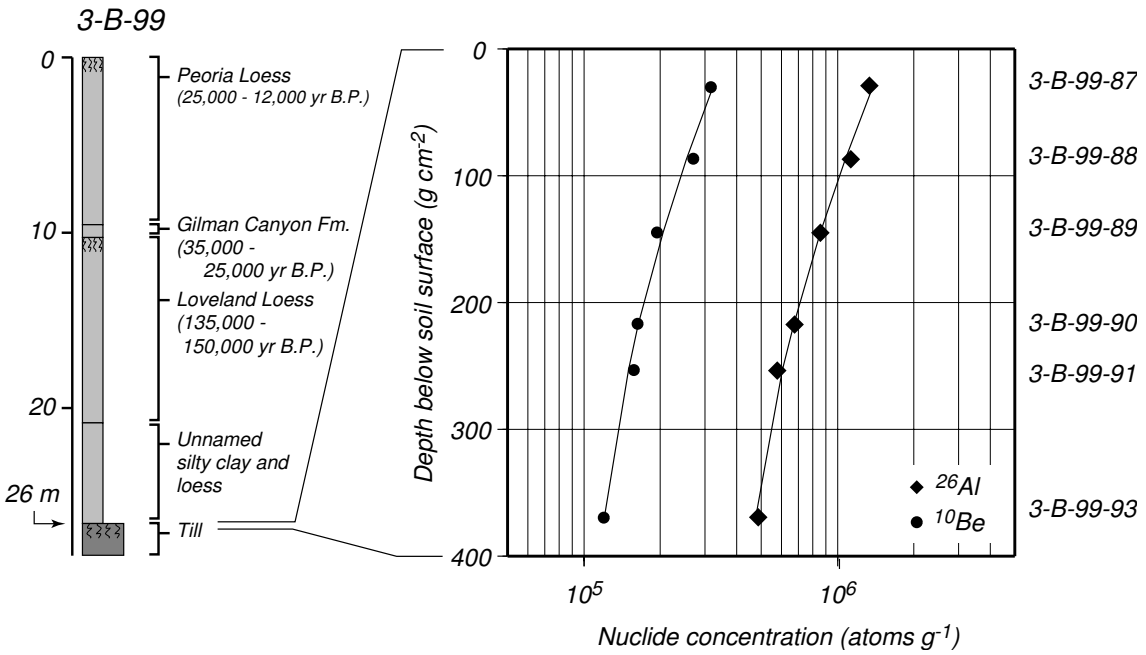

Figure 3.12: Left panel, stratigraphy of borehole 3-B-99 from eastern Nebraska. Right panel, ^{26}Al and ^{10}Be concentrations in quartz samples from paleosol at 26 m depth in borehole. Analytical errors are smaller than the symbols used to plot the data at this scale. Lines show nuclide concentrations predicted by best-fit burial history described in the text. These data are also reported in Balco et al. [2004b in review].

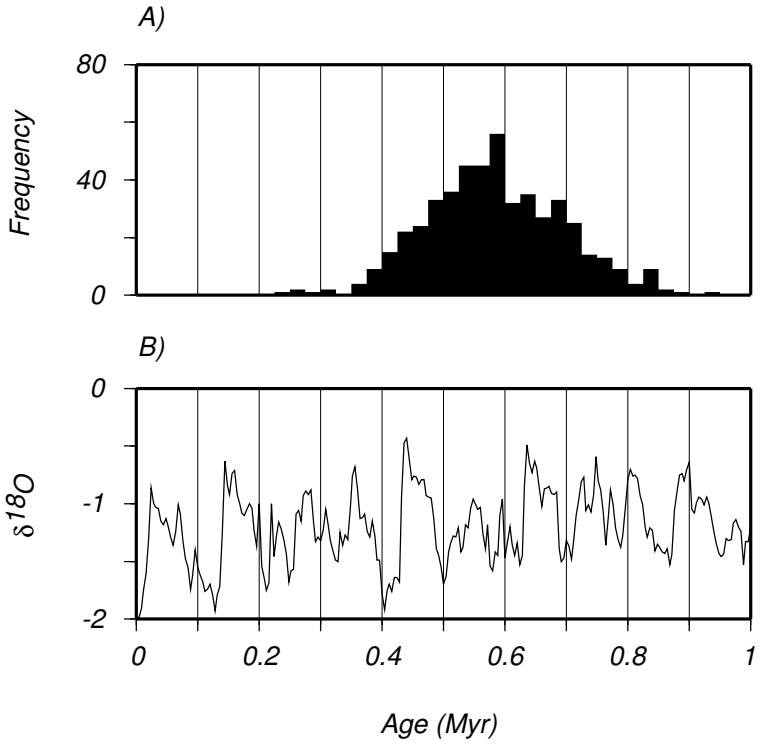

Figure 3.13: Error analysis for the age of the lowermost loess unit in borehole 3-B-99. A), probability distribution of best-fit ages generated by the Monte Carlo simulation described in the text. B), benthic δ^{18}O record from ODP core 806 [Berger et al., 1993]. This figure duplicates Figure 4 in Balco et al. [2004b in review].

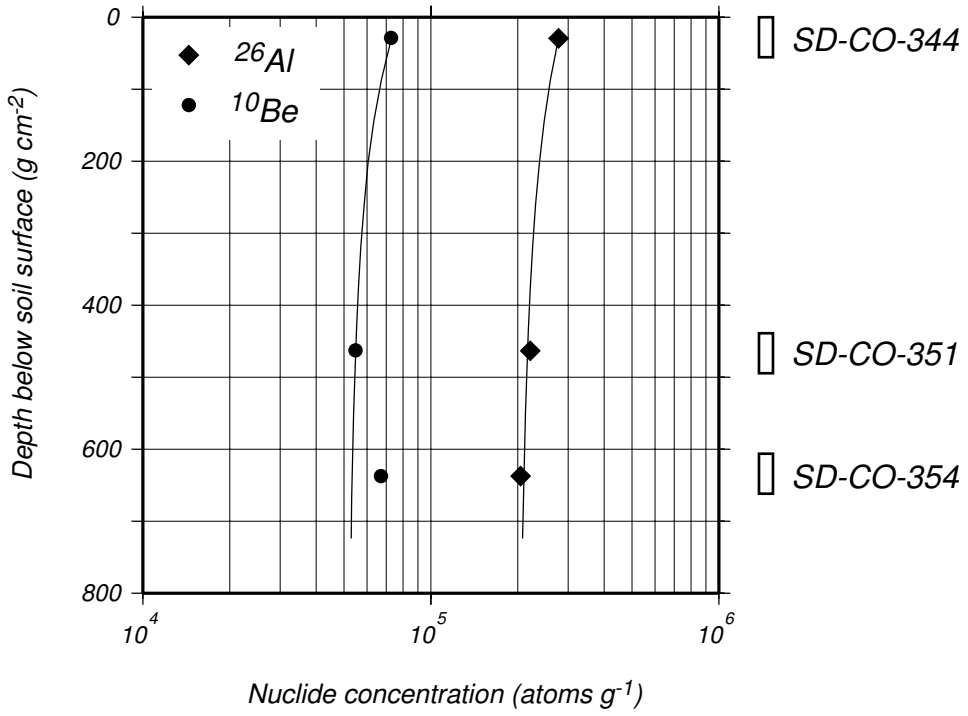

Figure 3.14: ^{26}Al and ^{10}Be concentrations in quartz from the paleosol at 103.8 m depth in borehole SD-CO. Analytical errors are smaller than the symbols used to plot the data at this scale. Boxes at right show length of core that we agglomerated to obtain each quartz sample. The lines show nuclide concentrations predicted by the best-fit burial history described in the text. We excluded the ^{10}Be measurement for SD-CO-354 in computing the fit, as described in the text.

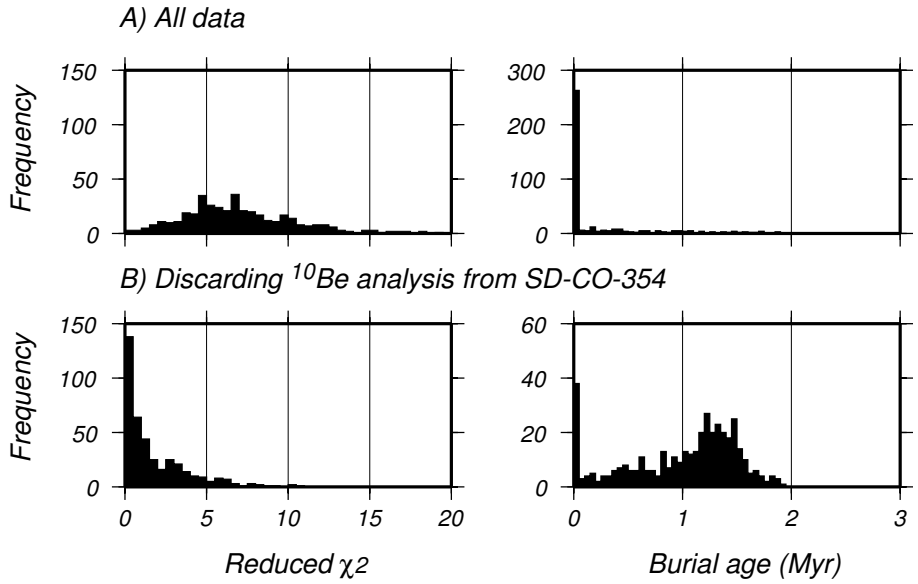

Figure 3.15: Error analysis for burial age of paleosol in borehole SD-CO, part I. Histograms show probability distributions for reduced χ^2 goodness-of-fit statistic (at left) and best-fit burial ages (at right) for exposure models generated by Monte Carlo analysis. A), all nuclide measurements included. The best-fit burial age is near zero but the fit to the data is unacceptable. B), omitting ^{10}Be measurement from SD-CO-354. Plausible burial ages near 1.3 Myr yield good ($\chi^2 \leq 1$) fits to the data. The muon cross-sections of Stone (unpublished data) and $Z_1 = 4300$ g $\cdot$ cm^{-2} were used in the calculation.

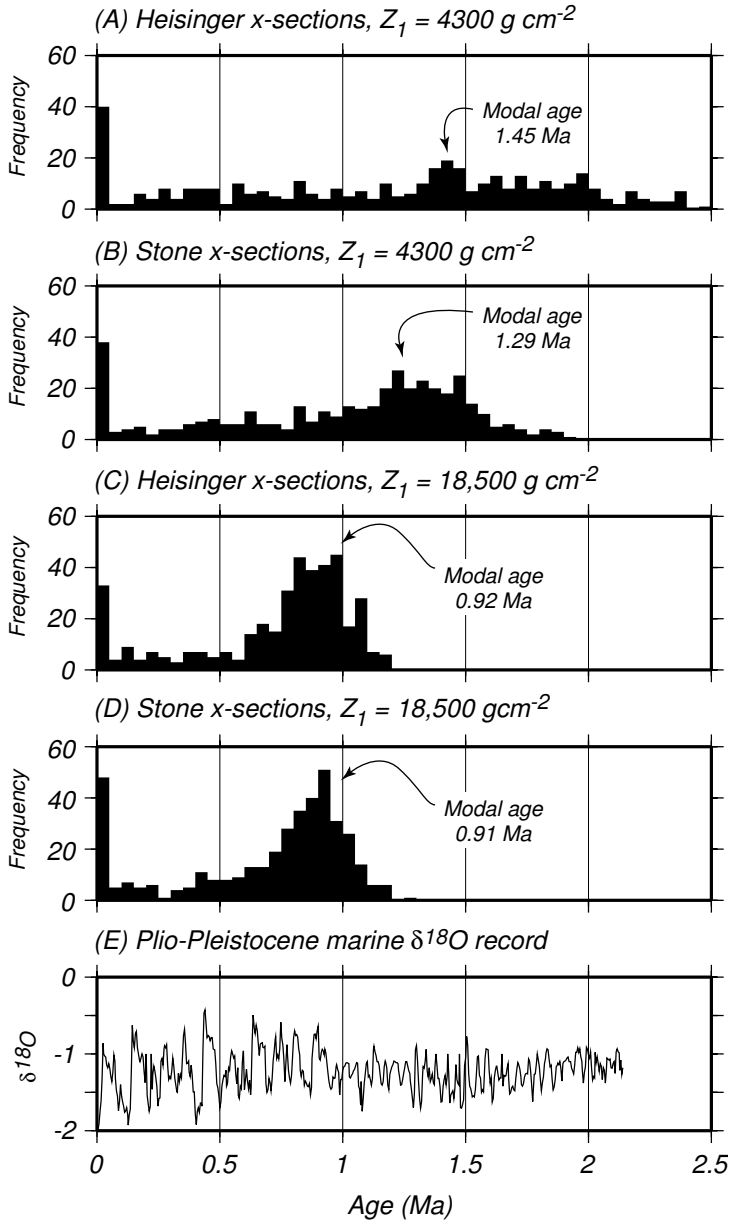

Figure 3.16: Error analysis for burial age of paleosol in borehole SD-CO, part II. Histograms A)-D) show results of Monte Carlo error analyses for bracketing assumptions about initial burial depth and muon interaction cross-sections. C) shows δ^{18}O record from core ODP 806 [Berger et al., 1993].

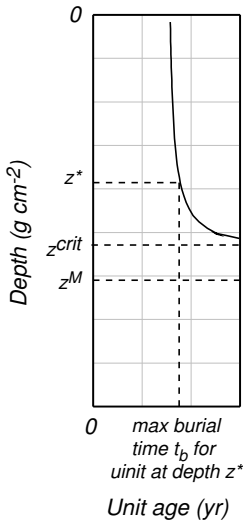

Figure 3.17: Diagram showing the relationship between maximum possible age of portions of the overburden and their depth relative to a particular sample.

Chapter 4

FATE OF THE PREGLACIAL REGOLITH BENEATH THE LAURENTIDE ICE SHEET

This chapter was submitted to the journal *Nature*. John Stone and Carrie Jennings were co-authors. Supplementary material that did not fit in the required format appears in Chapter 5.

4.1 Summary

Subglacial erosion and transport of deformable sediment influence the size, stability, and sensitvity to climate of large ice sheets. These processes may cause or sustain ice-sheet instabilities [MacAyeal, 1992], and perhaps dictate the periodicity of the Cenozoic ice ages [Clark and Pollard, 1998]. Subglacial erosion, however, is difficult to study. Where active at present, it is inherently difficult to observe, and, as with all eroding landscapes, the record of past events is effaced as the surface is removed. Here we use the cosmic-ray-produced radionuclide ^{10}Be, which is abundant in deeply weathered soils but absent in fresh bedrock, to investigate the sources of subglacial sediment exported from the Canadian Shield by the Laurentide Ice Sheet (LIS). We distinguish tills derived from erosion of fresh bedrock from those derived from regolith that predated glaciation. ^{10}Be-rich, regolith-derived till occurs only twice, first at the immediate onset of glaciation and then again in the middle Pleistocene during an apparent expansion of either the size of the ice sheet or the area of thawed-bed conditions.

4.2 Background

The streamlined and polished glacial landscapes of the northern continents have suggested to geologists of the last two centuries that erosion by Pleistocene glaciers has exhumed them from beneath hundreds of meters of crystalline bedrock. Flint [1947], on the other hand, calculated from the volume of terrestrial glacial sediment in North America that all of the Plio-Pleistocene advances of the LIS had accomplished only tens of meters of erosion of the Canadian Shield. White [1972] pointed out that this ignored sediment deposited in the oceans, and revised the estimate upward

once again; since then a large array of evidence has been marshaled to support one or the other of these positions [Bell and Laine, 1985, Sugden, 1976, 1978, 1989, Hall and Sugden, 1987, Kleman, 1994, Briner and Swanson, 1998, Bierman et al., 1999]. From our perspective the most important of this evidence concerns the morphologic similarity between glacially eroded surfaces and the chemical weathering front beneath deeply weathered, regolith-mantled terrains, and the numerous examples of surviving pre-glacial regolith in glaciated regions: these suggest that Plio-Pleistocene ice sheets may have done no more than remove a pre-existing blanket of deeply weathered regolith, the legacy of a temperate Tertiary climate acting on stable, low-relief cratonic surfaces over millions of years [Feininger, 1971, Lidmar-Bergstrom, 1988, 1997, Patterson and Boerboom, 1999].

This idea is relevant to paleoclimate studies because of the importance of subglacial sediment to ice-sheet dynamics and thence to climate change. Both glaciological theory [Cuffey and Alley, 1996] and observations from the West Antarctic Ice Sheet (WAIS) [Blankenship et al., 2001, Bindschadler et al., 2001] suggest that a supply of deformable subglacial sediment is needed to initiate and maintain fast, low-gradient stream flow within ice sheets: this type of flow is in turn required to support the physical instabilities believed to be responsible for quasi-periodic "collapses" of the WAIS [MacAyeal, 1992] and the LIS [MacAyeal, 1993a]. Physical arguments [Cuffey and Alley, 1996] indicate that the export of deformable sediment should greatly exceed the rate at which it is produced from fresh bedrock, suggesting that these instabilities rely on a pre-existing reservoir of subglacial sediment, and would cease with the exhaustion of this reservoir. Clark and Pollard [Clark and Pollard, 1998], in an effort to explain the enigmatic mid-Pleistocene transition between 40,000-yr and 100,000-yr frequencies in climate and ice sheet variability, proposed that the preglacial regolith on the Canadian Shield served as such a sediment reservoir, and that it was gradually exhausted in the core areas of the LIS during the middle Pleistocene. This in turn forced the LIS and the rest of the global ice-climate system into the longer-period, larger-amplitude oscillation characteristic of the last million years. Here we are motivated by the question of how the initial supply and eventual fate of deformable subglacial sediment is related to the long-term evolution of ice sheets, and, in particular, whether gradual regolith export from the LIS could, by reducing the thickness of deformable sediment beneath some threshold, have triggered the mid-Pleistocene climate transition.

4.3 Atmospherically-produced ^{10}Be in soil, regolith and till

Here we exploit the cosmic-ray-produced radionuclide ^{10}Be as a tracer to study the source of subglacial sediment, that is, till, exported by the LIS. Most terrestrial ^{10}Be is produced by spallation

of N and O nuclei in the atmosphere and transported to the Earth's surface by precipitation, where it adheres to soil particles. Under most natural conditions Be is nearly irreversibly bound to sediment [Brown, 1987], and regolith resulting from prolonged weathering becomes highly enriched in ^{10}Be (Figure 1). Eventually, such regolith reaches equilibrium between ^{10}Be deposition and loss by radioactive decay and surface erosion of soil particles [Pavich et al., 1984]. Deep weathering profiles on stable cratonic landscapes that were never glaciated have ^{10}Be inventories near 10^{12} atoms $\cdot$ cm^{-2}, and the regolith that covered the Canadian Shield prior to glaciation must have had a similar ^{10}Be inventory. In contrast, Pleistocene and Holocene soils that developed in glaciated regions during interglaciations of 10,000 – 60,000 yr have ^{10}Be inventories of $2-8\times10^{10}$ atoms $\cdot$ cm^{-2} (Figure 4.4).

We measured the bulk concentration of ^{10}Be in till from boreholes in southwest Minnesota and adjacent South Dakota (Figures 4.4,4.4; Table 4.1). This area is underlain by 100-300 m of Plio-Pleistocene glacial sediment, including at least 12 distinct tills that predate the most recent glaciation. We chose the area for two reasons. First, it is the most northerly extent of significant pre-Wisconsinan sediment accumulation, and therefore should provide the most accurate sample of till exported from the core area of the LIS, allowing the minimum opportunity for overriding and recycling of previously deposited glacial sediment. Second, the stratigraphy in this region consists primarily of till, with little evidence of soil development or prolonged interglacial exposure. This makes it more likely that the ^{10}Be concentration in our samples reflects the source material for the till and has not been affected by postdepositional ^{10}Be accumulation.

4.4 Discussion; conclusions

The ^{10}Be concentration in these tills varies over three orders of magnitude (Figure 4.4). The lowest tills in the region directly overlie saprolite or ^{10}Be-enriched silts (that presumably constitute the preglacial land surface), and thus appear to record the first Pleistocene ice advances. These tills contain $1-2\times10^{8}$ atoms $\cdot$ g^{-1} of ^{10}Be. Overlying, younger, tills have much lower ^{10}Be concentrations of $2-5\times10^{7}$ atoms $\cdot$ g^{-1}, with the exception of intermediate-age tills in two boreholes which have ^{10}Be concentrations as high as those in the lowest tills. The uppermost, Wisconsinan, tills have very low ^{10}Be concentrations $< 10^{7}$ atoms $\cdot$ g^{-1}. As ^{10}Be is radioactive ($t_{1/2} = 1.5\times10^{6}$ yr), if old and young tills were drawn from a source with constant ^{10}Be concentration, older tills would have lower ^{10}Be concentrations than younger due to decay. The fact that the oldest tills have the highest ^{10}Be concentration shows that older tills were derived from a ^{10}Be-enriched source material that is not present in most of the younger tills. We conclude that this ^{10}Be-enriched source was

the preglacial regolith. Early tills were derived from the regolith, and later tills from the erosion of unweathered bedrock.

The ^{10}Be concentration in till depends on a number of factors: the preglacial ^{10}Be inventory, the depth of subglacial erosion, the degree to which ^{10}Be-enriched regolith might be diluted with ^{10}Be-free sediment, the ^{10}Be inventory deposited during ice-free periods, the degree of mixing between a particular till and the stock of older glacial sediment that might be overrun and entrained; and the radioactive decay of the various ^{10}Be inventories. We used a simple box model that accounted for these factors to explore which possible processes could duplicate the observed sequence of ^{10}Be concentrations in successive tills. We found that the most important of our observations in this context were the ^{10}Be concentrations in the oldest tills, and the order-of-magnitude decrease in ^{10}Be concentration between the oldest tills and those directly overlying them. These can only be explained if two things are true. First, nearly the entire ^{10}Be inventory in the preglacial regolith must have been entirely removed from the core area of the LIS by the first one or two ice sheet advances. No matter what the dilution by possible ^{10}Be-free rock or sediment, the first ice sheet advance must have removed most of the regolith from the Canadian Shield. Second, very little of these lowest, high-^{10}Be, tills can have been recycled into subsequent tills. ^{10}Be concentrations in intermediate-age tills support this as well: the juxtaposition of tills with ^{10}Be concentrations that differ by nearly two orders of magnitude require that recycling of older till into younger be minimal.

The second important observation is that the extremely high ^{10}Be concentrations in intermediate tills in boreholes UMRB-1 and SD-CO, but not in tills above or below them, cannot be explained either by recycling of older glacial sediment or by ^{10}Be deposition during interglaciations. These tills likely record the mobilization of a previously undisturbed stock of preglacial regolith, either by an increase in the area of the ice sheet, the thawing of a region of the glacier bed that had previously been frozen, or a large-scale change in the direction of ice flow that could have mobilized regolith that was previously protected by the bed topography. Although we know only that these high-^{10}Be intermediate tills are younger than 1 Ma Balco et al. [2004a in review], these possibilities are all likely consequences of the growth of a larger ice sheet at the mid-Pleistocene transition evident in marine oxygen-isotope records.

In unglaciated areas at present, the entire regolith down to the bedrock weathering front is enriched in ^{10}Be. Thus, unless there existed another stock of ^{10}Be-free deformable sediment, the apparent result, that the entire preglacial ^{10}Be inventory was rapidly removed from the core area of the LIS by its earliest advances, is not consistent with the idea that regolith persisted until ~ 1

Ma and could have provided an internal trigger for ice sheet growth at the mid-Pleistocene climate transition. Instead, we suggest that the renewed export of ^{10}Be-rich till sometime after 1 Ma was a consequence, and not a cause, of a change in ice dynamics.

Table 4.1: Bulk ^{10}Be concentrations in till from boreholes in Minnesota and South Dakota. We measured ^{10}Be concentrations at both LLNL-CAMS and PRIME Lab; here and in data tables in Chapter 5, the PRIME Lab data have been corrected to LLNL internal standards, which are traceable to the ICN standard. Uncertainties are reported at $\pm 1\sigma$ and include all known sources of analytical error. Blank corrections are described in Section 5.2.

Sample name	Borehole	Depth (m)	Lithology	^{10}Be concentration (10^6 atoms $\cdot$ g^{-1})
UMRB-1-8	UMRB-1	2.4	till	7.73 ± 0.22
UMRB-1-14	UMRB-1	4.3	till	3.01 ± 0.1
UMRB-1-41	UMRB-1	12.5	till	15.05 ± 0.38
UMRB-1-63	UMRB-1	19.2	till	15.17 ± 0.42
UMRB-1-64	UMRB-1	19.5	till	15.15 ± 0.45
UMRB-1-65	UMRB-1	19.8	till	14.64 ± 0.42
UMRB-1-69	UMRB-1	21	till	14.2 ± 0.5
UMRB-1-68	UMRB-1	20.7	till	13.08 ± 0.38
UMRB-1-70	UMRB-1	21.3	till	16.67 ± 0.46
UMRB-1-72	UMRB-1	22	till	28.91 ± 0.76
UMRB-1-73	UMRB-1	22.3	till	381.22 ± 5
UMRB-1-74	UMRB-1	22.6	till	425.63 ± 5.46
UMRB-1-75U	UMRB-1	22.9	till	299.21 ± 3.85
UMRB-1-94	UMRB-1	28.7	till	712.61 ± 8.96
UMRB-1-116B	UMRB-1	35.4	till	78.1 ± 1.72
UMRB-1-146B	UMRB-1	44.5	till	98.82 ± 1.68
UMRB-1-153	UMRB-1	46.6	till	75.64 ± 2.39
UMRB-1-201	UMRB-1	61.3	till	88.98 ± 2.82
UMRB-1-218	UMRB-1	66.5	till	46.24 ± 1.47

continued on next page

Table 4.1: *continued*

Sample name	Borehole	Depth (m)	Lithology	^{10}Be concentration (10^6 atoms $\cdot$ g^{-1})
UMRB-2-19	UMRB-2	5.8	till	13.8 ± 0.36
UMRB-2-39	UMRB-2	11.9	till	14.32 ± 0.38
UMRB-2-111	UMRB-2	33.8	till	9.92 ± 0.27
UMRB-2-133	UMRB-2	40.5	till	9.12 ± 0.25
UMRB-2-140	UMRB-2	42.7	till	9.73 ± 0.27
UMRB-2-146	UMRB-2	44.5	till	9.46 ± 0.26
UMRB-2-164	UMRB-2	50	till	8.99 ± 0.25
UMRB-2-182	UMRB-2	55.5	till	12.32 ± 0.35
UMRB-2-194	UMRB-2	59.1	till	4.61 ± 0.15
UMRB-3-42	UMRB-3	12.8	till	13.58 ± 0.35
UMRB-3-70	UMRB-3	21.3	till	17.03 ± 0.44
UMRB-3-92	UMRB-3	28	till	23.72 ± 0.6
UMRB-3-95	UMRB-3	29	till	13.69 ± 0.36
UMRB-3-97	UMRB-3	29.6	till	12.94 ± 0.34
UMRB-3-99	UMRB-3	30.2	till	14.64 ± 0.38
UMRB-3-102	UMRB-3	31.1	till	16.2 ± 0.55
UMRB-3-110	UMRB-3	33.5	till	17.86 ± 0.46
UMRB-3-169	UMRB-3	51.5	till	20.87 ± 0.54
UMRB-3-170	UMRB-3	51.8	till	22.79 ± 0.58
UMRB-3-174	UMRB-3	53	till	93.82 ± 1.51
UMRB-3-188	UMRB-3	57.3	till	49.87 ± 1.25
UMRB-3-195	UMRB-3	59.5	till	264.24 ± 4.14
UMRB-3-196	UMRB-3	59.8	silt	121.94 ± 2.15
SWRA-3-188	SWRA-3	57.3	till	18.53 ± 0.48
SWRA-3-193	SWRA-3	58.8	till	14.86 ± 0.39
SWRA-3-228	SWRA-3	69.5	till	28.6 ± 0.72
SWRA-3-258	SWRA-3	78.7	till	121.09 ± 1.67

continued on next page

Table 4.1: *continued*

Sample name	Borehole	Depth (m)	Lithology	^{10}Be concentration (10^6 atoms $\cdot$ g^{-1})
SD-CO-10	SD-CO	3	till	82.24 ± 2.68
SD-CO-44	SD-CO	13.4	till	125.75 ± 4.08
SD-CO-65	SD-CO	19.8	till	181.23 ± 5.7
SD-CO-151	SD-CO	46	till	325.19 ± 9.85
SD-CO-219	SD-CO	66.8	till	20.17 ± 0.65
SD-CO-258	SD-CO	78.7	till	10.72 ± 0.36
SD-CO-293	SD-CO	89.3	till	11.47 ± 0.42
SD-CO-320	SD-CO	97.6	till	13.27 ± 0.46
SD-CO-367	SD-CO	111.9	till	11.08 ± 0.39
SD-CO-390	SD-CO	118.9	till	188.41 ± 5.84
SD-CO-401	SD-CO	122.3	silt	112.66 ± 3.72
SD-CO-402	SD-CO	122.6	silt	111.35 ± 3.66
SD-CO-402/2	SD-CO	122.6	silt	119.51 ± 3.82
SD-CO-402/4	SD-CO	122.6	silt	109.75 ± 3.51

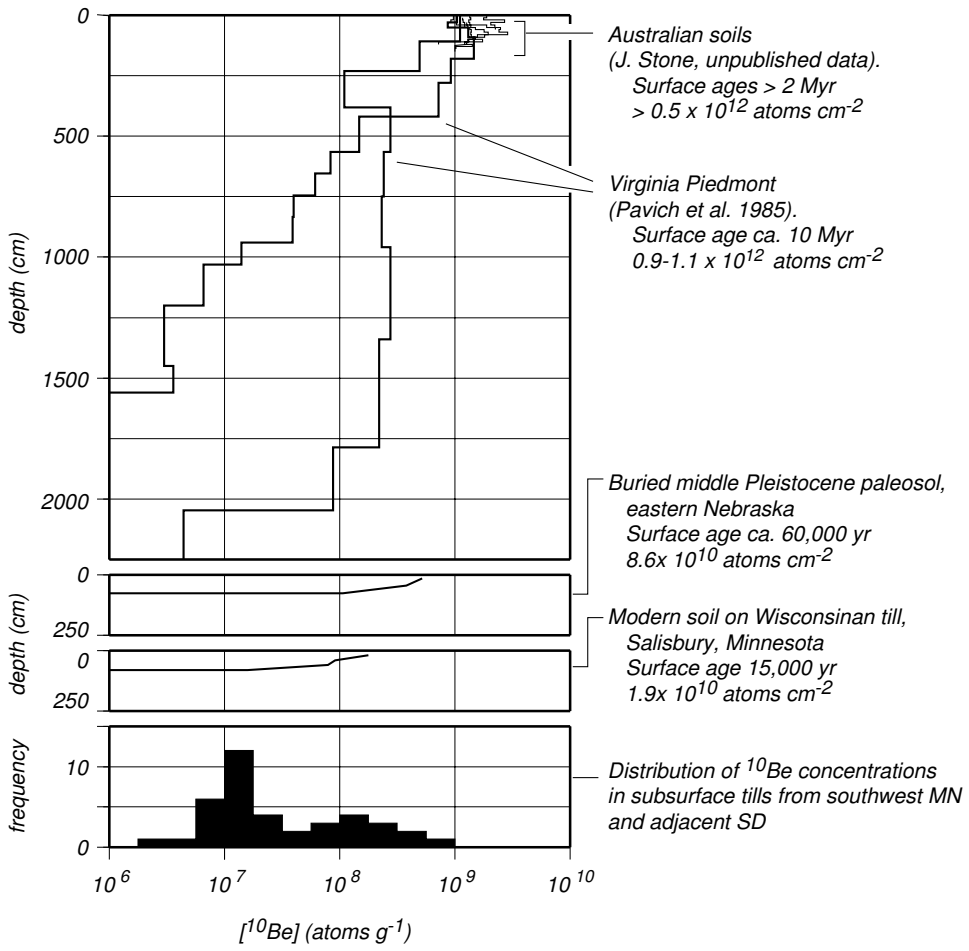

Figure 4.1: Bulk ^{10}Be concentrations in old and young soils. The paleosol from eastern Nebraska has been buried for ca. 600,000 yr Balco et al. [2004b in review]; we have corrected our measured ^{10}Be concentrations for radioactive decay during this time to better represent the ^{10}Be inventory at the time of burial. Analytical uncertainties are smaller than the size of the lines at this scale.

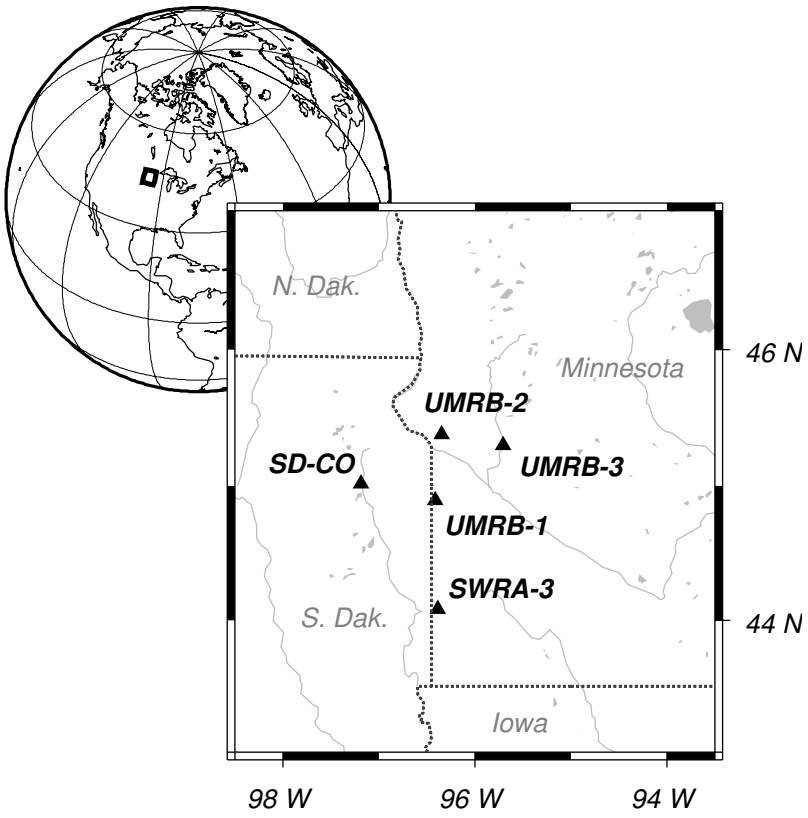

Figure 4.2: Map of study area showing location of boreholes mentioned in paper. Boreholes UMRB-X and SWRA-X were drilled by the Minnesota Geological Survey [Patterson, 1999, Setterholm, 1995]; borehole SD-CO was drilled by the South Dakota Geological Survey (SDGS, unpub. rpt.)

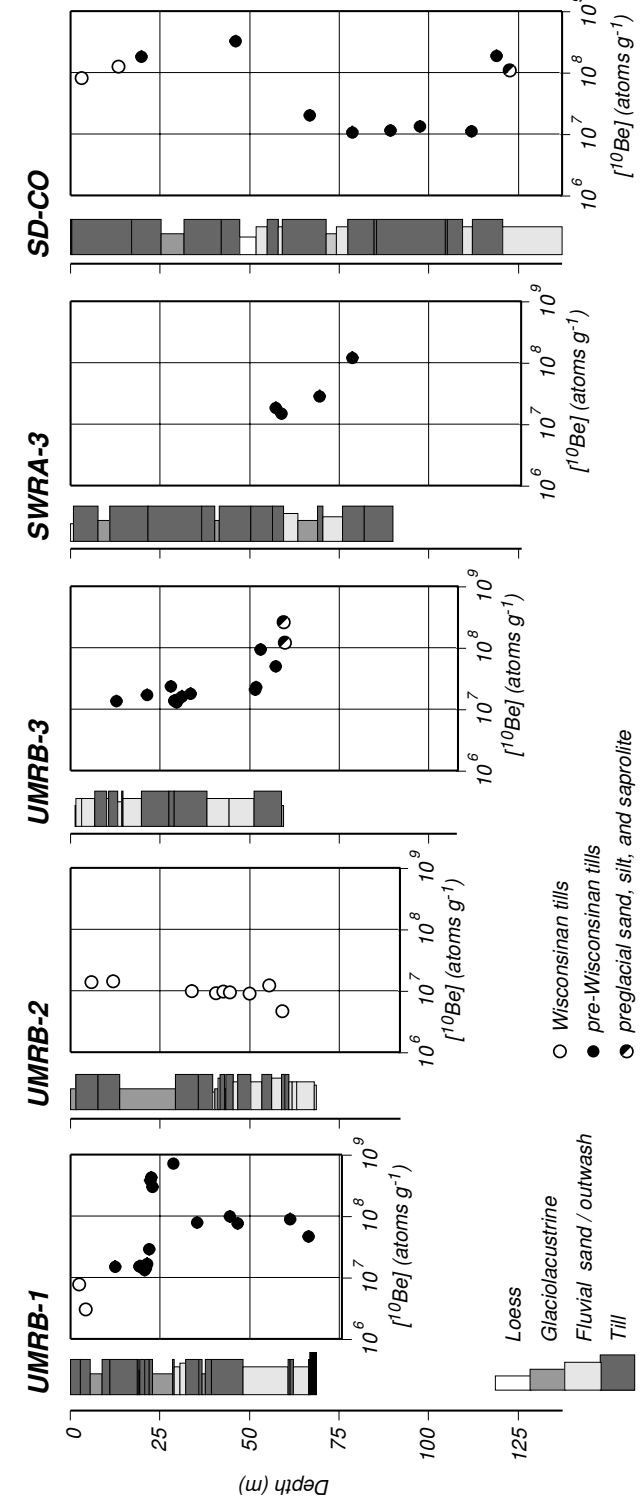

Figure 4.3: ^{10}Be concentrations in Plio-Pleistocene tills and preglacial sediment from boreholes in South Dakota and Minnesota.

Chapter 5

THE DETAILS OF MEASURING AND INTERPRETING THE ^{10}Be CONCENTRATION OF TILL

5.1 Introduction

Both this and the previous chapter describe measurements of the bulk ^{10}Be concentration of Laurentide Ice Sheet tills in the north-central U.S. The previous chapter is a manuscript of a paper whose length was limited; this chapter contiains supplemental material that did not fit there. First, we describe the analytical methods that we used and discuss the repeatability of measurements within individual tills. Second, we describe ^{10}Be measurements from modern and ancient soils that we used to estimate the ^{10}Be inventory that was likely deposited during interglaciations. Third, we describe the box model that we used for interpreting the ^{10}Be concentrations that we measured in tills.

5.2 Analytical methods

We measured ^{10}Be in samples of till by selecting $\sim$ 100 g samples of till from drillcore that appeared fresh, unweathered, and not affected by oxidation along joint surfaces, then drying them and grinding them in a shatterbox crusher. We added 400 μg commercial reagent Be solution as carrier and extracted Be from the sample by fusion in a KHF_2 melt. Stone [1998] describes this method. After extracting Be, we measured its isotope ratio by accelerator mass spectrometry at the Lawrence Livermore National Laboratory, Center for Accelerator Mass Spectrometry. Our Be carrier solution had $^{10}\mathrm{Be}/^{9}\mathrm{Be} = 1.5 \pm 0.2 \times 10^{-14}$, and our process blanks contained an additional $8 \pm 5 \times 10^4$ atoms ^{10}Be.

The method relies on complete fusion to ensure isotopic equilibration between sample and Be carrier [Stone, 1998]. This procedure had not previously been used for till, and we found that some till samples developed small (< 1 mm) refractory nodules which persisted throughout the fusion. In order to determine whether this was important, we analysed one sample of particularly refractory till (sample 4-A-75-83) twice. Small nodules survived the fusion in the first analysis but not in the second. The two analyses yielded 846 ± 26 and $942 \pm 29 \times 10^6$ atoms $\cdot\, \mathrm{g}^{-1}$. The difference

in these two analyses, although it has the sign we would expect if ^{10}Be remained sequestered in the nodules in the first analysis, is not significant at 95% confidence and is unimportant relative to the gross differences in till ^{10}Be concentrations that we observed.

We also tested for isotopic equilibration during fusion by analysing three aliquots of different weights for sample SD-CO-402 (duplicating the experiment in Stone [1998]). Figure 5.1 shows the results, which agreed within analytical error. Thus, we found no systematic difficulty in using this analysis procedure for samples of till.

5.3 Variability in ^{10}Be concentrations within individual tills; evidence of recyling of older into younger tills

In an effort to establish the extent to which tills are well-mixed with regard to their ^{10}Be concentrations, and to what extent we were justified in inferring the average ^{10}Be concentration of a till from a single sample, we measured ^{10}Be in multiple samples from several tills in boreholes from southwest Minnesota. In this section we have retained units of feet because our sample numbers follow the original borehole descriptions, which were denominated in feet. For example, sample UMRB-1-63 was collected at 63 feet depth in borehole UMRB-1. This is intended to make it easier for the reader to connect sample numbers in data tables with the discussion in the text. Figure 5.4 summarizes these data. The results of these experiments were as follows:

1. *Unnamed till at 129-158 ft (39-48 m) depth in borehole UMRB-1.* Two analyses at 146 and 153 feet (44.5 and 46.6 m) yielded similar results.

2. *Till at 63-68 ft (19.25-20.75 m) depth in UMRB-1.* Till unit 7 of Patterson [1999]. Four analyses at 63,64,65, and 68 feet (19.2, 19.5, 19.8, and 20.75 m) yielded indistinguishable results.

3. *Unnamed till at 68-72 ft (20.75-22 m) depth in UMRB-1.* Analyses at 69 and 70 feet (21 and 21.3 m) were indistinguishable. A third analysis at the bottom of the till at 75 feet (22 m) was higher, possibly reflecting mixing with the underlying till, which had a much higher ^{10}Be concentration. We discuss the effect of mixing below.

4. *Unnamed till at 72-75 ft (22-23) depth in UMRB-1.* This till had an extremely high ^{10}Be concentration in an initial analysis and we wished to determine whether or not this might reflect pedogenic ^{10}Be deposited after the emplacement of the till. Three analyses at 73,74,

and 75 ft (22.3, 22.6, and 23 m) all had similar, very high, ^{10}Be concentrations. The lowest sample did have a slightly lower concentration, which again may reflect mixing with underlying material that had a lower ^{10}Be concentration.

5. *Unnamed till at 95-125 ft (29-38 m) in borehole UMRB-3.* The top of this till unit had a blocky structure, suggesting a possible truncated soil profile [Patterson, 1999]. Five analyses at 0,2,4,7, and 15 ft (0, 0.6, 1.3, 2.1, and 4.6 m) below the till surface had similar ^{10}Be concentrations, slightly increasing with depth. If this till surface had been a soil surface in the past, we would expect higher ^{10}Be concentrations near the surface (see Section 5.5). If this till was pedogenically altered, the upper part of the soil must have been removed. The gradual increase with depth in these samples does resemble the lower part of the ^{10}Be concentration profiles in soils that we discuss below in 5.5, which show ^{10}Be minima and then gradual increases with depth 1-2 m below the surface. Thus, the ^{10}Be profile measured in this till would be consistent with a soil profile whose upper 1-2 m was removed during emplacement of the overlying till.

6. *Unnamed till at 168-193 ft (51-59 m) in UMRB-3.* This till appeared poorly mixed in core sections, being generally gray in color but containing seams and enclaves of red till. ^{10}Be analyses of this till were also more variable than for other tills. Analyses of grey and red enclaves at 169 and 170 feet (51.5 and 51.8 m) respectively were similar; another sample of the grey till at 174 ft (53 m) had a much higher concentration, and a fourth analysis of gray till at 188 ft (57.3 m) had an intermediate concentration. These data agree with the physical appearance of incomplete mixing.

7. *Till at 185-195 ft (56.4-59.5 m) depth in borehole SWRA-3.* Till unit 4 of Setterholm [1995]. Two analyses at intermediate depths in this till were similar.

8. *Unnamed till at 1-56 feet (0.3-17 m) depth in borehole SD-CO.* Two analyses were similar.

9. *Unnamed till at 278-337 feet (84.75-102.75 m) in borehole SD-CO.* Two analyses were indistinguishable.

From these data, we conclude that tills which appear lithologically well-mixed have well-mixed ^{10}Be concentrations. The one example of a poorly mixed till that we analysed suggests, as we

might expect, that tills which appear poorly mixed are not adequately represented by a single sample.

We found no evidence for significant pedogenic modification of ^{10}Be concentrations in any of these tills, which agrees with the general rarity of paleosols or other evidence of prolonged interglacial exposure periods in this region.

Third, there is some evidence (see items 3 and 4 above) that entrainment of underlying, older, till affected ^{10}Be concentrations near the base of a younger till. This is important in light of our interest in estimating the degree to which the ^{10}Be concentration in tills reflects a faraway source or recycling of local sediment; thus, we estimate the degree of mixing as follows. Assume that the tills at 63-68 feet (19.25-20.75 m) and 68-72 feet (20.75-22 m) in borehole UMRB-1 (see item 4 above and Figure 5.4) had similar source ^{10}Be concentrations, define concentration end member A N_A to be the mean of analyses from 63-69 feet (1.4×10^7 atoms $\cdot$ g^{-1}), and define concentration end member B N_B to be the mean of analyses at 73 and 74 feet (4×10^8 atoms $\cdot$ g^{-1}). For samples N_i for $i = 70$ and $i = 72$ feet, the fraction f of the "hot" lower till that has been incorporated into these samples by mixing is then:

$$f_i = \frac{N_i - N_A}{N_B - N_A} \tag{5.1}$$

.

This yields $f_{70} = 0.006$ and $f_{72} = 0.037$. Although we do not know the amount of time, transport distance, or erosion of the underlying till that was responsible for this mixing, it appears that: a) even with the extreme concentration gradient between tills in this example, the effect of mixing on the ^{10}Be concentration is relatively minor; and b) the effect of mixing is confined to close to the base of the till.

To summarize, for the majority of tills in this region that appear lithologically well-mixed, we conclude that a single ^{10}Be measurement from the middle of the till is adequately representative of the ^{10}Be concentration of the entire till.

5.4 Geographic variability of ^{10}Be concentration in correlated tills

In two cases we made ^{10}Be measurements on samples, from different boreholes, of a single widespread till that could be correlated between boreholes based on lithology and stratigraphy [Patterson, 1999]. Table 5.1 shows these data.

Two analyses of till unit 4 (an upper Wisconsinan till) differed by a factor of three between

boreholes, but, like other Wisconsinan tills, were very low relative to older tills. Analyses of till unit 7, (a pre-Wisconsinan till with distinctive lithology), were indistinguishable between boreholes. These data are not very comprehensive, but suggest that the geographic variability of ^{10}Be concentrations in an individual till is significantly smaller than the large differences between tills of different ages that we observe in most boreholes.

5.5 ^{10}Be *abundance in post- and inter-glacial soils*

In order to get an idea of the inventory of meteoric ^{10}Be that we might expect to accumulate in surface soils during interglaciations, we measured the ^{10}Be inventory in two soil profiles: first, a soil developed on Wisconsinan till of the Des Moines lobe at Salisbury, MN (samples designated MN-SAL-XX); and second, a middle Pleistocene paleosol buried by 26 meters of loess in Nebraska Conservation and Survey Division borehole 3-B-99 (samples designated 3-B-99-XX). Figure 3.3 shows the locations of these sites.

Figure 5.2 and Tables 5.2 and 5.3 show these measurements. These profiles reflect, first, the inherited ^{10}Be concentration in the soil parent material (till in both cases), and second, the nuclide inventory developed during soil formation. For both profiles, we take the inherited ^{10}Be concentration N_{IN} (atoms $\cdot$ g^{-1}) in the parent material to be the mean of the ^{10}Be concentration in the lowest three samples. We then compute the ^{10}Be concentration attributable to postdepositional ^{10}Be accumulation by subtracting N_{IN} from the measured ^{10}Be concentration in the other samples higher in the profile. That is, for sample i with measured ^{10}Be concentration N_i, the ^{10}Be concentration attributable to postdepositional nuclide accumulation is $N_{A,i} = N_i - N_{IN}$. We then calculate the total postdepositional ^{10}Be inventory by integrating over the depth range of each sample. In borehole 3-B-99, we collected depth-integrated samples. For the Salisbury soil profile, we collected point samples and assume that the ^{10}Be concentration at an arbitrary depth is equal to that in the nearest sample, which yields the assumed top and bottom depths shown in Table 5.2. The postdepositional inventory I (atoms $\cdot$ cm^{-2}) is then:

$$I = \sum_i N_{A,i} \rho (z_{bot,i} - z_{top,i}) \tag{5.2}$$

Where $z_{bot,i}$ and $z_{top,i}$ are the actual (for 3-B-99) or assumed (Salisbury) top and bottom depths of sample i. We used a density $\rho = 1.9$ g $\cdot$ cm^{-3}. Tables 5.2 and 5.3 show the results of this calculation.

The ^{10}Be inventory in a soil is related to the age of the soil [Pavich et al., 1984]. Disregarding

both erosion and radioactive decay of ^{10}Be, the soil age is approximately I/D, where D is the deposition rate of ^{10}Be (approx. 1.3×10^6 atoms $\cdot$ cm$^{-2} \cdot$ yr^{-1}; [Monaghan et al., 1986]). For the Salisbury soil profile, this yields a soil age of ca. 15,000 yr, in very good agreement with the time of deglaciation for this area (15,000 yr). For the 3-B-99 soil profile, this calculation yields a soil age of ca. 66,000 yr, which agrees with the time of soil exposure that we infer from *in-situ* nuclide measurements in Chapter 2.

5.6 Meteoric ^{10}Be *measurements in tills from Nebraska and Iowa*

We expect tills in in the southern part of our study area, that is, Iowa and Nebraska, to be less useful than the more ice-proximal tills in Minnesota and South Dakota for determining the ^{10}Be concentration in subglacial sediment exported from the central area of the Laurentide Ice Sheet, for two reasons. First, the increased distance that the ice sheet must travel over unconsolidated deposits from former glaciations to reach Iowa and Nebraska means that recycling of older glacial sediments into subsequent tills will probably be more pronounced. Second, tills in Iowa and Nebraska are relatively thin, and most tills show evidence of long periods of exposure and soil formation during interglaciations, suggesting that ^{10}Be concentrations at the time of till emplacement are more likely to be obscured by pedogenic ^{10}Be. The advantage of the Iowa-Nebraska region, on the other hand, is that the till stratigraphy has been well established by Boellstorff [1978a], C. Rovey (1996, unpublished report) and Roy et al. [2004]. Furthermore, Roy et al. [2004] (as well as others; see Ambrose [1964], Gravenor [1975], Boellstorff [1978a]) have pointed out that the lowermost units are enriched in clay minerals characteristic of weathered soils. This observation is the sole previous evidence pertaining to the fate of the preglacial regolith on the Canadian Shield, and we were particularly interested in determining whether or not the ^{10}Be concentrations in these tills were related to their clay mineral composition.

Figure 5.3 and Table 5.4 show bulk ^{10}Be measurements on tills from boreholes in Iowa and Nebraska described by Boellstorff [1978a]. We found that ^{10}Be concentrations were very variable between stratigraphically equivalent tills, and that ^{10}Be concentrations appeared better correlated with the depth of the sample below the till surface than with stratigraphic position. These observations suggest that deposition of ^{10}Be after till emplacement and subsequent pedogenic mixing is important in explaining these data. This agrees with the fact that tills in the southern part of the field area are thinner, fewer, and intercalated with paleosols. We conclude that we cannot use these data to infer the ^{10}Be concentration of these tills at the time they were emplaced without collecting enough additional samples to accurately separate the inherited and postdepositional

^{10}Be inventories.

5.7 Ancient saprolites from Minnesota

The easist way to establish the ^{10}Be concentration in the preglacial regolith would be to directly analyze some of the examples of preserved preglacial regolith that have been reported in glaciated areas throughout North America. Our field area in Minnesota does contain examples of saprolite exposed in river cuts and excavations beneath the Pleistocene till section [Patterson and Boerboom, 1999]. However, at least some of these saprolites are known to underlie Cretaceous deposits [Patterson and Boerboom, 1999]; as their age is much greater than the half-life of ^{10}Be, these units would be expected to be ^{10}Be-free, and in any case their ^{10}Be concentrations would be irrelevant to the problem of reconstructing Plio-Pleistocene regolith ^{10}Be concentrations. Despite this possibility, we measured ^{10}Be in four samples of saprolite formed from crystalline bedrock at two sites in southwest Minnesota (Table 5.5). Only one of these samples (BVP-50) had a ^{10}Be concentration that was distinguishable from zero, and the ^{10}Be in this sample is most likely the result of its relative proximity ($\sim$ 1 m) to the modern soil surface. Thus, we conclude that these saprolites are probably Cretaceous in age and are not useful for our purposes.

5.8 Simple box model for transport of ^{10}Be from the preglacial regolith in the sediment source area, into tills in the sediment deposition area.

This section describes a simple two-box model for the transport of ^{10}Be from some source area in the erosional portion of the Laurentide Ice Sheet to a sink area where the ice sheet deposits till. The point of this model is that, obviously, there are a large number of factors that affect the ^{10}Be concentration of tills that we observe in our field area in Minnesota; this is an attempt to combine many of these factors at least semi-quantitatively, determine which ones are important, and investigate what we can actually learn from a sequence of till ^{10}Be concentrations. In the model we consider two stocks of sediment: first, a source which represents material on the Canadian Shield that is available to be eroded by the Laurentide Ice Sheet; and second, a sink, which represents all the sediment deposited by advances of the Laurentide Ice Sheet. During each glaciation, the ice sheet moves a certain amount of sediment from source to sink. Sediment is conserved, and everything is normalized to area, so that the amount of erosion in the source area during an ice sheet advance E is equal to the amount of deposition in the sink area, and has units of cm. The sediment in the sink area is assumed to have a dry bulk density $\rho_T = 2$ g $\cdot$ cm^{-3}, which is typical

of till.

5.8.1 *Initial* ^{10}Be *inventory in the source area prior to glaciation*

The initial ^{10}Be inventory in the source area prior to the first glaciation is $I(z)$, where the function I yields the cumulative ^{10}Be inventory in the regolith above the depth z. I has units of atoms $\cdot$ cm^{-2} and z has units of cm. The only existing data that are relevant to the question of what the ^{10}Be inventory on the Canadian Shield may have been at the onset of Northern Hemisphere glaciation are ^{10}Be measurements from a pair of 20-m cores through soil and saprolite in a deep weathering profile in the Virginia Piedmont. Pavich et al. [1985] and Brown et al. [1988] describe these cores. We reproduce their cumulative inventory functions in Tables 5.8.7 and 5.8.7 as well as Figure 4.4. These cores have total ^{10}Be inventories of 8.8×10^{11} and 1×10^{12} atoms $\cdot$ cm^{-2}. These are the only measurements of the complete ^{10}Be inventory in a deep regolith/saprolite cover. The ^{10}Be inventory in the preglacial regolith that covered the Canadian Shield was likely similar in order of magnitude to that in the Virginia Piedmont, but would have varied locally according to rates of sediment erosion and deposition. However, as there are no other data available, we take these as the best available approximation of the initial inventory prior to glaciation.

5.8.2 ^{10}Be *inventory transported by each ice sheet advance*

Ice sheet advances are denoted by subscripts $j = 1...n$. There are n ice sheet advances and the total amount of erosion in the source area for the entire series of glaciations is thus En (cm). During an ice sheet advance, the inventory of ^{10}Be that is transported from source to sink consists of the ^{10}Be in the preglacial regolith as well as whatever ^{10}Be was deposited during the preceding interglacial. A fraction f_K of the source area consists of 'bedrock' whose ^{10}Be concentration is zero. The ^{10}Be from the preglacial regolith transported during ice sheet advance j is therefore:

$$I_{R,j} = [I(jE) - I(jE - E)]\,(1 - f_K) \tag{5.3}$$

The ^{10}Be deposited in the source area, during the interglaciation prior to ice sheet advance j, that must then be transported by that ice sheet advance is $I_{d,j}$. This inventory is much smaller than the initial inventory in the preglacial regolith. In the absence of soil erosion and radioactive decay, the ^{10}Be inventory in a soil is approximately Pt, where P is the global average deposition rate of ^{10}Be (1.3×10^6 atoms $\cdot$ cm^{-1} $\cdot$ yr^{-1}; Monaghan et al. [1986]) and t is time (yr). I_d is assumed to be zero for the first ice advance where $j = 1$. So, for an interglaciation that is 15,000 yr long, we expect a soil ^{10}Be inventory of approximately 2×10^{10} atoms $\cdot$ cm^{-2}. We measured the ^{10}Be inventory of

a soil profile on 15,000 yr old till in Minnesota and found that it was 2×10^{10} atoms $\cdot$ cm^{-2}, so this is probably a good starting value. This, of course, assumes that ^{10}Be deposited on top of the ice sheet during interglaciations does not wind up in till, which might or might not be true.

Thus, the total inventory of ^{10}Be that must be transported from source to sink during an ice sheet advance is:

$$I_{R,j} + I_d = [I(jE) - I(jE - E)]\,(1 - f_K) + I_d \tag{5.4}$$

This doesn't apply f_K to the interglacial deposition (because I_d is a rather weakly constrained parameter anyway, and one can obtain the same effect by adjusting I_d by a factor of $(1 - f_K)$).

5.8.3 ^{10}Be *concentration in till*

We take the ^{10}Be concentration in till to be the same as the average ^{10}Be concentration of all the sediment, till or not, transported by the ice sheet from source to sink during an ice sheet advance. This assumption is related to the assumption that I_d does not include ^{10}Be deposited on top of the ice sheet during a glaciation. If we believed that only the interglacial ^{10}Be deposited in the glaciated region between periods of ice cover wound up in the till, and supraglacial ^{10}Be was transported away from the ice margin and never delivered to the ice sheet bed, we would choose I_d to be small; if we believed the opposite we would choose I_d to reflect all the ^{10}Be deposited during the entire glacial-interglacial cycle. Regardless, the concentration of ^{10}Be in the till deposited by ice sheet advance j is C_j and has units of atoms $\cdot$ g^{-1}. If there is no recycling of previously deposited till into till j, then the ^{10}Be inventory that was transported from the source area is distributed over the thickness of the deposited sediment:

$$C_j = \frac{[I(jE) - I(jE - E)]\,(1 - f_K) + I_d}{E\rho_T} \tag{5.5}$$

If previously deposited glacial sediment is recycled into till j, then we need a fraction f_R that describes what proportion of till j is composed of mixed-in older tills. We assume that the mixed-in material has the average ^{10}Be concentration of all the previous tills. This average ^{10}Be concentration $C_{avg,j}$ (atoms $\cdot$ g^{-1}) is the total inventory of ^{10}Be mobilized in advances 1...$(j-1)$, divided by the total thickness of sediment mobilized:

$$C_{avg,j} = \frac{I(jE - E)(1 - f_K) + (j - 2)I_d}{\rho_T(jE - E)} \tag{5.6}$$

The factor of $(j-2)$ on I_d reflects the fact that $I_d = 0$ for $j = 1$. So the ^{10}Be concentration in till j when recycling is taken into account is:

$$C_j = \frac{(1-f_R)}{E\rho_T}\Big(\left[I(Ej) - I(jE-E)\right](1-f_K) + I_d\Big) + \frac{f_R}{\rho_T E(j-1)}\Big[I(jE-E)(1-f_K) + (j-2)I_d\Big] \tag{5.7}$$

Since there can be no recycling when $j = 1$, at which time $I_d = 0$ and $I(0) = 0$ as well, there is a slightly simpler expression for C_1:

$$C_1 = \frac{(1-f_K)I(E)}{E\rho_T} \tag{5.8}$$

5.8.4 Accounting for radioactive decay

Accounting for radioactive decay is not of major importance, because the oldest tills in North America are probably only about 2.5 Ma; thus, decay has about a factor-of-two effect on the eventual nuclide concentrations, which is smaller than the order-of-magnitude differences we seek to explain. Also, it requires adding yet another speculative parameter, in this case the duration D (yr) of each glacial-interglacial cycle, which presumably varied over time. The modifications to the above scheme are as follows:

First, we account for decay of the preglacial ^{10}Be inventory in the source area until the end of period j. This changes Equation 5.3 to:

$$I_{R,j} = \left[I(jE) - I(jE-E)\right](1-f_K)e^{-\lambda jD} \tag{5.9}$$

The decay constant λ is 4.83×10^{-7} yr^{-1} for ^{10}Be.

Second, the interglacial inventory I_d must decay only for the duration of period j. In reality both accumulation and decay would take place during the entire period of accumulation, but this approximation has a negligible effect on the result. This changes the ^{10}Be inventory that must be transported from source to sink (see Equation 5.4), to:

$$\left[I(jE) - I(jE-E)\right](1-f_K)e^{-\lambda jD} + I_d e^{-\lambda D} \tag{5.10}$$

Third, the concentration C_j that we observe at the end of period n must account for decay between the end of period j and the end of period n. Thus, in the absence of recycling, the concentration C_j is given by: (replacing Equation 5.5):

$$C_j = \frac{e^{-\lambda D(n-j)}}{E\rho^T}\Big(\left[I(jE) - I(jE-E)\right](1-f_K)e^{-\lambda jD} + I_d e^{-\lambda D}\Big) \tag{5.11}$$

Fourth, the expressions that account for recycling become rather more complicated. The total inventory transported prior to period j, allowed to decay until the end of period j, is:

$$I(jE-E)(1-f_K)e^{-\lambda Dj} + \sum_{i=2}^{j-1} I_d e^{-\lambda Di} \tag{5.12}$$

Note the implicit assumption that all the mixing takes place at the end of period j. Then the average ^{10}Be concentration in all the tills deposited prior to period j, at the end of period j, is (updating Equation 5.6):

$$\frac{I(jE-E)(1-f_K)e^{-\lambda Dj} + \sum_{i=2}^{j-1} I_d e^{-\lambda Di}}{\rho_T(jE-E)} \tag{5.13}$$

We can then mix this concentration with the concentration in till j in the correct proportions, leading to the final expression for C_J (updating Equation 5.7), which gives the ^{10}Be concentrations C_j (atoms $\cdot$ g^{-1}) that are observed at the end of period n:

$$\begin{aligned} C_j = {} & \frac{(1-f_R)e^{-\lambda D(n-j)}}{E\rho^T}\Big(\left[I(jE) - I(jE-E)\right](1-f_K)e^{-\lambda jD} + I_d e^{-\lambda D}\Big) \\ & + \frac{f_R e^{-\lambda D(n-j)}}{\rho_T(jE-E)}\Big(I(jE-E)(1-f_K)e^{-\lambda Dj} + \sum_{i=2}^{j-1} I_d e^{-\lambda Di}\Big) \end{aligned} \tag{5.14}$$

The simplified expression for C_1 is:

$$C_1 = \frac{I(E)(1-f_K)e^{-\lambda Dn}}{E\rho_T} \tag{5.15}$$

Note also that the sum in Equation 5.14 can't be evaluated when $j = 2$; fortunately this sum is supposed to be zero for $j = 2$.

5.8.5 Parameters; results

The parameters that we need to specify are as follows.

1. The function $I(z)$ that describes the depth dependence of the initial ^{10}Be inventory in the source area. We have already specified this to be the ^{10}Be profile from one of the regolith cores of Pavich et al. [1985] and Brown et al. [1988]. z has units of cm. $I(z)$ has units of atoms $\cdot$ cm^{-2}.

2. The ^{10}Be inventory deposited during interglacials I_d. Units of atoms $\cdot$ cm^{-2}.

3. The area fraction f_K of non-^{10}Be-contributing bedrock in the source area. Dimensionless.

4. The fraction of each till f_R which is composed of recycled older till. Dimensionless.

5. The amount of erosion and deposition in each ice sheet advance E. Units of cm.

6. The duration of each glacial-interglacial cycle D. Units of yr.

Figure 5.8.7 shows an example with some parameters that agree with many of our observations. Here we took I_d from Table 5.8.7, and used the parameters: $I_d = 2 \times 10^{10}$ atoms $\cdot$ cm^{-2}, $f_K = 0.1$, $f_R = 0.1$, $E = 800$ cm, $n = 20$ and $D = 10^5$ yr.

5.8.6 What exactly do we learn from this? Discussion and conclusions

This model has quite a number of parameters, we do not know the value of any of these parameters, and we are trying to account for a rather sparse data set where each of our boreholes contains only a discontinuous subset of the total sequence of Plio-Pleistocene tills. It would not be very useful to attempt a formal inversion, but we can use certain aspects of the data to get an idea about some of the parameters, as follows.

Inferences about erosion from ^{10}Be *concentrations in Wisconsinan tills*

Wisconsinan tills in most of our boreholes have the lowest ^{10}Be concentrations of any tills that we analysed, approximately $0.5 - 1.5 \times 10^7$. We can compare these concentrations to those that our model predicts for steady-state concentrations long after the initial ^{10}Be inventory in preglacial regolith has been exhausted. In this situation, $I_R = 0$, and recycling becomes unimportant because, in the steady state, the average nuclide concentration in the stack of previously deposited tills converges on the nuclide concentration in the most recently deposited till. For large j, the nuclide concentration C_j converges on:

$$C_j = \frac{I_d}{E\rho_T} \tag{5.16}$$

Thus, the nuclide concentration in Wisconsinan tills should only depend on two of the parameters, the interglacial ^{10}Be inventory I_d and the erosion in the source area E. If we take $I_d = 2 \times 10^{10}$ atoms $\cdot$ cm^{-2} as discussed above, and $C_j = 1 \times 10^7$ atoms $\cdot$ g^{-1}, then $E = 1 \times 10^3$ cm $= 10$ m.

For the reasonable end members of $I_d = 1.3 \times 10^{10}$ atoms $\cdot$ cm^{-2}(a 10,000-yr interglaciation) and $I_d = 8 \times 10^{10}$ atoms $\cdot$ cm^{-2}(a 60,000-yr interglaciation), E would be 7 or 40 m, respectively. This exercise tells us that E is probably on the order of 10 m.

Inferences about total Pleistocene erosion from average till ^{10}Be *concentration*

We can also get an idea of the most reasonable value for E by considering a back-of-the-envelope estimate of the total ^{10}Be mass balance throughout the entire series of glaciations. The total amount of ^{10}Be that must be transported consists of the preglacial inventory in the regolith (approx. 9×10^{11}) and the total amount of ^{10}Be deposited during the interglaciations. If the total sequence of glaciations is 2 Myr long, the preglacial inventory, wherever it is, has by now decayed to $\sim 3.5 \times 10^{11}$ atoms $\cdot$ cm^{-2}. The total ^{10}Be inventory deposited in the source area, accounting for deposition and decay, during the entire 2 Myr is 1.7×10^{12} atoms $\cdot$ cm^{-2}. Thus, there is a total ^{10}Be inventory of $\sim 2 \times 10^{12}$ atoms $\cdot$ cm^{-2} that must be somewhere in the resulting glacial sediment of any age. Call this I_{total}. The total thickness of material eroded from the source area is E_{total}. Then the average concentration in all tills must be $C_{avg} = I_{total}/E_{total}\rho_T$. The average ^{10}Be concentration in all the tills we measured is approximately 1×10^8 atoms $\cdot$ g^{-1}. This is a rather gross oversimplification which can certainly only be expected to give an idea of the rough order of magnitude of subglacial erosion, but it yields $E_{total} = 100$ m, which compares very well with the 120 m average depth of erosion by the Laurentide Ice Sheet since 3 Ma estimated from marine sediment volumes by Bell and Laine [1985]. If there have been approximately 25 ice sheet advances (another highly speculative estimate) into Minnesota, this suggests that we should choose E to be approximately 4 m.

Thus, these two rather vague calculations give the idea that E is somewhere around 5 or 10 meters.

Inferences about erosion depth and recyling from basal and near-basal tills

The other important feature of our data that allows us to limit parameter values is the fact that, in several boreholes, we find a basal till with a very high ^{10}Be concentration overlain by several tills with much lower ^{10}Be concentrations. Even without knowing the age of the tills, if we assume that they represent consecutive ice advances, we can use these data to estimate not only the depth of erosion by the first till but also the amount of recycling of the first till into subsequent tills.

In three separate cases where we have boreholes that appear to penetrate the base of the glacial section, the basal one or two tills have about an order of magnitude more ^{10}Be than the subsequent

till (boreholes SD-CO, UMRB-3, SWRA-3). These data are reproduced with the model results in Figure 5.8.7. It stands to reason that there is no way to generate this relationship between the earliest and the next tills unless: a) most of the preglacial ^{10}Be inventory is removed by the first one or two ice sheet advances, and b) there is very little mixing of earlier tills into later tills. The box model reinforces this conclusion. One can trade off the rock fraction f_K with the depth of erosion E to produce the desired concentration in the first till C_j, but the decrease in concentration between C_1 and C_2 is a function only of E and f_R. We cannot duplicate these data with the box model unless E is greater than approximately 7-10 m and f_R is less than approximately 0.1. These results, that the initial inventory was rapidly removed from the system and that recycling of older into younger tills must be very weak, are the most important results of the modeling exercise. Note that our conclusion of very weak recycling of old into young tills agrees with the comparison of adjacent tills with very different ^{10}Be concentrations in Section 5.3.

Significance of high-^{10}Be *tills in the middle of the sequence*

In UMRB-1 and SD-CO we observed tills with very high ^{10}Be concentrations, equal to those in basal tills overlying preglacial sediment. Some have higher concentrations than basal tills, even when decay is taken into account. None of the processes in the model can produce ^{10}Be-rich tills sandwiched between ^{10}Be-poor tills in the middle of the sequence. These tills cannot result only from the recycling of previously deposited tills, unless recycling processes specifically selected only the lowest, and thus least accessible, units of a pre-existing stack of sediment, which is geometrically implausible. If these intermediate ^{10}Be-rich tills originated from the transport of interglacial soils, they would require erosion depths of only a few centimeters, with no incorporation of any deeper material, which is also difficult to envision. Thus it appears that these intermediate, high-^{10}Be, tills can only arise from the introduction of new preglacial regolith that was not previously disturbed by prior glaciations.

5.8.7 Summary

Even though we do not know the age of all of the tills that we sampled and thus cannot directly compare box model results with a dated sequence of tills, and even though the number of parameters needed in the box model results in a rather underdetermined situation, we can say a few things with reasonable confidence. First, the depth of subglacial erosion during the average glaciation was likely near 5-10 m. Second, the rapid exhaustion of the preglacial ^{10}Be inventory in the lowest tills in a few boreholes requires, first, that the majority of the preglacial ^{10}Be inventory be

removed from the system by the first ice sheet advance, and, second, that recycling of previously deposited tills into new tills be small. Third, high-^{10}Be tills in the middle of our sequences cannot be explained by recycling of previously deposited tills, and must reflect the introduction of an additional source of undisturbed preglacial regolith.

Table 5.1: ^{10}Be concentrations in correlated till samples from Minnesota River Valley boreholes. Till unit designations from Patterson [1999]. In this and subsequent data tables, ^{10}Be measurements are reported relative to LLNL internal standards, which are traceable to the ICN standard. Uncertainties are reported at $\pm 1\sigma$ and include all known sources of analytical error. Blank corrections are described in Section 5.2.

Till unit	Borehole	Depth (ft)	[^{10}Be] (10^6 atoms $\cdot$ g^{-1})
4	UMRB-1	14	3.01 $\pm$ 0.1
4	UMRB-2	111	9.92 $\pm$ 0.27
7	UMRB-1	63-68 (mean)	14.51 $\pm$ 0.99
7	UMRB-3	42	13.58 $\pm$ 0.35

Table 5.2: Bulk ^{10}Be measurements and interpretation for Salisbury, MN road cut soil profile.

Sample name	Sample depth(cm)	$z_{top,i} - z_{bot,i}$	N_i (10^6 atoms $\cdot$ g^{-1})	$N_{A,i}$ (10^6 atoms $\cdot$ g^{-1})
MN-SAL-20	20	0-30	218.4 ± 8.24	199.67 ± 9.23
MN-SAL-40	40	30-50	121.59 ± 3.96	102.87 ± 5.74
MN-SAL-60	60	50-70	107.85 ± 3.37	89.13 ± 5.35
MN-SAL-80	80	70-90	36.62 ± 1.3	17.9 ± 4.35
MN-SAL-100	100	-	21.87 ± 0.71	-
MN-SAL-160	160	-	14.02 ± 0.47	-
MN-SAL-220	220	-	20.29 ± 1.27	-
Inherited ^{10}Be concentration (10^6 atoms $\cdot$ g^{-1})				18.73 ± 4.15
Total inventory I (10^9atoms $\cdot$ cm^{-2})				19.36 ± 0.63

Table 5.3: Bulk ^{10}Be measurements and interpretation for paleosol at 26 m depth in borehole 3-B-99.

Sample name	$z_{top,i}$ (cm below soil surface)	$z_{bot,i}$	$N_i(10^6$ atoms $\cdot$ g$^{-1})$	$N_{A,i}(10^6$ atoms $\cdot$ g$^{-1})$
3-B-99-87	0	30	695.4 ± 20.63	585.25 ± 20.63
3-B-99-88	30	61	534.97 ± 16.72	424.83 ± 16.73
3-B-99-89	61	91	229.43 ± 8.67	119.29 ± 8.68
3-B-99-90	107	122	104.08 ± 3.3	-
3-B-99-91	122	145	102.45 ± 3.29	-
3-B-99-93	175	213	123.9 ± 4.13	-

Inherited ^{10}Be concentration (10^6 atoms $\cdot$ g^{-1})	110.14 ± 0.48
Total inventory I (10^9atoms $\cdot$ cm^{-2})	65.93 ± 1.63
I, corrected for 0.58 Myr decay (10^9atoms $\cdot$ cm^{-2})	86.19 ± 2.13

Table 5.4: ^{10}Be concentrations in Nebraska and Iowa tills. Till designations from C. Rovey (1996, unpub. rpt.)

Sample	Borehole	Sample depth (m)	Unit top depth (m)	Unit	[^{10}Be] (10^6 atoms $\cdot$ g^{-1})
4-A-75-33	4-A-75	10.0	9.4	A2	161.59 ± 5.09
4-A-75-83	4-A-75	25.1	24.2	A3	862.12 ± 26.36
4-A-75-83B	4-A-75	25.1	24.2	A3	941.66 ± 29.01
1-A-76-85	1-A-76	25.7	24.2	A3	68.28 ± 2.29
17-A-76-121	17-A-76	36.6	26.9	A3	70.12 ± 2.28
4-A-75-116	4-A-75	35.0	33.2	B2	59.63 ± 2.89
1-A-76-145	1-A-76	43.8	33.2	B2	47.57 ± 1.38
4-A-75-155	4-A-75	46.8	40.5	B3	63.01 ± 2.24
5-A-75-160	5-A-75	48.3	25.7	B3	54.21 ± 1.65
5-A-75-167B	5-A-75	50.5	50.2	C	64.2 ± 2.25
17-A-76-150	17-A-76	45.3	41.4	C	100.69 ± 3.11

Table 5.5: ^{10}Be concentrations in saprolite from southwest Minnesota.

Sample	Site description	[^{10}Be] (10^6 atoms $\cdot$ g^{-1})
RP-1	Ramsey Park, Redwood Falls, MN. Roadside outcrop in saprolitized gneiss and schist.	0.11 ± 0.05
RP2-3	Ramsey Park, Redwood Falls, MN. Riverbank cut in similar saprolitized gneiss and schist across river from RP-1 outcrop. Sample collected from 3 m below modern soil surface.	0.02 ± 0.04
BVP-50	Abandoned kaolin pit near Belview, MN. 1-3 meters of buff-colored clay, presumably kaolinite, overlying saprolitized gneiss. Clay unconformably overlain by gravel lag deposit from glacial River Warren. Sample from 50 cm below clay/gravel contact.	0.22 ± 0.04
BVP-100	Same location, 100 cm below clay/gravel contact.	0.02 ± 0.04

Table 5.6: Cumulative ^{10}Be inventory in a soil/saprolite core on weathered gneiss in Virginia, as a function of depth. Reproduced from Pavich et al. [1985].

Cumulative ^{10}Be inventory (atoms $\cdot$ cm^{-2}) $I(z)$	Depth (cm) z
0	0
5.60E+10	30
9.40E+10	50
1.87E+11	90
4.37E+11	180
6.21E+11	280
7.92E+11	420
8.31E+11	565
8.45E+11	655
8.56E+11	745
8.63E+11	837.5
8.72E+11	942.5
8.75E+11	1032.5
8.78E+11	1202.5
8.80E+11	1450
8.81E+11	∞

Table 5.7: Cumulative ^{10}Be inventory in a soil/saprolite core on weathered granite from Virginia. Reproduced from Brown et al. [1988].

Cumulative ^{10}Be inventory (atoms $\cdot$ cm^{-2}) $I(z)$	Depth (cm) z
0	0
2.02E+11	107
3.05E+11	230
3.33E+11	380
4.20E+11	565
4.95E+11	750
5.77E+11	958
7.56E+11	1340
9.23E+11	1787
9.62E+11	2046
1.02E+12	∞

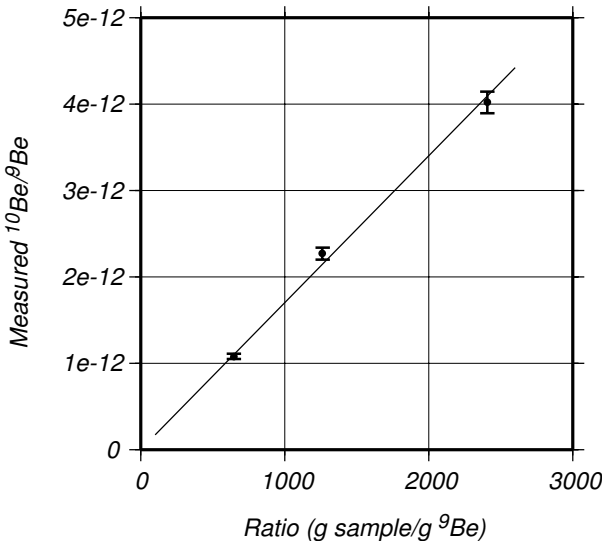

Figure 5.1: Isotopic equilibration of sample and carrier Be. Symbols with (1σ) error bars show isotope ratios measured for varying weights of sample SD-CO-402 fused with 0.4 mg ^{9}Be carrier. Line reflects expected relationship for average ^{10}Be concentration in this sample of 1.14×10^{8} atoms $\cdot$ g^{-1}.

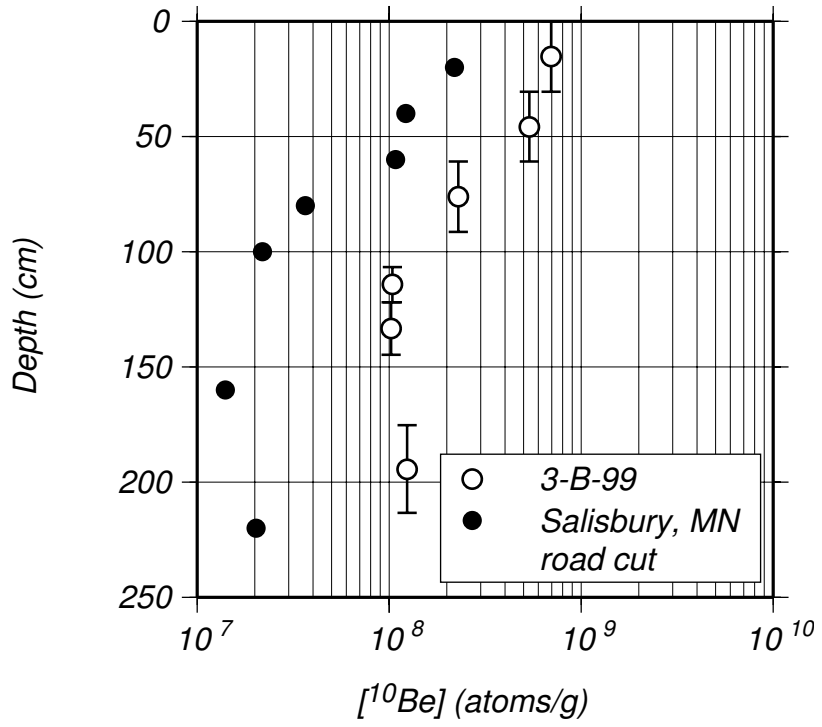

Figure 5.2: Bulk ^{10}Be concentrations in soil profiles. Vertical error bars show size of depth-integrated samples in 3-B-99. Analytical errors in measuring ^{10}Be concentrations are smaller than the data points at this scale.

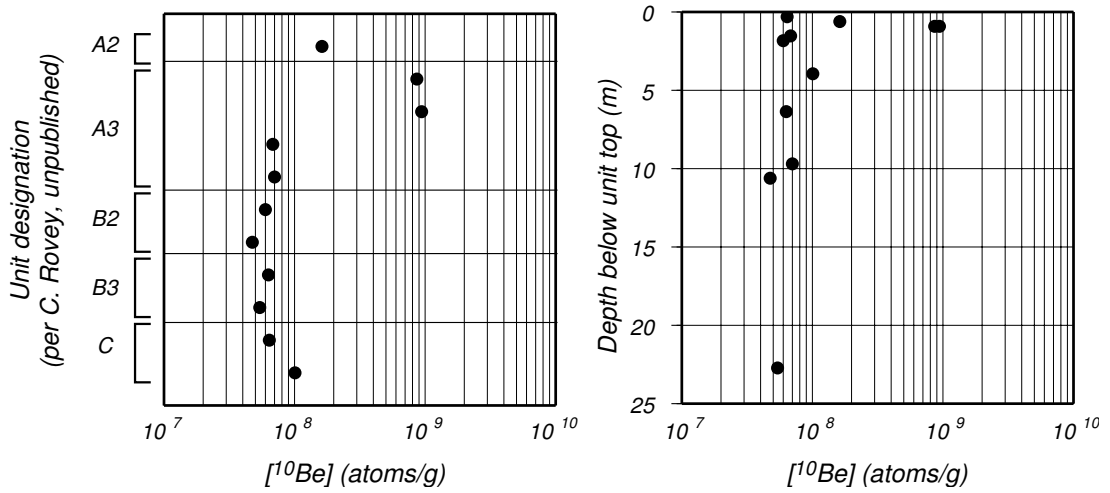

Figure 5.3: Bulk ^{10}Be concentrations in tills from boreholes in Iowa and Nebraska. Left panel, ^{10}Be measurements in stratigraphic order as described in text. Unit designations from Rovey (unpub. rpt.). Right panel, relationship between ^{10}Be concentration and the depth that samples were collected below the surface of the till unit. The same data appear in both figures.

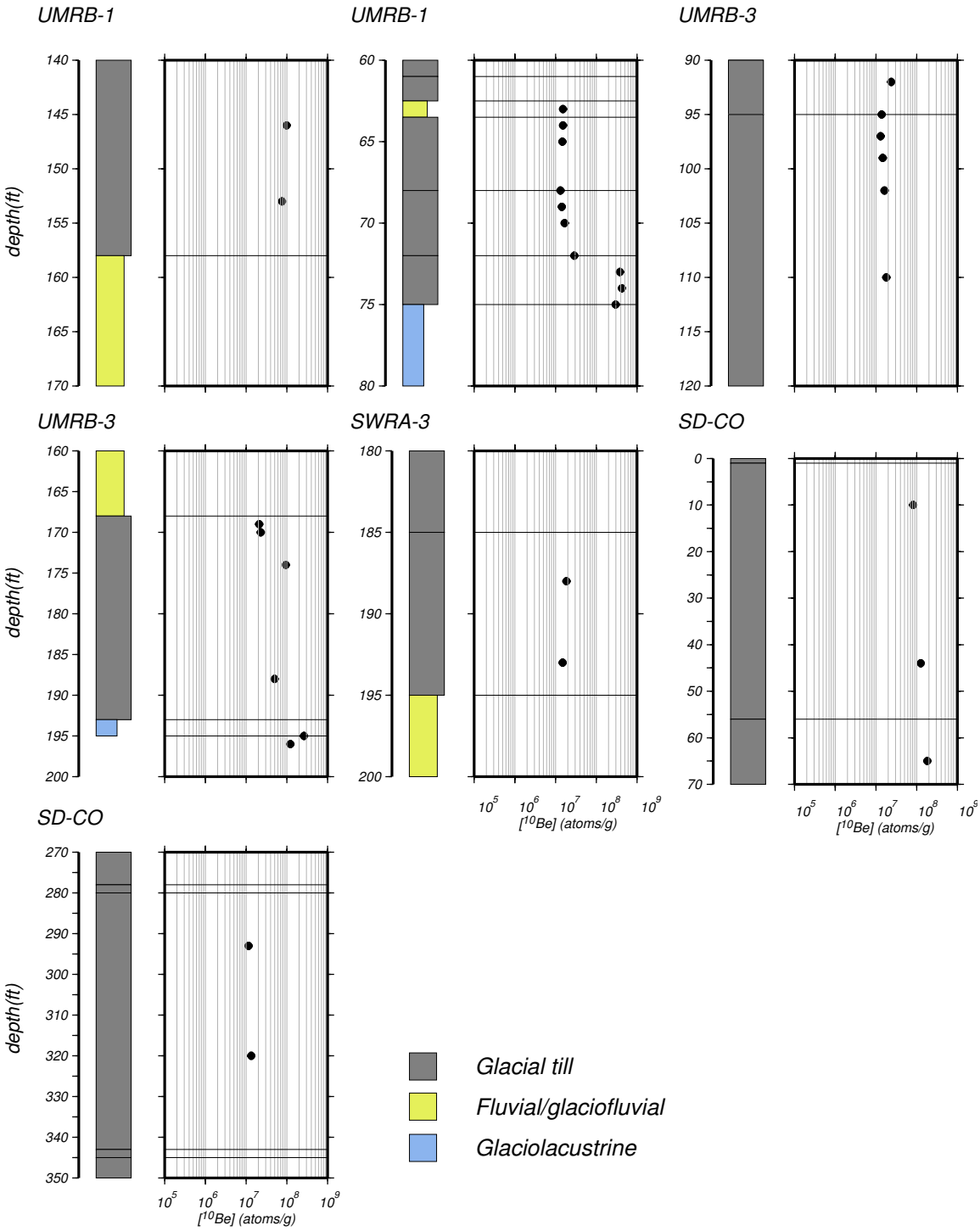

Figure 5.4: Results of multiple ^{10}Be analyses on various tills from southwestern Minnesota. Analytical errors are smaller than symbols used to plot data at this scale.

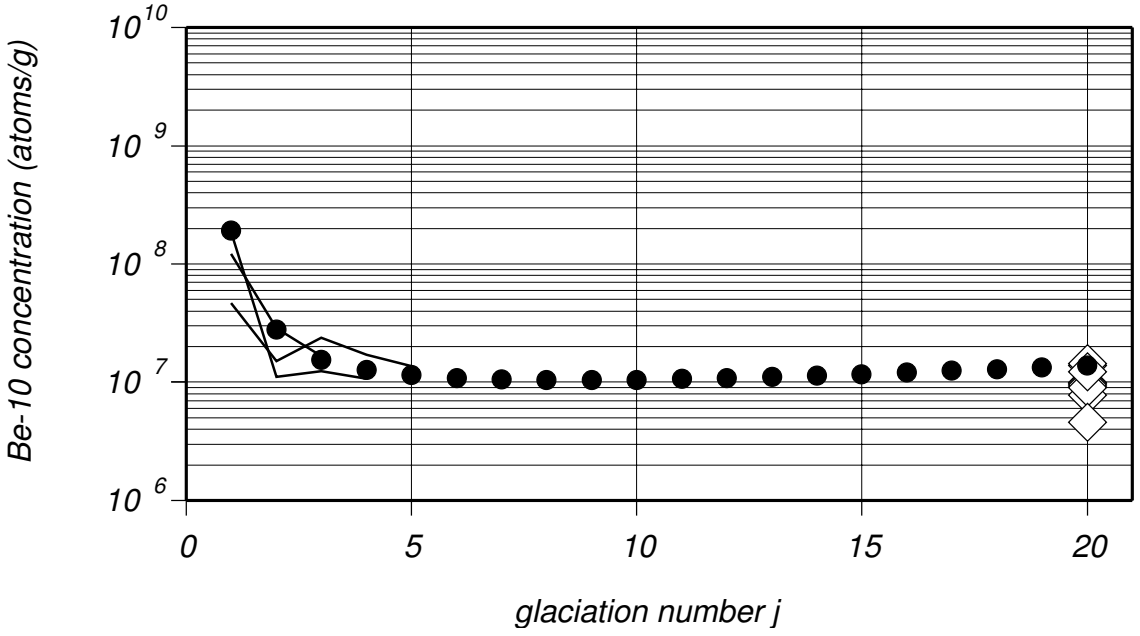

Figure 5.5: Example results of box model for ^{10}Be transport in till.The black circles are the model results for the parameters described in the text, the lines are ^{10}Be concentrations in the first few basal tills in three boreholes where we found what we believe to be the base of the glacial section, and the white diamonds are ^{10}Be concentrations in Wisconsinan tills.

BIBLIOGRAPHY

J.W. Ambrose. Exhumed paleoplains of the Precambrian shield of North America. *American Journal of Science*, 262:817–857, 1964.

G. Balco. Measuring the density of rock, sand, and till. UW Cosmogenic Nuclide Lab Procedures., 2004a. URL `http://depts.washington.edu/cosmolab/chem.html`.

G. Balco. *The sedimentary record of subglacial erosion beneath the Laurentide Ice Sheet*. Unpublished Ph.D. thesis, University of Washington, 2004b.

G. Balco, J.O.H. Stone, and C. Jennings. Dating Plio-Pleistocene glacial sediments using the cosmic-ray-produced radionuclides ^{10}Be and ^{26}Al. *American Journal of Science*, 2004a in review.

G. Balco, J.O.H. Stone, and J. Mason. Numerical ages for Plio-Pleistocene glacial sediment sequences by ^{26}Al/^{10}Be dating of quartz in buried paleosols. *Earth and Planetary Science Letters*, 2004b in review.

M. Bell and E. Laine. Erosion of the Laurentide region of North America by glacial and glacifluvial processes. *Quaternary Research*, 23:154–174, 1985.

W.H. Berger, T. Bickert, H. Schmidt, G. Wefer, and M. Yasuda. Quaternary isotope record of planktonic foraminifers. In *Proceedings of the Ocean Drilling Program, scientific results, Vol. 130*, pages 363–379. Ocean Drilling Program, College Station, TX, 1993.

E.A. Bettis III. Holocene alluvial stratigraphy and selected aspects of the Quaternary history of western Iowa. In *Midwest Friends of the Pleistocene, 37th Field Conference Guidebook.*, page 197. Iowa City, IA, 1990.

E.A. Bettis III, D.R. Muhs, H.M. Roberts, and A.G. Wintle. Last Glacial loess in the conterminous U.S.A. *Quaternary Science Reviews*, 22:1907–1946, 2003.

P. R. Bierman, K. A. Marsella, C.J. Patterson, P. T. Davis, and M. Caffee. Mid-Pleistocene cosmogenic minimum-age limits for pre-Wisconsinan glacial surfaces in southwestern Minnesota and southern Baffin Island: a multiple nuclide approach. *Geomorphology*, 27(1-2):25–39, 1999.

R. Bindschadler, J. Bamber, and S. Anandakrishnan. Onset of streaming flow in the Siple Coast region, West Antarctica. In R. Bindschadler and R. Alley, editors, *The West Antarctic Ice Sheet: Behavior and Environment*, page 123. American Geophysical Union, Washington, DC, 2001.

D. Blankenship, D. Morse, C. Finn, R. Bell, M. Peters, S. Kempf, S. Hodge, M. Studinger, J. Behrendt, and J. Brozena. Geologic controls on the initiation of rapid basal motion for West Antarctic ice streams: a geophysical perspective including new airborne radar sounding and laser altimetry results. In R. Bindschadler and R. Alley, editors, *The West Antarctic Ice Sheet: Behavior and Environment*, page 105. American Geophysical Union, Washington, DC, 2001.

J. Boellstorff. Chronology of some late Cenozoic deposits from the central United States and the ice ages. *Transactions of the Nebraska Academy of Sciences*, VI:35–48, 1978a.

J. Boellstorff. A need for redefinition of North American Pleistocene stages. *Transactions of the Gulf Coast Association of Geological Societies*, XXVIII:65–74, 1978b.

J. Boellstorff. North American Pleistocene stages reconsidered in light of probable Pliocene-Pleistocene continental glaciation. *Science*, 202:305, 1978c.

J. P. Briner and T. W. Swanson. Using inherited cosmogenic ^{36}Cl to constrain glacial erosion rates of the Cordilleran ice sheet. *Geology*, 26(1):3–6, 1998.

L. Brown. ^{10}Be as a tracer of erosion and sediment transport. *Chemical Geology*, 65:189–196, 1987.

L. Brown, M.J. Pavich, R.E. Hickman, J. Klein, and R. Middleton. Erosion of the eastern United States observed with ^{10}Be. *Earth Surf. Processes Landf.*, 13:441–457, 1988.

S C Cande and D V Kent. Revised calibration of the geomagnetic polarity timescale for the Late Cretaceous and Cenozoic. *Journal of Geophysical Research, B, Solid Earth and Planets*, 100(4): 6093–6095, 1995.

E.M. Clapp, P.R. Bierman, A.P. Schick, J. Lekach, Y. Enzel, and M. Caffee. Sediment yield exceeds sediment production in arid region drainage basins. *Geology*, 28(11):995–998, 2000.

P.U. Clark and D. Pollard. Origin of the middle Pleistocene transition by ice sheet erosion of regolith. *Paleoceanography*, 13:1–9, 1998.

K. Cuffey and R. Alley. Is erosion by deforming subglacial sediments significant? (Toward till continuity). *Annals of Glaciology*, 22:17–24, 1996.

R.G. Ditchburn and N.E. Whitehead. The separation of ^{10}Be from silicates. In *Third workshop of the South Pacific Environmental Radioactivity Association*, pages 4–7, 1994.

C. Emiliani. Pleistocene temperatures. *Journal of Geology*, 63:538–578, 1955.

T. Feininger. Chemical weathering and glacial erosion of crystalline rocks and the origin of till. Technical report, U.S. Geological Survey Professional Paper 750-C, pp. C65-C81, 1971.

R.F. Flint. *Glacial Geology and the Pleistocene Epoch*. J. Wiley and Sons, New York, 1947.

R.F. Flint. Pleistocene geology of eastern South Dakota. Technical report, U.S. Geological Survey Professional Paper 262, 1955.

S.L. Forman, III Bettis, E.A., T.J. Kemmis, and B.B. Miller. Chronologic evidence for multiple periods of loess deposition during the late Pleistocene in the Missouri and Mississippi River Valley, United States: implications for the activity of the Laurentide Ice Sheet. *Palaeogeography, Palaeoclimatology, Palaeoecology*, 93:71–83, 1992.

S.L. Forman and J. Pierson. Late Pleistocene luminescence chronology of loess deposition in the Missouri and Mississippi River valleys, United States. *Palaeogeography, Palaeoclimatology, Palaeoecology*, 186:25–46, 2002.

C.A. Gansecki, G.A. Mahood, and M. McWilliams. New ages for the climactic eruptions at Yellowstone; single-crystal ^{40}Ar/^{39}Ar dating identifies contamination. *Geology (Boulder)*, 26(4): 343–346, 1998.

J.P. Gilbertson and J.D. Lehr. Quaternary stratigraphy of northeastern South Dakota. In J.P. Gilbertson, editor, *Guidebook for the Friends of the Pleistocene Field Conference 3*, pages 1–13. 1989.

A. R. Gillespie and P. R. Bierman. Precision of terrestrial exposure ages and erosion rates estimated from analysis of cosmogenic isotopes produced in situ. *Journal of Geophysical Research*, 100 (B12):24,637–24,649, 1995.

J. C. Gosse and F. M. Phillips. Terrestrial in situ cosmogenic nuclides: theory and application. *Quaternary Science Reviews*, 20(14):1475–1560, 2001.

D. E. Granger, D. Fabel, and A. N. Palmer. Pliocene-Pleistocene incision of the Green River, Kentucky, determined from radioactive decay of cosmogenic ^{26}Al and ^{10}Be in Mammoth Cave sediments. *Geological Society of America Bulletin*, 113(7):825–836, 2001.

D. E. Granger, J. W. Kirchner, and R. C. Finkel. Quaternary downcutting rate of the New River, Virginia, measured from differential decay of cosmogenic ^{26}Al and ^{10}Be in cave-deposited alluvium. *Geology*, 25(2):107–110, 1997.

D. E. Granger, J.W. Kirchner, and R. Finkel. Spatially averaged long-term erosion rates measured from in situ-produced cosmogenic nuclides in alluvial sediment. *Journal of Geology*, 104:249–257, 1996.

D.E. Granger and P.F. Muzikar. Dating sediment burial with in situ-produced cosmogenic nuclides: theory, techniques, and limitations. *Earth and Planetary Science Letters*, 188(1-2):269–281, 2001.

C.P. Gravenor. Erosion by continental ice sheets. *American Journal of Science*, 275:594–604, 1975.

A.M. Hall and D.E. Sugden. Limited modification of mid-latitude landscapes by ice sheets: the case of northwest Scotland. *Earth Surf. Processes Landf.*, 12:531–542, 1987.

G.R. Hallberg. Pre-Wisconsinan glacial stratigraphy of the central Plains region in Iowa, Nebraska, Kansas, and Missouri. In V. Sibrava, D.Q. Bowen, and G.M. Richmond, editors, *Quaternary Glaciations of the Northern Hemisphere*, pages 11–15. Pergamon Press, Oxford, 1986.

G.R. Hallberg and T.J. Kemmis. Stratigraphy and correlation of the glacial deposits of the Des Moines and James lobes and adjacent areas in North Dakota, South Dakota, Minnesota, and Iowa. In V. Sibrava, D.Q. Bowen, and G.M. Richmond, editors, *Quaternary Glaciations of the Northern Hemisphere*, pages 65–68. Pergamon Press, Oxford, 1986.

Michael J Hambrey, Peter J Barrett, and Ross D Powell. Late Oligocene and early Miocene glacimarine sedimentation in the SW Ross Sea, Antarctica; the record from offshore drilling. In J.A. Dowdeswell and O.C. Colm, editors, *Glacier-influenced sedimentation on high-latitude continental margins.* Geological Society of London, London, 2002.

J. Harbor, D. Fabel, A. Stroeven, and D. Elmore. Constraining erosion rates under the Fennoscandian Ice Sheet: new evidence from cosmogenic isotopes. *Abstracts with Programs, Geological Society of America*, 31(7):48, 1999.

H. Heinrich. Origin and consequences of cyclic ice rafting in the northeast Atlantic Ocean during the past 130,000 years. *Quaternary Research*, 29:142–152, 1988.

B. Heisinger, D. Lal, A. J. T. Jull, P. Kubik, S. Ivy-Ochs, K. Knie, and E. Nolte. Production of selected cosmogenic radionuclides by muons: 2. Capture of negative muons. *Earth and Planetary Science Letters*, 200(3-4):357–369, 2002a.

B. Heisinger, D. Lal, A. J. T. Jull, P. Kubik, S. Ivy-Ochs, S. Neumaier, K. Knie, V. Lazarev, and E. Nolte. Production of selected cosmogenic radionuclides by muons 1. Fast muons. *Earth and Planetary Science Letters*, 200(3-4):345–355, 2002b.

J. Klein, R. Middleton, R. Giegengack, and P. Sharma. Revealing histories of exposures using in situ produced ^{26}Al and ^{10}Be in Libyan desert glass. *Radiocarbon*, 28:547–555, 1988.

J. Kleman. Preservation of landforms under ice sheets and ice caps. *Geomorphology*, 9:19–32, 1994.

D. Lal. Cosmic ray labeling of erosion surfaces: in situ nuclide production rates and erosion models. *Earth Planet. Sci. Lett.*, 104:424–439, 1991.

D. Lal and B. Peters. Cosmic ray produced radioactivity on the earth. In K. Sitte, editor, *Handbuch der Physik*, pages 551–612. Springer, Berlin, 1967.

K. Lidmar-Bergstrom. Preglacial weathering and landform evolution in Fennoscandia. *Geografiska Annaler*, 70A:273–276, 1988.

K. Lidmar-Bergstrom. A long-term perspective on glacial erosion. *Earth Surf. Processes Landf.*, 22:297–306, 1997.

J.M. Lineburg. *Sedimentology and stratigraphy of pre-Wisconsin drifts, Coteau des Prairies, eastern South Dakota*. M.S. thesis, University of Minnesota, 1993.

D.R. MacAyeal. Irregular oscillations of the West Antarctic Ice Sheet. *Nature*, 359:29–32, 1992.

D.R. MacAyeal. Binge/purge oscillations of the Laurentide Ice Sheet as a cause of the North Atlantic's Heinrich Events. *Paleoceanography*, 8:775–784, 1993a.

D.R. MacAyeal. A low order model of the Heinrich event cycle. *Paleoceanography*, 8:767–773, 1993b.

D.R. MacAyeal and T.K. Dupont. A finite-element model of the Hudson Strait ice stream purge cycle using a statistical mechanics treatment of the subglacial bed. *EOS, Trans. AGU*, 75(44, suppl.):240–241, 1994.

J. Mangerud, E. Jansen, and J. Y. Landvik. Late Cenozoic History of the Scandinavian and Barents Sea ice sheets. *Global and Planetary Change*, 12:11–26, 1996.

J.A. Mason. Surficial geology of the Fort Calhoun and Kennard quadrangles, Nebraska. Conservation and Survey Division Open-File Report 56, 2001.

Mathworks, Inc. *Optimization Toolbox User's Guide*. The Mathworks, Inc., Natick, MA, 2000.

M.C. Monaghan, S. Krishnaswami, and K.K Turekian. The global average deposition rate of ^{10}Be. *Earth and Planetary Science Letters*, 76:279–287, 1986.

K. Nishiizumi, E.L. Winterer, C.P. Kohl, J. Klein, R. Middleton, D. Lal, and J.R. Arnold. Cosmic ray production rates of ^{26}Al and ^{10}Be in quartz from glacially polished rocks. *J. Geophys. Res.*, 94:17,907–17,915, 1989.

T.C. Partridge, D. E. Granger, M. Caffee, and R.J. Clarke. Lower Pliocene hominid remains from Sterkfontein. *Science*, 300(5619):607–612, 2003.

C.J. Patterson. Surficial geology of southwestern Minnesota. In C.J. Patterson, editor, *Contributions to the Quaternary Geology of Southwestern Minnesota. Minnesota Geological Survey Report of Investigations No. 47*. University of Minnesota, St. Paul, MN, 1997.

C.J. Patterson. Quaternary geology - upper Minnesota River basin, Minnesota. Minnesota Geological Survey Regional Hydrologic Assessment RHA-4, 1999.

C.J. Patterson and T.J. Boerboom. The significance of pre-existing, deeply weathered crystalline rock in interpreting the effects of glaciation in the Minnesota River Valley, U.S.A. *Annals of Glaciology*, 28:53–58, 1999.

M. J. Pavich, L. Brown, J.N. Vallette-Silver, J. Klein, and R. Middleton. ^{10}Be analysis of a Quaternary weathering profile in the Virginia Piedmont. *Geology*, 13:39–41, 1985.

M.J. Pavich, L. Brown, J. Klein, and R. Middleton. ^{10}Be accumulation in a soil chronosequence. *Earth Planet. Sci. Lett.*, 68:198–204, 1984.

J. Putkonen and T. Swanson. Accuracy of cosmogenic ages for moraines. *Quaternary Research*, 59:255–261, 2003.

M. Roy, P.U. Clark, R.W. Barendregt, J.R. Glasmann, and R.J. Enkin. Glacial stratigraphy and paleomagnetism of late Cenozoic deposits of the north-central United States. *Geological Society of America Bulletin*, 116(1/2):30–41, 2004.

D.R. Setterholm. Quaternary geology – southwestern Minnesota. Minnesota Geological Survey Regional Hydrologic Assessment Series RHA-2, 1995.

N.J. Shackleton, J. Backman, H. Zimmerman, D.V. Kent, M.A. Hall, D.G. Roberts, D. Schnitker, J.G. Baldauf, A. Desprairies, R. Homrighausen, P. Huddlestun, J.B. Keene, A.J. Kaltenback, K.A.O Krumsiek, A.C. Morton, J.W. Murray, and J. Westberg-Smith. Oxygen isotope calibration of the onset of ice-rafting and history of glaciation in the North Atlantic region. *Nature*, 307:620–623, 1984.

N.J. Shackleton and N.D. Opdyke. Oxygen-isotope and paleomagnetic stratigraphy of equatorial Pacific core V28-238: oxygen isotope temperatures and ice volumes on a 10^5 and 10^6 year scale. *Quaternary Research*, 3:39–55, 1973.

B.H. Sheldrick, editor. *Analytical Methods Manual 1984*. Land Resource Research Institute, Research Branch, Agriculture Canada, 1984.

D.R. Soller and P.H. Packard. Digital representation of a map showing the thickness and character of Quaternary sediments in the glaciated United States east of the Rocky Mountains. USGS Digital Data Series DDS-38, 1998.

J. Stone. A rapid fusion method for separation of beryllium-10 from soils and silicates. *Geochimica Et Cosmochimica Acta*, 62(3):555–561, 1998.

J. Stone. Extraction of Al and Be from quartz for isotopic analysis. UW Cosmogenic Nuclide Lab Methods and Procedures., 2004. URL `http://depts.washington.edu/cosmolab/chem.html`.

J. O. Stone. Air pressure and cosmogenic isotope production. *Journal of Geophysical Research*, 105(B10):23753–23759, 2000.

J. O. H. Stone, J. M. Evans, L. K. Fifield, G. L. Allan, and R. G. Cresswell. Cosmogenic chlorine-36 production in calcite by muons. *Geochimica Et Cosmochimica Acta*, 62(3):433–454, 1998.

J. O. H. Stone, L. K. Fifield, J. Beer, M. Vonmoos, C. Obrist, M. Grajcar, P. Kubik, R. Muscheler, R. Finkel, and M. Caffee. Co-precipitated silver-metal oxide aggregates for accelerator mass spectrometry of ^{10}Be and ^{26}Al. *Nuclear Instruments and Methods B*, 2004 in press.

D.E. Sugden. A case against deep erosion of shields by ice sheets. *Geology*, 4:580–582, 1976.

D.E. Sugden. Glacial erosion by the Laurentide Ice Sheet. *Journal of Glaciology*, 20:367–391, 1978.

D.E. Sugden. Modification of old land surfaces by ice sheets. *Zeitschrift fur Geomorphologie*, 72: 163–172, 1989.

W.A. White. Deep erosion by continental ice sheets. *Geological Society of America Bulletin*, 83: 1037–1056, 1972.

Appendix A

STRATIGRAPHY AND ANALYTICAL DATA FOR BOREHOLES MENTIONED IN TEXT

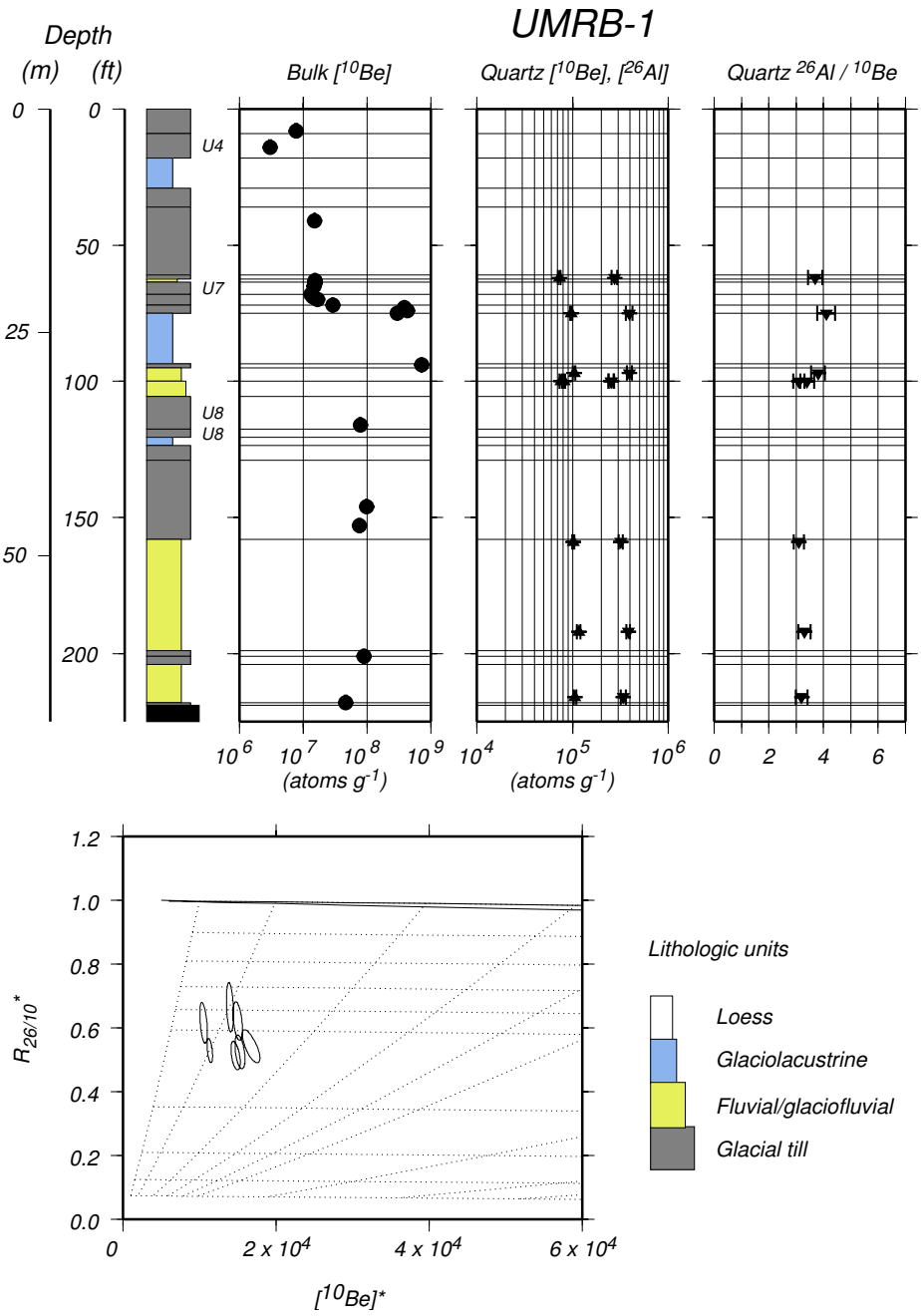

Figure A.1: Stratigraphy and analytical data for boreholes discussed in text. This page, borehole UMRB-1. Core log to left. Till unit designations refer to Patterson [1999]. Panels to right of core log show ^{10}Be and ^{26}Al analyses. "Bulk" ^{10}Be refers to ^{10}Be of atmospheric origin (so-called "meteoric" or "garden-variety" ^{10}Be) measured in bulk sediment. Error bars for these analyses are smaller than the plotting symbol at this scale. "Quartz" ^{10}Be and ^{26}Al data refer to measurements of *in-situ*-produced nuclides in purified quartz separates. The two-nuclide plot in the lower panel is described in Figure 3.2 and shows 68% confidence ellipses for *in-situ*-produced ^{10}Be and ^{26}Al measurements. The light lines in background are trajectories and isochrons for burial at infinite depth (Figure 3.2).

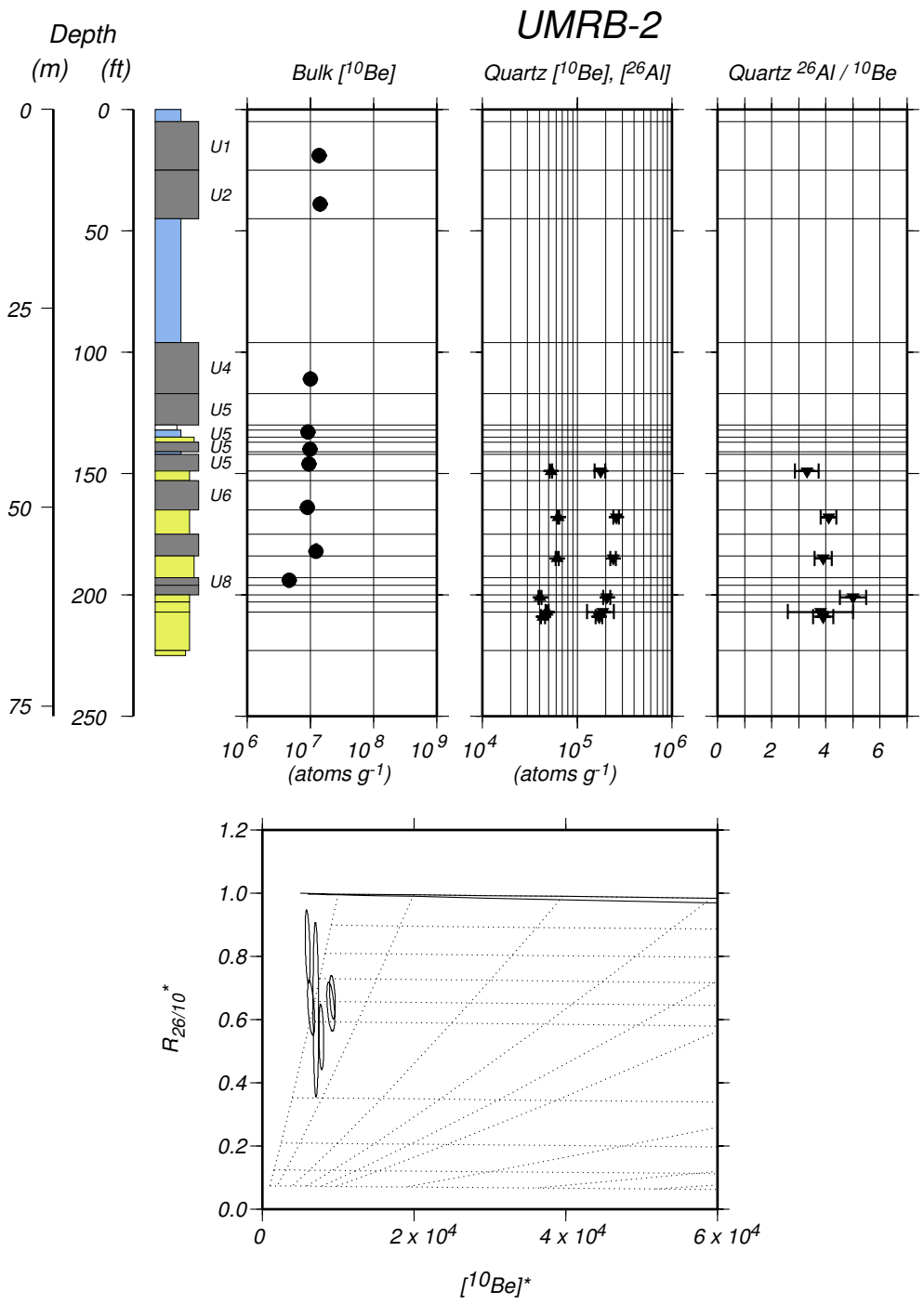

Figure A.1b: Borehole UMRB-2. Till unit designations refer to Patterson [1999].

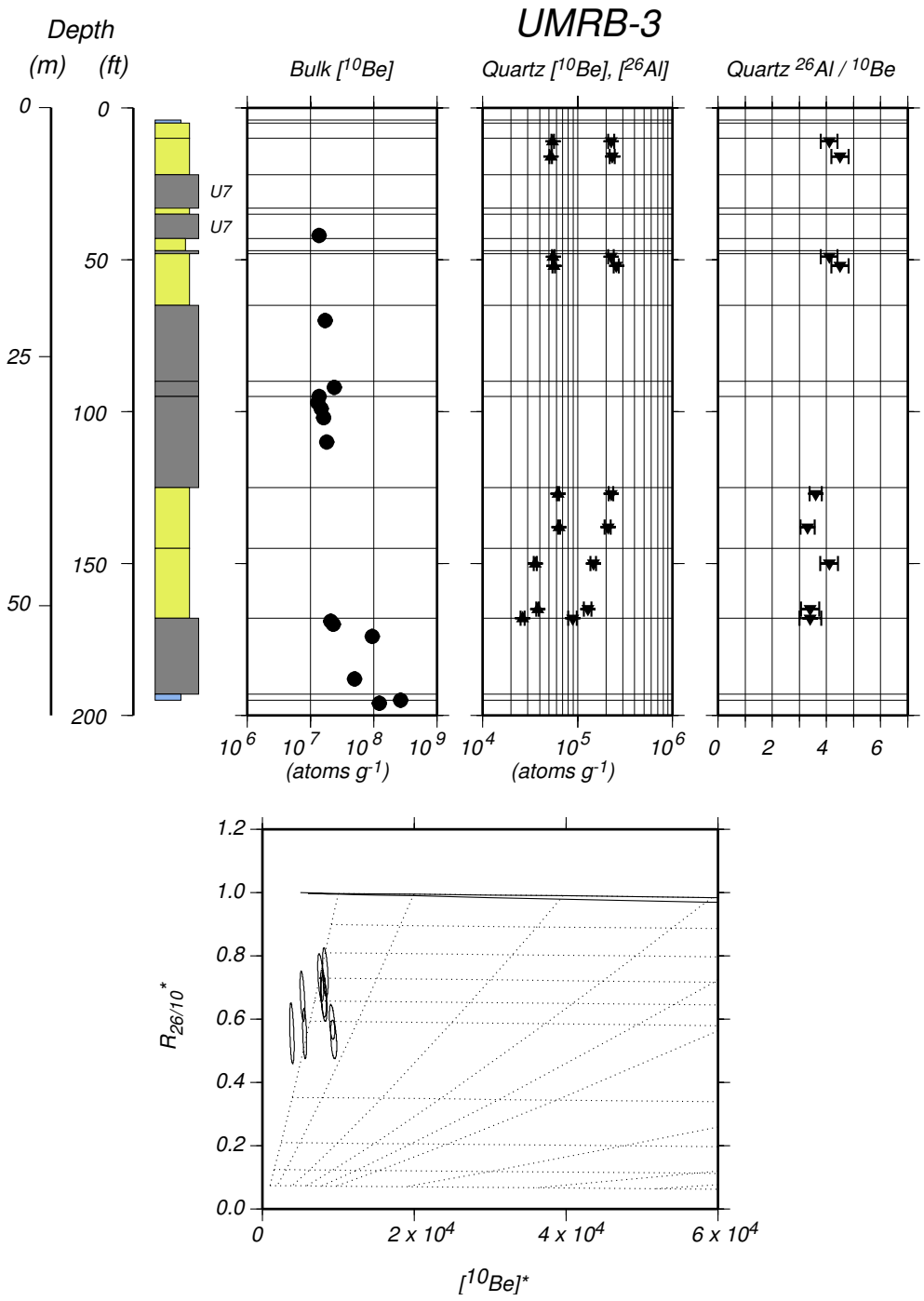

Figure A.1c: Borehole UMRB-3. Till unit designations refer to Patterson [1999].

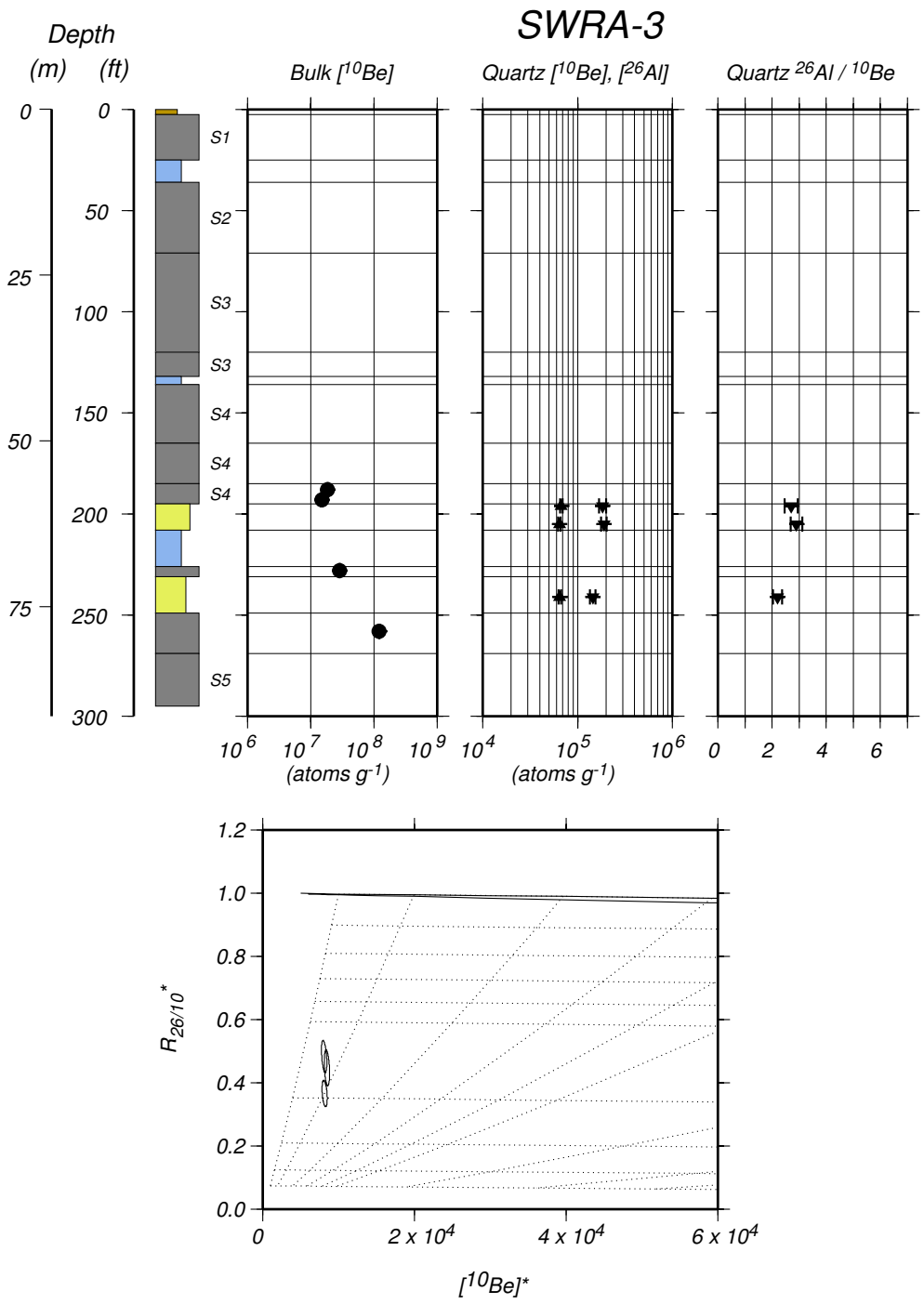

Figure A.1d: Borehole SWRA-3. Till unit designations refer to Setterholm [1995].

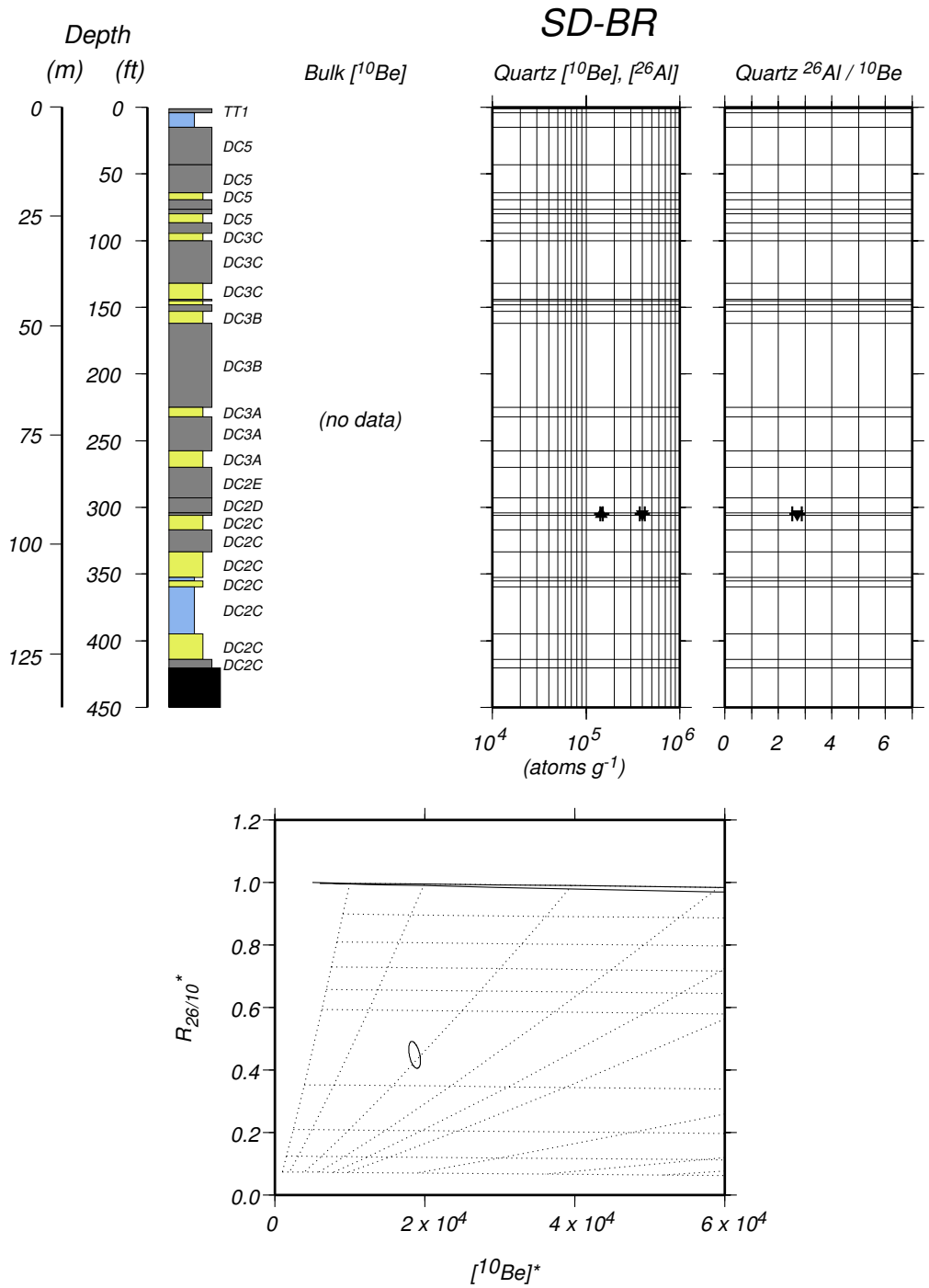

Figure A.1e: Borehole SD-BR. Till unit designations refer to Lineburg [1993].

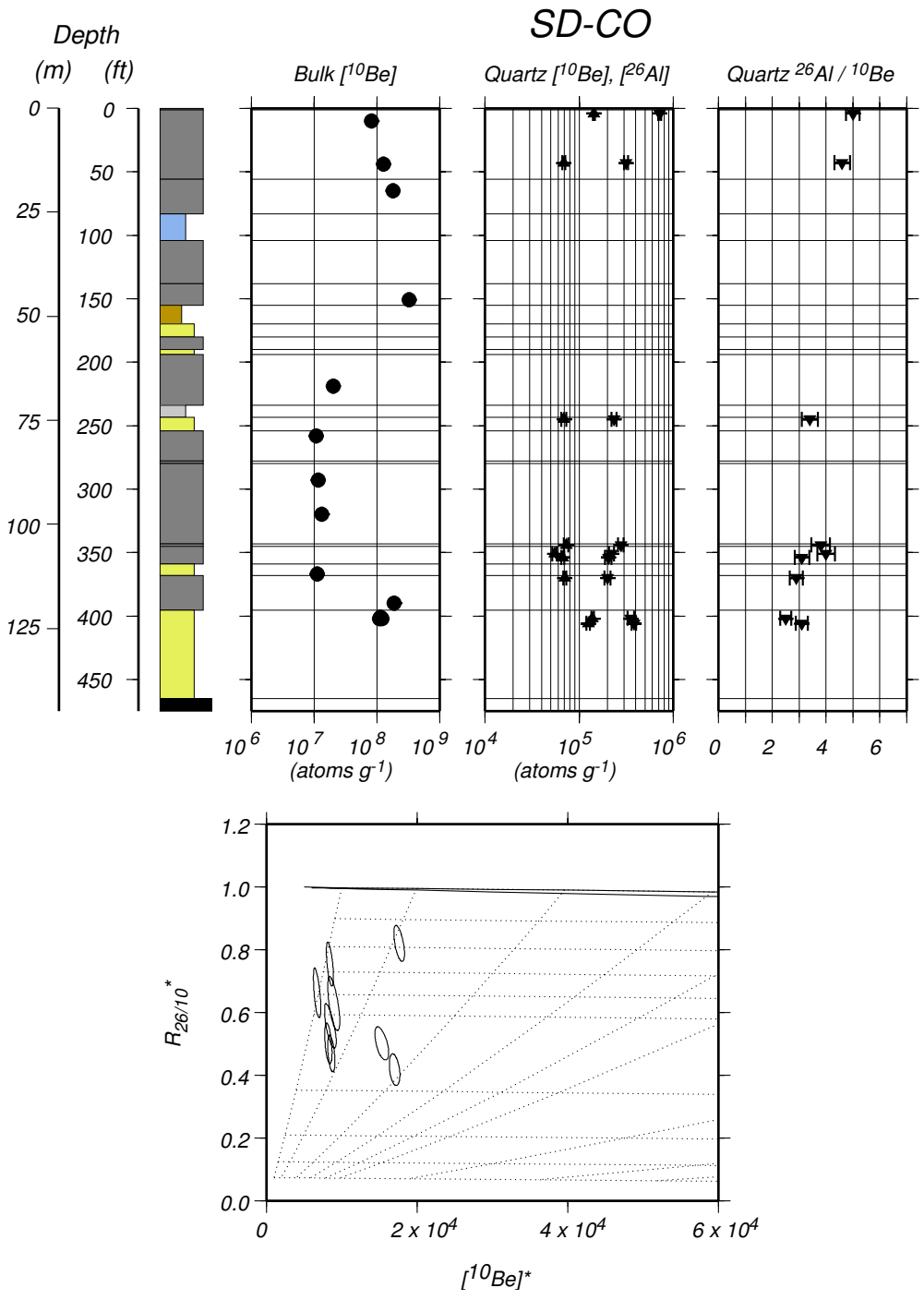

Figure A.1f: Borehole SD-CO.

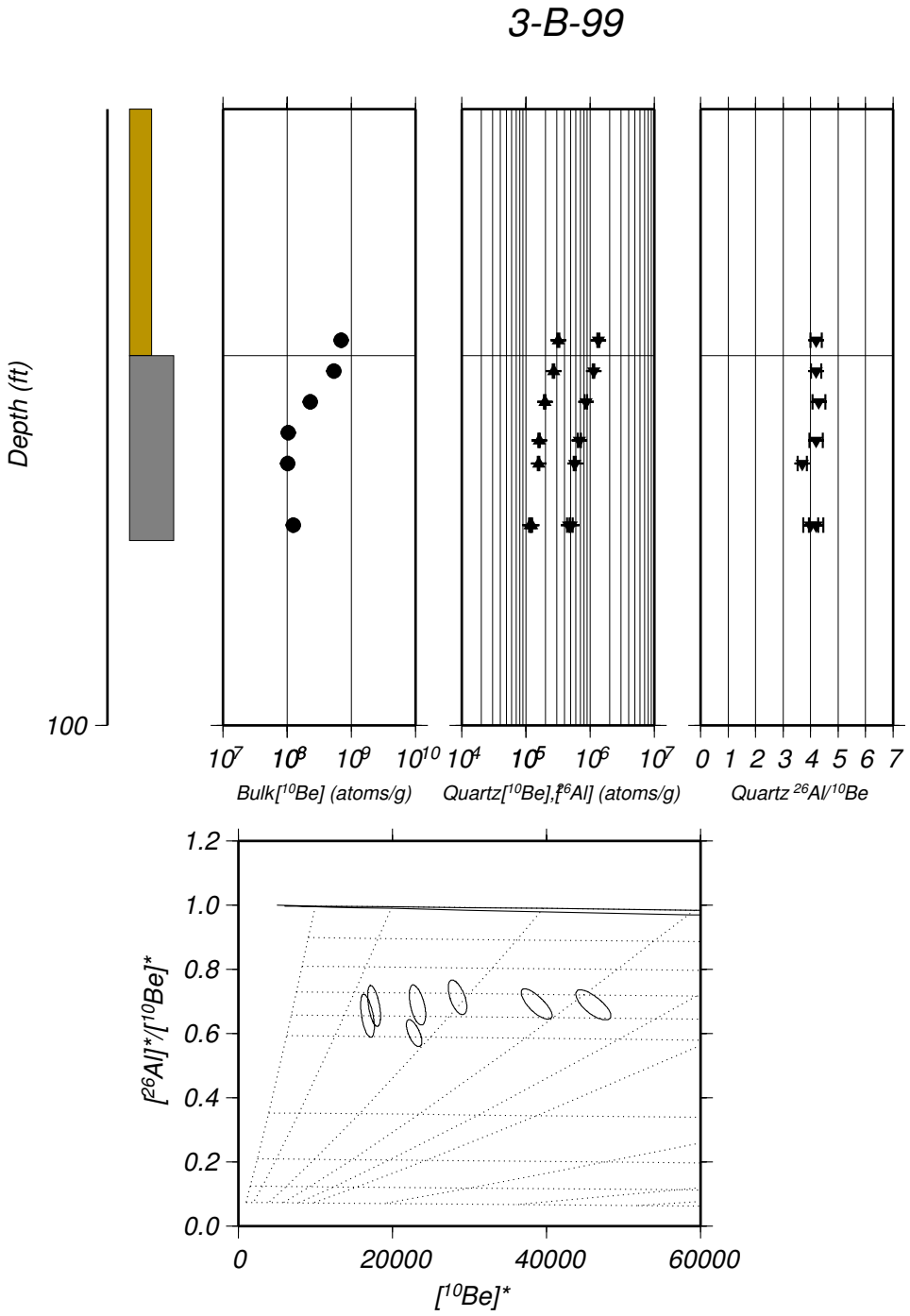

Figure A.1g: Borehole 3-B-99.

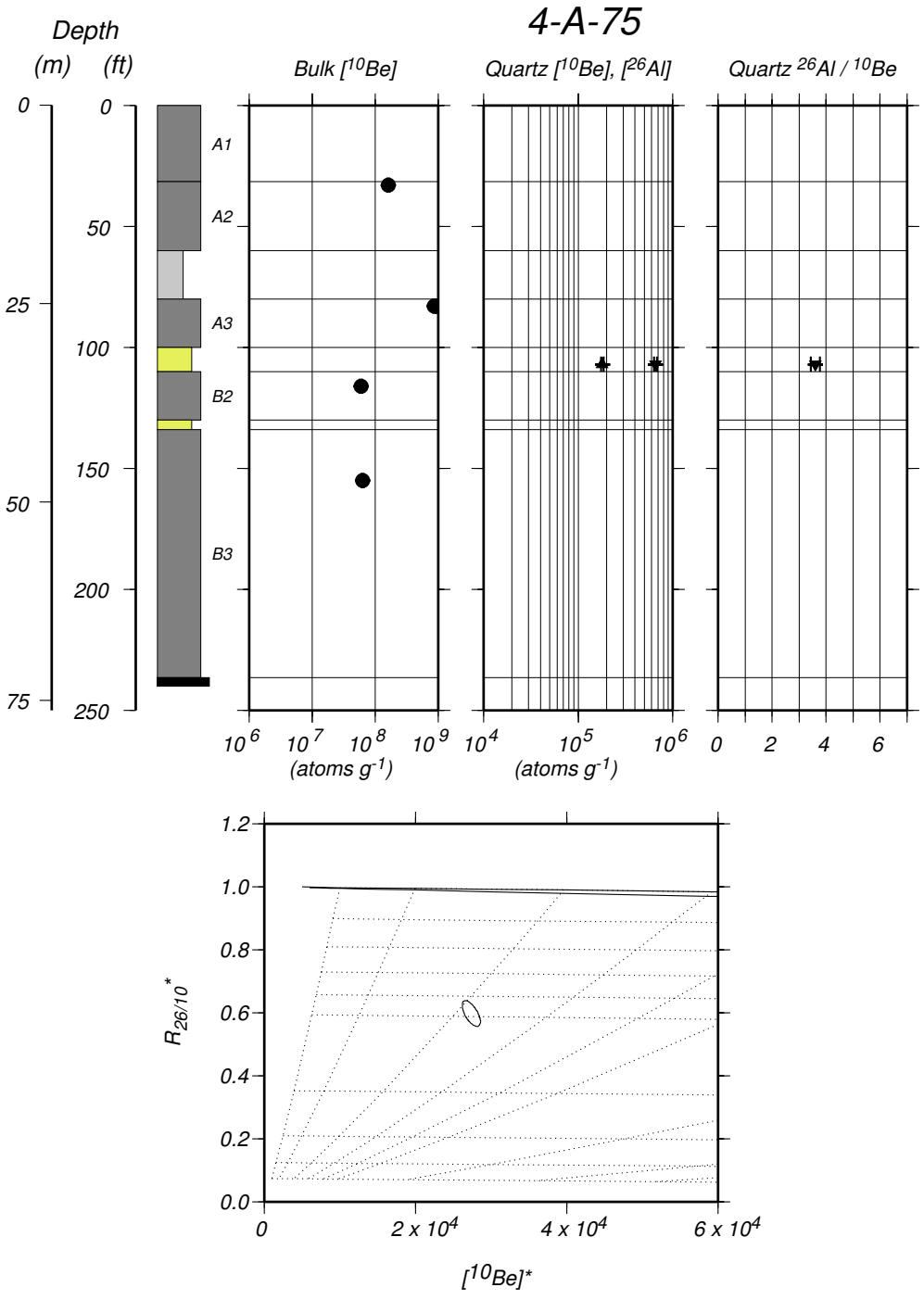

Figure A.1h: Borehole 4-A-75. Till unit designations refer to Boellstorff [1978a] and C. Rovey (unpublished report).

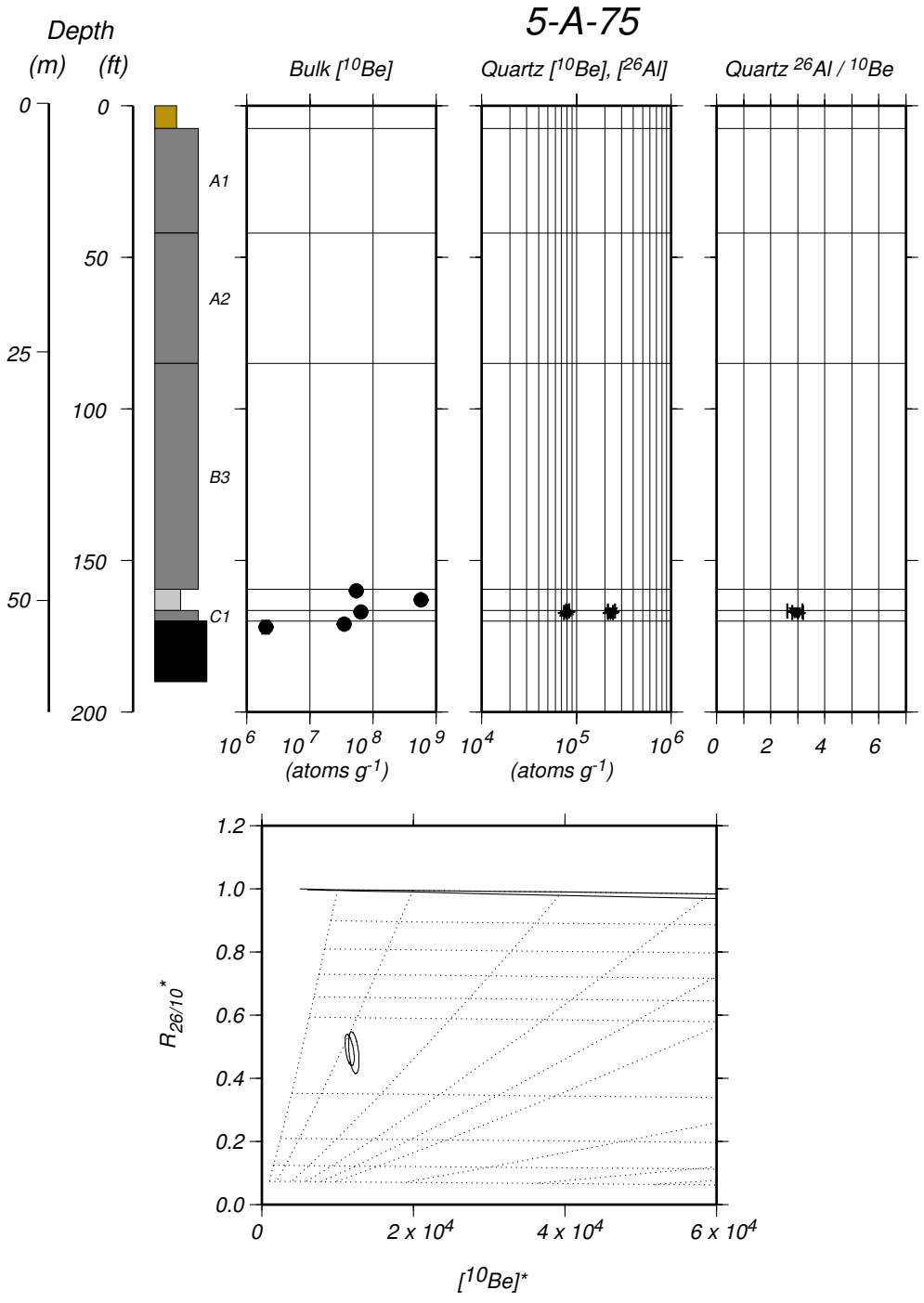

Figure A.1i: Borehole 5-A-75. Till unit designations refer to Boellstorff [1978a] and C. Rovey (unpublished report).

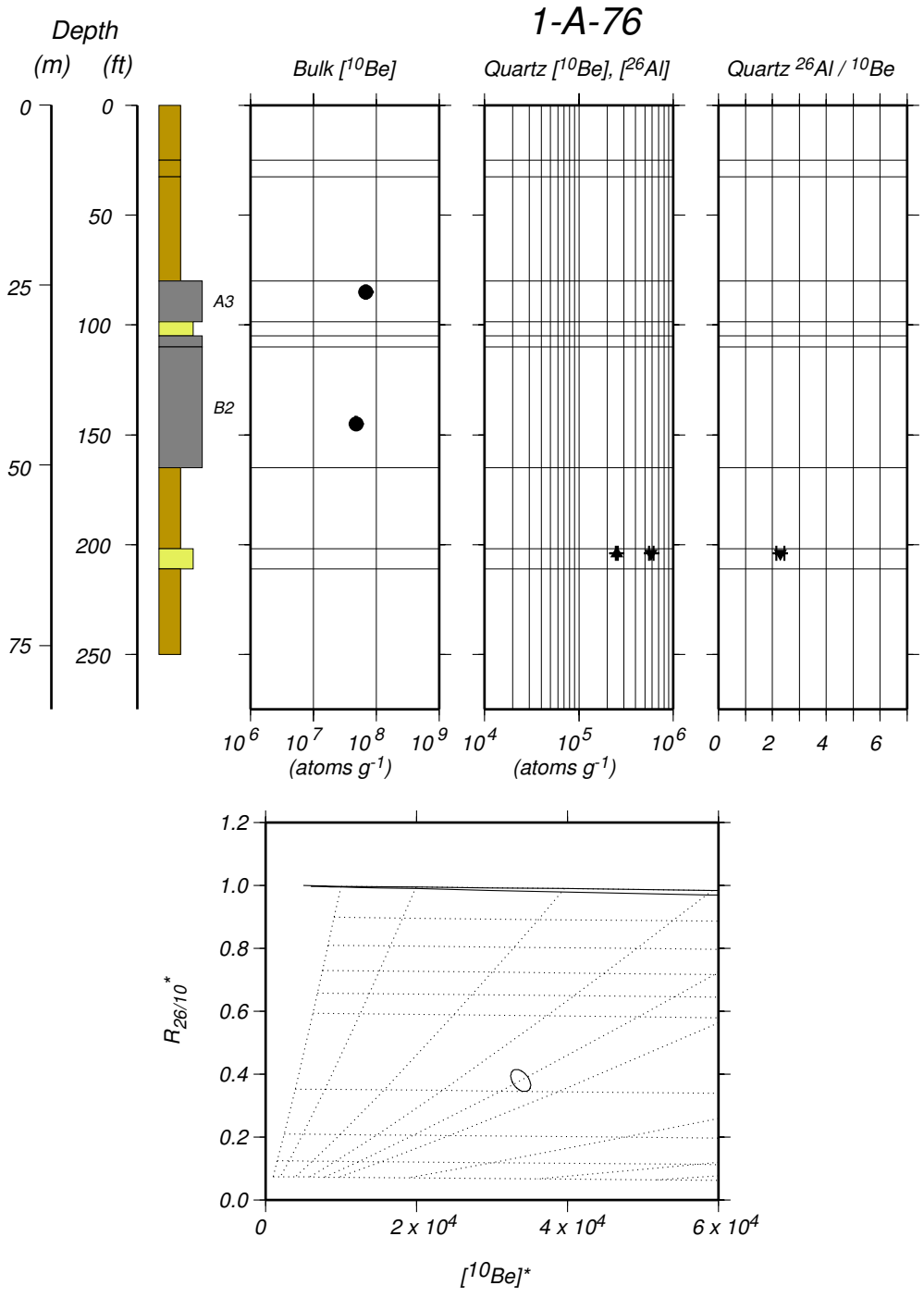

Figure A.1j: Borehole 1-A-76. Till unit designations refer to Boellstorff [1978a] and C. Rovey (unpublished report).

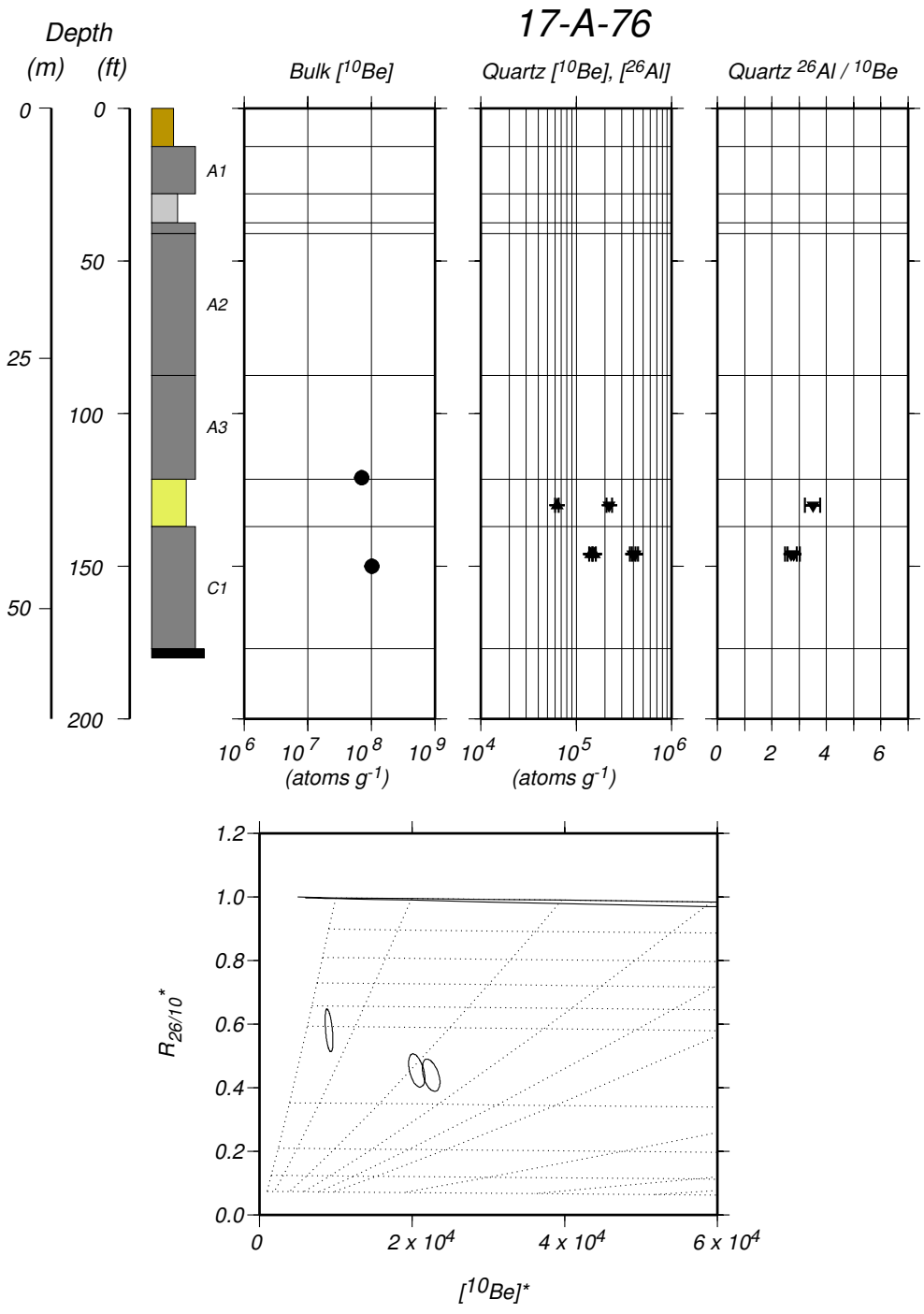

Figure A.1k: Borehole 17-A-76. Till unit designations refer to Boellstorff [1978a] and C. Rovey (unpublished report).

VITA

Greg Balco's chief accomplishment has been to remain alive and in reasonable health since 1970. He received a B.A. from Williams College in 1992, and a M.S. in Geological Sciences from the University of Maine in 1997. This is his second work of fiction.